DBM-98

International Workshop on

Deuteration of Biological Molecules for Structural and Dynamic Studies. Applications to Neutron Scattering and NMR

Frank Laboratory of Neutron Physics
Joint Institute for Nuclear Research

Dubna, Russia
May 19-25, 1998

JOINT INSTITUTE FOR NUCLEAR RESEARCH

Proceedings of the

International Workshop on

Deuteration of Biological Molecules for Structural and Dynamic Studies. Applications to Neutron Scattering and NMR

Frank Laboratory of Neutron Physics
May 19-25, 1998
Dubna, Russia

Dubna, 1998

International Advisory Committee:

V.L.Aksenov (Russia)
A.V.Belushkin (Russia)
G.Buildt (Germany)
R.May (France)
J.Parello (France)
D.Worcester (USA)

Organizing Committee:

Chairmen:
I.Serdyuk (JINR, Dubna, Russia)
P.Timmins (ILL, Grenoble, France)

Scientific secretary:
M.Avdeev (JINR, Dubna, Russia)

Coordinators:
T.Drozdova (JINR, Dubna, Russia),
A.Korol (JINR, Dubna, Russia)

ISBN 5-85165-515-1

Preface

The international workshop "Deuteration of Biological Molecules for Structural and Dynamic Studies. Applications to Neutron Scattering and NMR (DBM-98)" was organized by the Frank Laboratory of Neutron Physics (FLNP) of the Joint Institute for Nuclear Research (JINR) and held in Dubna, Russia, on May 19-25, 1998. This workshop was intended to bring together scientists from around the world who are interested in application of the neutron scattering and the NMR techniques for structural and dynamic studies of biological molecules.

The main objectives of DBM-98 were

- generalization of newest experimental experience in application of biological macromolecules deuteration to investigations of their structure and dynamics by neutron scattering and NMR methods;
- mapping out new approaches to selective deuteration of biological macromolecules aimed at extraction of structural information with highest possible spatial resolution;
- discussion of technological aspects of biomass deuteration to have the highest possible yield at reasonable expenditures;
- establishing contacts between representatives of different fields of science, such as physics, biology, medicine, etc., to seek new approaches to investigations of structural fundamentals of biological macromolecule functioning using neutron scattering and NMR methods.

These Proceedings comprise about 20 reports given at the workshop and present latest achievements in the field of elastic-inelastic neutron scattering and nuclear magnetic resonance on biological molecules and production of deuterated materials.

The Organizing Committee is sincerely grateful to the Russian Ministry of Science and Technology, the Russian Fund for Basic Research (RFBR) and the European Research Office (ERO) of the United States Army for the financial support of the workshop.

We believe that shared experience is valuable for an effective use of neutrons and NMA for biological studies. DBM-98 is a second in a series following the lines of the first workshop (Autrans, 1994) and we hope that the tradition will continue.

P.Timmins and I.Serdyuk

Chairmen of DBM-98


D
DEUTERATION
OF BIOLOGICAL
MOLECULES.
APPLICATIONS
TO NEUTRON
SCATTERING
AND NMR

Contents

APPLICATION OF DENSE CULTURE FOR *IN VIVO* DEUTERATION OF MICROORGANISMS.

Kalju Vanatalu, Katrin Tomson, Toomas Paalme, Kalle Tiisma and Raivo Vilu.

Institute of Chemical Physics and Biophysics, Akadeemia tee 23, EE0026 Tallinn, Estonia

For the NMR and neutron scattering studies large amounts (~hundreds of grams) of deuterated biomass is needed. The use of deuterated substrates and heavy water environment has a strong inhibitory effect on cellular physiology causing the slow down of growth rate and may also result changes in morphology and in nutritional requirements. Additional restrictions are set due to the high price of ^2H labelled compounds including heavy water. This brings along the need from one side to choose the less expensive substrates and use them in an economical way and from the other side choose the growth conditions which enable the biosynthesis of required cell components in the biologically active state. We have established a method of large scale preparation of deuterium labelled microbial cells using computer-controlled fed-batch cultivation. The main advantages of this technique are achievement of high cell densities and and stable growth conditions throughout the cultivation by constant control of the growth rate.

The only acceptable by price fully deuterated growth substrates for *E.coli* are succinate and acetate. According to our observation the growth of *E.coli* in merely acetate is very poor and unstable, but it is utilised extensively if succinate is also present. As D-acetate is significantly cheaper than D-succinate it is advantegous to optimise the acetate/succinate ratio in the feeding solution.

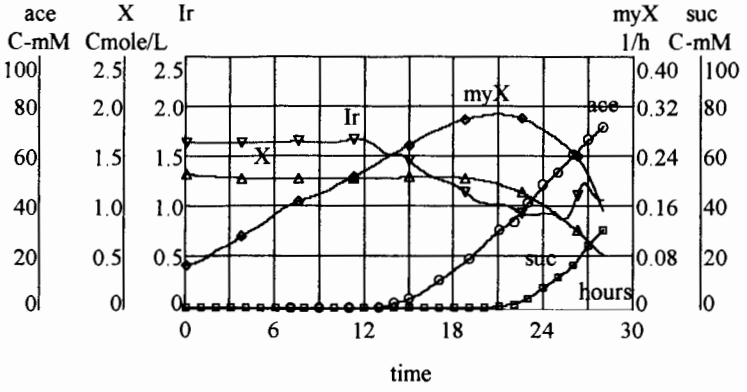

Fig.1. Growth of *E.coli* in the mixture of acetate+succinate in normal protonated conditions. Designations: ace- concentration of acetate in the fermentor; X- biomass concentration; Ir- ratio of consumption of acetate/succinate by the culture; myX- specific growth rate of cells; suc- succinate concentration in the fermentor.

For the production of partially deuterated biomass one can use H-glucose. On fig.1 are shown the results of A-stat[3,5] experiment of *E.coli* grown in the mixture of succinate and acetate in normal protonated conditions.

All the acetate is used up by the culture until the growth rate approaches $0.22h^{-1}$ which equals the maximal specific growth rate on acetate alone (table 1). After that the ratio of consumption of acetate/succinate decreases. Thus, the ratio of utilisation of acetate/succinate is inversely proportional to the growth rate. From table1 it is seen that in all cases under study the accumulation of acetate (or succinate in case of using it as the sole carbon source) starts at lower growth rate than μ_{max}. It is well known that acetate concentrations already in the range of 1 g/L inhibit the growth rate of *E.coli* significantly[6]. As in the case of batch cultivation the growth proceeds at maximal rate it is clear that only low biomass densities can be reached.

Table 1. Main growth characteristics of *E.coli* cultivated in A-stat in normal protonated media. Designations: μ_{crit}- growth rate value, where acetate (in case of succinate the substrate) accumulation starts; μ_{max}- maximal specific growth rate; C/C- carbon moles

Carbon source	μ_{crit} (h^{-1})	μ_{max} (h^{-1})	$Y_{x/s}$(C/C), $\mu<\mu_{crit}$	$Y_{x/s}$(C/C), $\mu>\mu_{crit}$	substrate concentration (C-mM) at $\mu=\mu_{max}$
acetate	0.15	0.22	0.25	0.35	~30
succinate	0.29	0.4	0.36-0.39	0.39	~30
acetate+ succinate	0.22	0.32	0.30	0.35	acetate ~30
glucose	0.48	0.58	0.53	0.44	acetate ~10

In order to avoid the accumulation of substrate or metabolic by-products and maintain continuous growth the growth rate must be kept below μ_{crit}. On the other hand, if the growth rate is chosen too low the cultivation time increases. As the substrate expenditures for the maintenance of cellular functions per unit of time remain the same but the increase of cell mass is slow this brings along the overall decrease of biomass yield at very low growth rates[7]. Thus the optimal cultivation point is at growth rate slightly below μ_{crit}.

To accomplish continuous growth of the culture at pregiven growth rate we have established a μ-stat fed-batch cultivation technique[1].

The feeding of the culture is carried out by increasing the substrate pumping rate pmp(t) into the fermentor according to the exponential growth law:

$$pmp(t)=pmp(0)*\exp(\mu_{pre}*t) \quad (1),$$

where μ_{pre} designates the pregiven feeding rate. After some time the growth rate of the culture stabilizes at the value $\mu=\mu_{pre}$. On fig.2 is depicted the simulated change of growth rate of culture by choosing different initial conditions at start of feeding with $\mu=0.05\ h^{-1}$.

It can be seen, that the culture reaches asymptotically the condition $\mu=\mu_{pre}$ irrespective of the starting value of pmp(0) on condition that μ_{pre} is chosen not above μ_{crit}.

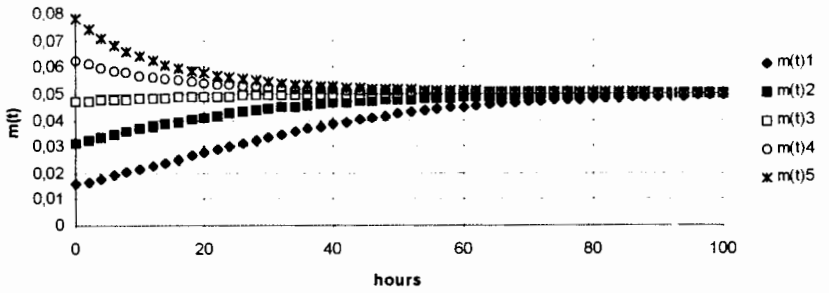

Fig.2. Simulation of transitions from batch to fed-batch. Exponential feeding of substrate with μ_{pre}=0.05 h^{-1} was switched on at 0 h. The amount of biomass was 2g and the biomass yield coefficient 0.25 g/g. Growth rates m(t)1...5 correspond to the initial pumping rates resp. 0.125, 0.25,0.375, 0.5 and 0.625 g/h.

In practice the fed-batch is carried out under automatic increase of the pumping controlled by the computer. We have used an expert system BioXpert (BioExpert Ltd., Tallinn) enabling to control the fermentation process by programmed algorithms. Also different on-line parameters(pO_2, pH, temperature, O_2 and CO_2 levels in the effluent gas) are collected at 1 to 10 min. intervals. This enables to estimate continuously the state of the culture in the fermentor. Substrate level in the medium is analysed by HPLC.

When the cells of *E.coli* are transferred to deuterated medium the values of μ_{max} and μ_{crit} decrease. Due to to big volumes of media chemostat or even A-stat experiments cannot be carried out in D_2O. For the start of fed-batch in D_2O the necessary initial parameters μ_{max}, μ_{crit} and Y_{xs} are estimated from the batch growth in the fermentor and later corrected during fed-batch.

A typical growth curve of μ-stat fed-batch of *E.coli* on D_2O fed with deuterated acetate+succinate is depicted on fig.3. As it can be seen the biomass increased exponentially until the aeration capacity of the system became limiting followed by constant feeding rate as a chemostat culture. Using fed-batch cultivation biomass densities above 100g/L wet weight could be achieved in D_2O. As revealed by the neutron scattering analysis the produced ribosomes had high level of deuteration with matching point equal to 121% of coherent neutron scattering density of D_2O. The NMR analysis have shown 98.5-99.0% deuteration of the growth medium in the end of high-biomass density fermentations. The ribosomes had biological activity and good homogeneity of label. Such approach has been used to produce fully and partially deuterated *E.coli* MRE600 biomass for neutron scattering studies of ribosomes[2] and recombinant tRNAs[4]

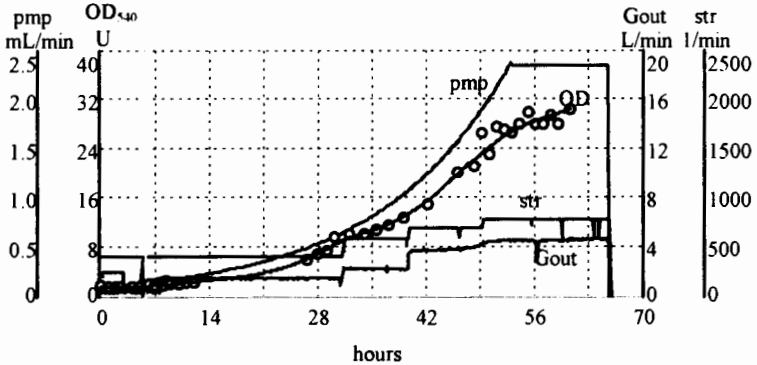

Fig.3. Computer controlled fed-batch cultivation of *E.coli* MRE600 rif on fully deuterated medium. Designations: OD_{540}-optical density of culture at 540 nm; pmp- pumping rate of feeding solution; str- stirrer speed; Gout-air flow rate for aeration

Table 2 compares the growth parameters of different *E.coli* strains overproducing tRNAs during fed-batch in D_2O. The overproduction of tRNAs by fed-batch grown cells was 3-4 fold for $tRNA^{Phe}$ by the plasmid plppMetPhe and 1.5 fold by the pPhe normalized to the cellular content of $tRNA^{Leu}$. In the case of pMet the overexpression of $tRNA^{met}$ was up to 2 fold. The produced biomass was of high biological activity and sufficient for large-scale purification of specific deuterium labelled tRNAs.

Table2. Growth characteristics of *E.coli* MRE600 carrying different plasmids with genes of $tRNA^{Phe}$ and $tRNA^{met}$

plasmid	μ_{max} (h^{-1})	μ_{crit} (h^{-1})	succinate/acetate in feeding solution (C-molar)	$Y_{x/s}$(C-moles)	X_{max}(g WW/L)
pPhe	0.08	0.035	2.66/3.90	0.25	80
pMet	0.13	0.05	2.66/3.90	0.29	110
plppMetPhe	0.15	0.025	3.06/3.90	0.31	70
without	0.13	0.08	2.66/3.90	0.30	125

E.coli B MV10-17 is a mutant strain lacking protein L1 of the ribosomal 50S subunit. Use of such ribosomes in deuterated form enables to insert a protonated L1 protein as a label in structural studies using small angle neutron scattering. The unfavourable circumstance however, was that the strain grew only on mineral media with remarkable amounts of rich supplement added. It was established by cultivation in selective addition of aminoacids that the strain was an auxotroph for 3 aminoacids: leucine, isoleucine and valine. Therefore it was decided to use in addition to succinate and acetate a supplement of hydrolyzed deuterated *E.coli* or a methylotrophic yeast biomass for provision of the leu, ile and val. As the hghest obtainable cell density of the methylotrophic yeast was below 30 optical density units it was more favourable to use *E.coli* for making protein hydrolyzate. In the preliminary experiments it was observed that after the depletion of rich supplement in the

medium the cells of auxotrophic *E.coli* were still expending succinate unproductively without biomass synthesis. Basing on this fenomenon the idea of the fed-batch strategy was developed. In fact, by measuring the rates of utilization of hydrolyzate, succinate and acetate it is possible to find out the approximate ratios of those components in the feeding. Then by increasing slightly the amount of succinate and decreasing that of acetate in the feeding it is possible to ensure the complete utilization of the other two components without a danger of succinate accumulation as it can be utilised even in the absence of the rich supplement. According to these considerations cultivations in H_2O and D_2O were carried out in two stages: a) batch growth with the estimation of necessary growth characteristics and b) based on the initial data fed-batch for achieving high cell densities. The results are shown in table 3. The ratios of consumption of acetate and succinate were different for batch growth in H_2O and D_2O. It can be assumed that the different ratios of consumption of acetate/succinate may (partly) be caused due to more than two times lower growth rate during batch in D_2O compared to the experiment in H_2O. Nevertheless the overall biomass yield remained around 0.2 (C/C moles) in both cases. As shown in table 3 the cells were able to extensively utilize succinate unproductively both in H_2O and D_2O but practically could not utilise acetate in D_2O when the source of aminoacids was depleted. Based on the data of consumption of the hydrolyzate; succinate and acetate in batch growth the feeding for fed-batch was prepared where the succinate was added in excess. This enabled to carry out balanced feeding and achieving cell density of 70 g/l of wet weight in fully deuterated medium. No feeding components were found accumulating in the growth medium in significant levels during the whole cultivation as checked by HPLC and aminoacid analyses. Obviously during the fed-batch in D_2O the ratio of unproductively used succinate can be decreased but this increases the risk of overfeeding with acetate or the hydrolyzate.

Table 3. Growth parameters of auxotrophic *E.coli* B MV17-10 in batch and fed-batch cultivation in normal and deuterated media. The growth parameters for batch growth are mean values estimated in the middle of logarithmic growth.

	Batch		Fed-batch	
medium:	H_2O	D_2O	H_2O	D_2O
1) growth rate: μ (h^{-1})	0.37	0.16	0.12	0.02-0.04
2) consumption of succinate and acetate: $1/Y_{x/suc}$ (g/g)	2.4	1.9	2.2	3.9
$1/Y_{x/ac}$ (g/g)	1.4	2.0	1.1	2.0
Sum: $1/Y_{x/suc}+1/Y_{x/ac}$ (g/g)	3.8	3.9	3.3	5.9
3) consumption of hydrolysate: secondary:primary biomass	1:1.6	1:1.5	1:1.4	1:1.4
4) unproductive consumption of succinate(q_{suc}) and acetate(q_{ac}): q_{suc} (g/g*h)	0.93	0.36		
q_{ac} (g/g*h)	0.29	0.02		

The hydrolyzate prepared from *E.coli* was in all cases consumed in the ratio of about 1:1.5 (g biomass produced: g biomass hydrolysed). Taking into account that the yield of the limiting aminoacids preparation was about 70% it follows that practically all of the growth-limiting aminoacids (leu, ile, val) were switched into the biomass without metabolization. The method developed can be used in many other cases of fed-batch culture of auxotrophic organisms enabling to minimize the amount of very expensive labelled rich supplement (cell hydrolyzate, aminoacids, nucleotides) by using cheaper substrates as mair sources of carbon and energy.

In summary the μ-stat fed-batch is an effective method for the cultivation of *E.coli* and other microbial cells in deuterated media. The main advantages are achievement of high biomass density and the ability to keep the cells in stabile growth conditions. For the setup of fed-batch preliminary study of the strain is necessary to carry out to estimate the main growth parameters. For this task the A-stat experiments in H_2O can be combined with the batch experiments in D_2O in small volumes.

1. Paalme, T., K. Tiisma, A. Kahru, K. Vanatalu, R. Vilu (1990) Glucose-limited Fed-Batch Cultivat on of *Escherichia coli* with Computer-Controlled Fixed Growth Rate. Biotechnology and Bioengineering, *35*, 312-319.
2. Vanatalu, K., Paalme, T., Vilu, R., Burkhardt, N., Jünemann, R., May, R., Rühl, M.,Wadzack, J., Nierhaus, K.H. (1993) Large-scale preparation of fully deuterated cell components. Ribosomes from *Escherichia coli* with high biological activity. Eur. J. Biochem., *216* , 315-321
3. Paalme, T., Kahru, A., Elken, R., Vanatalu, K., Tiisma, K., Vilu, R. (1995) The computer-controlled continuous culture of *Escherichia coli* with smooth change of dilution rate (A-stat). Journal of Microbiological Methods, *24*, 145-153
4. Jünemann, R., Wadzack, J., Triana-Alonso, F.J., Bittner, J.-U., Caillet, J., Meinnel, T., Vanatalu, K. , Nierhaus, K.H.(1996) In vivo deuteration of transfer RNAs: overexpression and large-scale purification of deuterated specific tRNAs. Nucleic Acids Research, *24*, 5, 907-913.
5. Paalme, T., Elken, R., Kahru, A., Vanatalu, K., Vilu, R.(1997) The growth rate control in *Escherichia coli* at near to maximum growth rates: the A-stat approach. Antonie van Leeuwenhoek *71*:217-230
6. Lawford,H.G. and Rousseau, J.D. (1993) Effects of pH and acetic acid on glucose and xylose metabolism by a genetically engineered ethanologenic *Escherichia coli*. Appl. Biochem. Biotechnol. *39-40*, 301-322
7. Pirt, S.J. (1965) The Maintenance Energy of Bacteria in Growing Cultures. Proc. R. Soc. Ind., *163*, 224-231

BIOSYNTHETIC DEUTERATION OF THERMUS THERMOPHILUS

Inna V. Shcherbakova, Igor N. Serdyuk

Institute of Protein Research, RAS
142292 Pushchino, Moscow Region, Russia

INTRODUCTION

Thermus thermophilus appears to have considerable promise because its macromolecules are readily crystallized objects. For example, noticeable progress has been achieved in determining the atomic structure of individual ribosomal elements, such as ribosomal proteins. A considerable amount of research is devoted nowadays to locate these elements inside the ribosome.

Stable crystals of appropriate sizes of *Thermus thermophilus* ribosomes were obtained. Low and middle resolution diffraction patterns were collected. However, at present the problem of the determination of the three-dimensional structure of the 70S ribosome at a resolution of about 20Å is far from being solved. The achievements in crystallization of both the whole particle and its subparticles let the researchers cling to the hope that their structure could be determined easily using X-ray analysis. However, due to the difficulties encountered, especially the phase problem and large dimensions of elementary cells, many investigators concluded that decoding the three-dimensional structure of the integral ribosome at a high resolution is a task for the next century.

On the other hand with recent achievements in cryoelectron microscopy modern structural ribosomology approached a resolution of 15-20 Å. But construction of a high resolution three-dimensional model of the ribosome and an adequate structural description of the mechanism of protein synthesis are impossible without clear distinction between the protein and RNA molecules in the ribosomal structure. Both X-ray crystallography and electron microscopy do not suit well to make such distinction as the contrast between proteins and RNA is rather low. Contrast variation in neutron scattering is the method of choice allowing clear separation between the two main ribosomal components. The contrast variation study of fully protonated ribosome is usually not enough. It has significantly different matching points for RNA and protein, whereas the fully deuterated ribosome is essentially uniform for neutron It means that at every contrast we will have shape scattering. First part of our work was devoted to optimization of the conditions for *T.thermophilus* cultivation on fully deuterated medium.

The possibilities of neutron scattering experiments are enhanced by selective deuteration of main ribosomal components. The standard way for solving this problem has been to study hybrid isotopic particles obtained by reconstitution from protonated and deuterated components (Nierhaus, 1990). The main disadvantage is that this approach is time-consuming and expensive. Moreover, the procedure of reconstitution is well developed only for *E.coli* ribosomal particles, but not for the ribosomes from thermophilic and halophilic microorganisms.

Growing microbial cultures on media with different D_2O content suggests itself as a powerful way for solving the problem of deuterium incorporation. However it does not lead to a significant change in the relative contrast (ratio of of scattering amplitudes densities) of the RNA and proteins components (Moore, 1979). The only way of contrasting different components is the use of a combination of protonated and deuterated substrates during growth, rather than a monosubstrate (Moore, 1977).

The aim of second part of our study is to develop a general approach to the RNA nad protein labelling problem based on metabolic regulation. Applied to ribosomes, this approach could allow to obtain a set of ribosomal particles with different ratios of scattering amplitude densities of the RNA and protein components, suitable for neutron measurements in 95 – 100% D_2O, where the incoherent background is very low, and good quality data are obtainable to relatively large scattering vector values. Initial experiment were performed with MRE600 *Escherichia coli* but the study was extended to thermophilic bacteria cultivation.

MATERIALS AND METHODS

Strain

Strain HB8 *Thermus thermophilus* were adapted to fully deuterated medium in two–step manner. The adaptation steps are presented in the Table I.The cell culture was stored in the synthetic medium (Findling *et al.*, 1986) containing 40% glycerol at –70°C. The inoculum volume was usual no more than 5% of final cultivation volume.

Deuterated materials

Deuteration of inorganic components of the medium was achieved by means 2– or 3–fold evaporation after dissolving in D_2O. Deuterated glycerol and succinate were synthetized by Dr. Lenskikh (Institute of Protein Research, RAS). According the NMR measurements, the deuteration of the substrates was no less than 96%.

Fermentation

The fermentor ANK–210 (Russia) was used with a 10 liter vessel. Sterilization of the fully deuterated medium was achieved by filtration through a culture capsule filter with 0.2 μm pores. The fermentor was autoclaved at 110°C for 1 hour and dried by sterile air. The temperature of the fermentor was 75°C, the pH of about 7.5 was controlled automatically by titration of the medium. The rate of air flow and the pump rate for feeding medium was changed manually. The growth rate was monitored by absorbance measurements at 590 nm.
Batch cultivation involved growing up to the minimal amount of biomass (A_{590} = 1.5). It corresponds to the yield of about 2 grams of wet biomass per 1 liter of growth medium.
The biomass density was increased to relatively high values by the feeding into the fermentor of a concentrated solution of nutritional substrates upon the fed–batch cultivation. The composition of starting and feeding solutions is presented in the Table II. The fed–batch cultivation was followed by the continuous cultivation.

Table I. Adaptation of HB8 *T.thermophilus* to fully deuterated medium.

Step	% D_2O in growth medium	Carbon source	Maximum culture density A_{590}
I	75%	H–glycerol, H–succinate	2.5
II	98%	D–glycerol, D–succinate	1.7

Table II. Composition of starting and feeding medium for *T.thermophilus* fermentation.

Component	Concentration, per 1 liter of starting medium	Concentration, per 1 liter of feeding solution
$MgSO_4*7H_2O$	0.1 g	2 g
$CaCl_2*2H_2O$	5.8 mg	116 g
KCl	76 mg	760 g
Na_2SO_4	0.114 g	1 14 g
NaCl	0.53 g	5.3 g
NH_4Cl	0.51 g	15.8 g
Tris	4.84 g	43.4 g
$K_2HPO_4*3H_2O$	0.64 g	
KH_2PO_4	0.30 g	5 g
biotin	8 μg	160 μg
EGTA	15 mg	135 mg
$NaHCO_3$	0.42 g	4.2 g
Glycerol	5 g	112 g
Sodium succinate	5 g	28 g
$FeC_6H_5O_7$	1.1 mg	22 mg
$MnSO_4*H_2O$	1.6 mg	32 mg
$ZnSO_4*7H_2O$	0.56 mg	11.2 mg
$Na_2MoO_4*2H_2O$	28 μg	0.56 mg
$CoCl_2*6H_2O$	50 μg	1 mg
$CuSO_4*5H_2O$	0.25 mg	5 mg
Titrant	10% HCl	

Isolation of the ribosomes

The ribosomes of *T.thermophilus* were isolated according the slightly modified procedure, described by Gogiya *et al.*, 1986. The stages for removing lipid membranes were necessary. Tight–coupled ribosomes were isolated by means hydrophobic chromatography on Butyl–ToyoPearl 650S. The quality of the samples were estimated by sedimentation control.

Neutron scattering experiments

Two sets of neutron scattering data were obtained. The first one was obtained using D11 small–angle camera at the Laue–Langevin Institute (Grenoble, France). The second set was obtained at the small–angle camera of Risoe National Laboratory (Roskilde, Denmark).

Experiments on selective biosynthetic deuteration of different components of the ribosome.

Strain MRE 600 *Escherichia coli* was used in the initial experiments because it has a low level of RNase activity and sufficient adaptation to growvery well on a completely deuterated synthetic medium. Cultures were performed in medium M9. 1 g/l of NH_4Cl was used as a nitrogen source and 5 g/l of glycerol and succinate were used as carbon sources. The necessary amount of nucleosides was added to the medium with a

simultaneous two-fold decrease in the concentrations of glycerol and succinate when it was required to grow *E.coli* in a medium containing nucleosides. Vitamin B1 at a concentration of mg/l was added during growth. In the experiments on incorporation of labelled precursors of RNA and protein, the specific radioactivity of the medium was 1 μCi/ml. The radioactivity of total cellular RNA and protein was determining after fractionation.

To isolate *E.coli* ribosomes, the standard procedure described in (Spirin *et al.*, 1987) was used. Ribosomal RNA was isolated by deproteinization with phenol (Marmur, 1961) and ribosomal protein by deproteinization with acetic acid (Hardy *et al.*, 1969).

The percentage of deuteration was determined as a ratio of the integral intensity of ^{1}H-NMR spectra of a preparation with unknown incorporation of deuterium to the integral intensity of a completely protonated preparation. Protein and RNA preparations for NMR analysis were obtained as described in (Moore, 1979).

RESULTS AND DISCUSSIONS

Cultivation of *T.thermophilus* on the synthetic media

Fig.1 demonstrates the growth curves of *T.thermophilus* fermentation on fully protonated and fully deuterated mineral media. Under batch fermentation, the culture quickly reaches the stationary phase. Optical density of the culture measured at 590 nm was about 1.7. Rather low amount of the biomass was harvested (about 2 grams of wet biomass per 1 liter of the growth medium). The fed–batch cultivation was used to increase the yield of the biomass. The growth rate for protonated culture was about 0.6 hours^{-1}, for deuterated one – about 0.1 h^{-1}.We tried to maintain the growth rate at a high level to obtain highly active ribosomes in large amounts. In the case of a fully deuterated medium, the increase of the biomass density by more than 8 units A_{590} was followed by a decrease of the growth rate and growth inhibition. The fed–batch cultivation was followed by the cultivation in the continuous regime.

Isolation of the fully deuterated *T.thermophilus* ribosomes

The isolation technique for *T.thermophilus* ribosomes was well developed (Gogiya *et al.*, 1986). The hydrophobic chromatography of the ribosomes on Butyl–ToyoPearl is the excellent method for obtaining tight–coupled nonaggregating ribosomes. The Guinier plot of neutron scattering data obtained at Risoe National Laboratory of fully deuterated 70S in H_2O is presented in the Figure 2. Almost no aggregation was observed under the conditions of isolation. The sedimentation control shows the presence of the one component in the solution with sedimentation constant of about 70S.

Figure 3 demonstrates the dependence of $(I(0)/cTl)^{1/2}$ on the % D_2O in buffer for measurements. The intercept with the X–axis give the matching point of whole ribosome, which is about 120% D_2O.Thus, proposed procedure of the *T.thermophilus* cultivation brings into obtaining relatively large quantity of deuterated ribosome, homogeneous and nonaggregating.

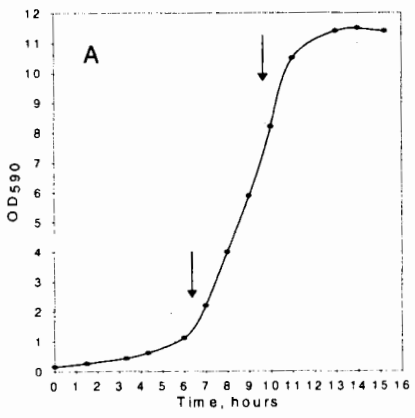

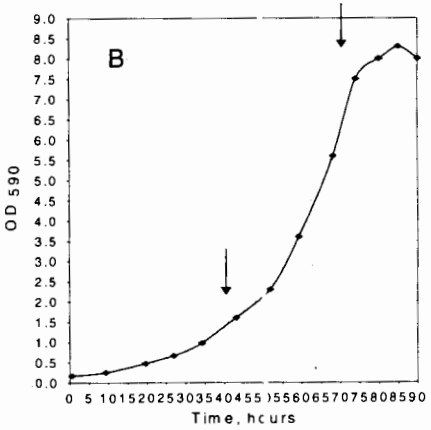

Figure 1. Growth curves of *T.thermohilus* cultivation on fully protonated (A) and fully deuterated (B) media with glycerol and succinate as carbon sources. Arrows indicate beginning of fed–batch and continuous cultivation.

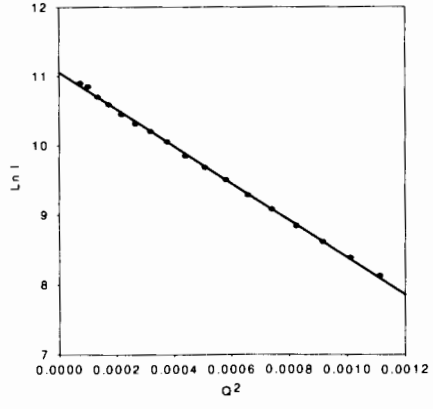

Figure 2. Guinier plot of neutron scattering intensities of the fully deuterated ribosomes.

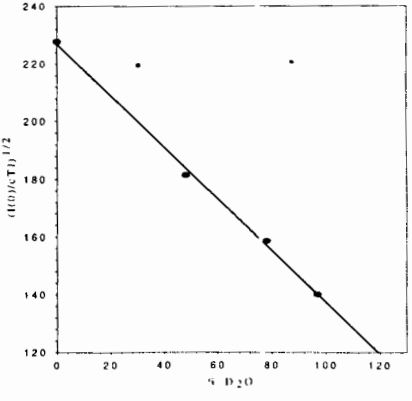

Figure 3. Match – point plot (I(0)/cTl *vs.* % D_2O in buffer) for fully deuterated ribosomes

Selective deuteration of different components of the *E.coli* ribosomes

Prokaryotic cells utilise costly substrates (from the point of view of intracellular energetics) as direct precursors of biopolymers. This avoids both the energetically disadvantageous stage of their breakdown into simpler substances and subsequent synthesis of monomers necessary for the cell. Substrates concentrations play a key role in growth. For example, a substrate in excess will be involved by the cell in different catabolic pathway transformations with simultaneous energy release.

Initially, we believed like Moore, that for specific labelling of the RNA and protein components it was sufficient to add labelled nucleosides and amino acids to the growth medium. However, it appeared that it is impossible to inhibit anabolic pathways leading from amino acids to nucleotides. Our first results showed that even at a chosen concentration of amino acids not involved directly in nucleotide synthesis, the lowest incorporation of [^{14}C]-amino acids into the RNA components is 15% as compared to their incorporation into the protein component of the cell. The percentage of incorporation into RNA increased with changes in the conditions of cultivation. It is therefore inappropriate to use a medium containing amino acids as substrates.

For the part of our work we have used strain MRE 600 *E. coli* for the first estimations because *E.coli* cultivation was much easier and it was widely believed that metabolic pathways are very similar for the two gram – negative species.

Initially we monitored the incorporation of ^{14}C-labeled nucleosides into different components of the cell as the function of D_2O content of the medium and protonated or deuterated glycerol and succinate. It was found that at a total concentration of nucleosides below 1 mM, incorporation of the label into the protein component was no more than 8% of that in the RNA component. In this low nucleoside substrate concentrations, incorporation into the protein component increased sharply at uridine concentrations higher than 0.5 mM, whereas an increase in purine concentration from 0.2 to 1 mM resulted in a slow linear increase in the incorporation into protein. In the nucleoside concentrations interval from 0.1 to 1.2 mM, incorporation into the protein component was less than 10% as compared with 100% incorporation into the RNA component. Figure 4 shows the kinetics of incorporation of the labelled carbon from adenosine into the RNA and protein components of the cell at nucleoside concentration 0.4 mM upon growing in heavy water and deuterated glycerol and succinate. However the deuteration of RNA in these conditions calculated from NMR spectra showed significant synthesis from usual carbon and nitrogen sources suggesting that at 0.4 mM the supplemented nucleoside concentration is too low.

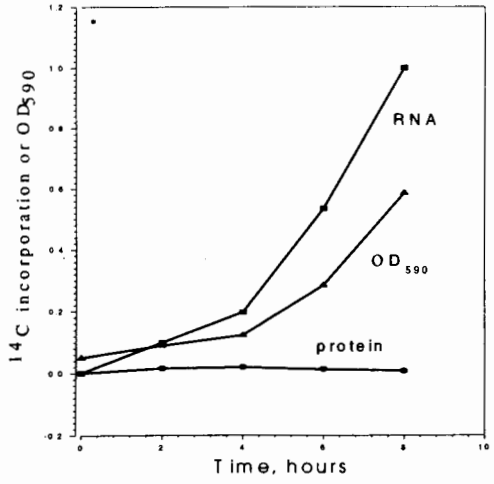

Figure 4. The kinetics of incorporation of the labelled carbon from adenosine into the RNA and protein components of the cell at nucleoside concentrations 0.4 mM upon growing in heavy water and deuterated substrates.

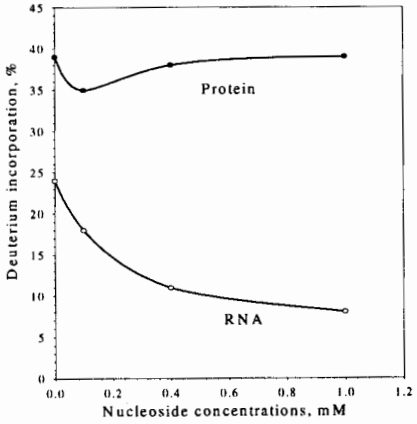

Figure 5. Incorporation of deuterium into different components of the ribosome at various nucleoside concentrations in growth media containing 65% D_2O, protoniated glycerol and succinate

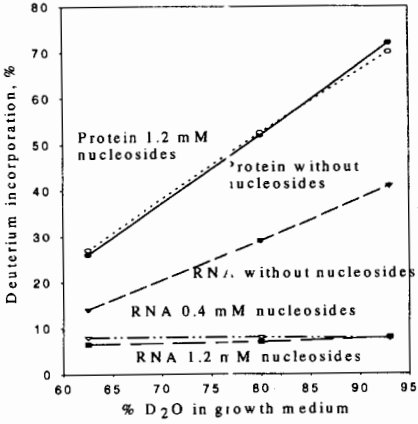

Figure 6. Incorporation of deuterium into different components of the ribosome when *E.coli* is grown in media containing percentage of D_2O and different nucleosides concentrations (0.4 mM and 1.2 mM). Protonated glycerol and succinate were used as carbon sources.

Figure 5 shows the incorporation of deuterium from water into different components of the ribosomeas a function of nucleoside concentration. It is seen that the extent of deuteration of the protein does not change essentially increasing from 35% to 38% with an increase in the total concentration of nucleosides from 0.16 mM to 1.2 mM. In parallel, deuteration of the RNA drops from 24% to 8%. These data were the basis for plotting the dependence of deuterium incorporation into the nonexchangeable part of the RNA and protein component of the ribosome on the percentage of deuterium in the growth medium for two various concentrations of nucleosides (0.4 mM and 1.2 mM) as compared with the medium free of nucleosides (Fig. 6). The plots show that at concentrations of nucleosides from 0.4 to 1.2 mM, they incorporate only into the RNA component of the ribosome while the protein is synthesised from standard substrates.

Table III lists four types of ribosomal particles characterised by different extents of contrast for neutrons as well as conditions for growing culture for their preparation.

We use low percentage of deuterium in growth media. Initially it was believed that it was possible to achieve an appreciable difference using only various combinations of H-and D-substrates. But it appeared that under those circumstances the extent of deuteration of the 'deuterated' component is insufficient and, consequently, it is not enough contrasted as compared to the protonated component. That is why it was decided to correct deuterium incorporation into the 'deuterated' component by low percentage of D_2O in the growth medium affecting minimally the protonated component. Experiments were done on determination of deuterium incorporation into the protein and RNA components of the cell in a system with adjusted concentration of nucleosides. The data obtained are given in Table IV.

It is shown that when growing bacteria in a medium containing low concentrations of heavy water, the protein is not practically deuterated in the case of H-substrates and is

highly deuterated when growing in 25% heavy water and D-substrates (the contrast-match point being 93% D_2O). Deuterium from D-substrates does not incorporate into the ribosomal RNA.

We hoped we could extend the approach to other microorganisms cultivation, namely to *T.thermophilus* cultivation. It is widely believed that the metabolic pathways of those microorganism are similar. However after *T.thermophilus* cultivation on the media presented in the Table III there was no pronounced selectivity in deuteration of ribosomal components (Table V).

For the third type of ribosome deuterium from deuterated carbon sources was incorporated into every component of the ribosome, but into RNA components to a greater extend. For the forth type of ribosome where the deuterated nucleotides were used the protein component was deuterated to a greater extend than the RNA one. So, metabolic pathways are likely to differ for the two species. The simplest evidence for the difference is that cultivation medium become more acidic upon *E.coli* fermentation, and it become more alkaline upon *T.thermophilus* fermentation when identical carbon and nitrogen sources are used.

Table III. Growth conditions for obtaining of the set of the ribosomal particles (ribosomes and their subunits) for neutron scattering experiments

Particle	Growth medium	Contribution in D_2O
I	H_2O, [^{1}H]glycerol, [^{1}H]succinate	RNA, protein
II	D_2O, [^{2}H]glycerol, [^{2}H]succinate	Shape scattering
III	25% D_2O, [^{2}H]glycerol, [^{2}H]succinate, [^{1}H]nucleosides	RNA
IV	25% D_2O, [^{1}H]glycerol, [^{1}H]succinate, [^{2}H]nucleosides	Protein

Table IV. Incorporation of deuterium into nonexchangeable positions of main ribosomal components

Growth media	Deuterium incorporation into proteins		Deuterium incorporation into RNAs	
	% from NMR studies	calculated match point	% from NMR studies	calculated match point
10% D_2O, [^{1}H]glycerol, [^{1}H]succinate, 1 mM [^{1}H]-nucleosides	2	42	0	70
25% D_2O, [^{1}H]glycerol, [^{1}H]succinate, 1 mM [^{1}H]-nucleosides	3	42	2	72
10% D_2O, [^{2}H]glycerol, [^{2}H]succinate, 1 mM [^{1}H]-nucleosides	47	82	1	71
25% D_2O, [^{2}H]glycerol, [^{2}H]succinate, 1 mM [^{1}H]-nucleosides	60	93	2	72

Table V. Deuteration of *T.thermophilus* ribosomal components upon cultivation on the nucleosides containing media. The extend of deuteration of protein component was obtained from NMR measurements (Moore, 1979). The extend of deuteration of RNA components was calculated from neutron scattering data (Fan *et al.*, 1997) obtained at the D11 instrument in ILL (Grenoble, France).

Particle type	Growth medium	Deuterium incorporation	
		into protein	into RNA
I	H_2O, [^{1}H]glycerol, [^{1}H]succinate	0%	0%
II	D_2O, [^{2}H]glycerol, [^{2}H]succinate	~96%	~96%
III	25% D_2O, [^{2}H]glycerol, [^{2}H]succinate, [^{1}H]nucleosides	17%	30%
IV	25% D_2O, [^{1}H]glycerol, [^{1}H]succinate, [^{2}H]nucleosides	24%	11%

CONCLUSIONS

1. Fermentation procedure for large-scale preparation of fully deuterated biomass of *T.thermophilus* is proposed.
2. The new approach for metabolic selective deuteration of *E.coli* ribosome without reconstitution stage was developed. For this purpose the combination of deuterated and protonated substrates in growth medium was used.
3. The approach is to be modified for *T.thermophilus* cultivation because of essential differences in metabolic pathways of the two microorganisms.

REFERENCES

Findling K.L., Yoshida T., Fee J.A., *J.Biol.Chem. 259*, 123-125 (1984)
Gogiya Z.V., Yusupov M.M., Spirina T.N., *Mol.Biologia (Russia) 20*, 519-526 (1986)
Hardy S.J.S., Kurland C.G., Voynov P., Mora G., *Biochemistry 8*, 2897-2899 (1969)
Marmur J., *J.Mol.Biol.3*, 208-218 (1961)
Moore P.B., *Anal.Biochem.82*, 101 (1977)
Moore P., *Methods Enzymol.49*, Part G, 639-655 (1979)
Nierhaus K.H., in *Ribosomes and Protein Synthesis*, IRL Press Oxford, 161-189 (1990)
Spirin A., Baranov V., Polubesov G., Serdyuk I., May R., *J.Mol.Biol.194*, 119-128 (1987)

CHOICE OF *E.COLI* HOST STRAINS FOR OVERPRODUCTION OF DEUTERATED PROTEINS

Oleg PALIY, Debra BLOOR, David BROCKWELL and Jill BARBER
School of Pharmacy and Pharmaceutical Sciences, University of Manchester,
Oxford Road, Manchester M13 9PL, UK

In the time since two-dimensional nuclear magnetic resonance (2D NMR) has been developed it has become an extremely valuable tool for studying the three-dimensional conformation of large proteins and their complexes with ligands. In order to study protein-effector interactions it is necessary in some cases to make protein deuterated prior to NMR studies. To achieve full deuteration of protein its overexpression in cells (usually bacterial, such as *Escherichia coli*) which are able to grow on deuterated media is needed. However, cells usually grow very slowly on such media and good expression levels of recombinant protein are hard to achieve [7].

Although during last twenty years many researchers have used *Escherichia coli* (*E.coli*) cells to produce deuterated components, few strains have been grown on deuterated medium. The most heavily used strains are MRE600 [1,2], MRE600D (created in our laboratory by adaptation of MRE600 strain to deuterated succinate medium) and MG1655 [3,4]. Among other *E.coli* strains that were used for deuteration studies are DL39 [3], XA90 [5] and AR120 [6].

In our studies we used *E.coli* strain MRE600D to produce a large amount of fully deuterated *E.coli* Elongation Factor Tu (EFTu). MRE600D strain was made by gradual adaptation of wild-type MRE600 strain to deuterated succinate medium [7]. We included two steps of cell cultivation on solid medium in order to achieve homogeneity and purity of culture. During our work with the MRE600D strain bearing recombinant plasmid we have discovered some other problems: i) low efficiency of cell recovery on deuterated succinate agar medium after transformation, ii) instability of plasmid DNA that led to reduced protein expression, iii) strain homogeneity must be maintained or expression level is reduced. Nevertheless, by maintaining homogeneity and high-sterile handling of cultures we have obtained an extremely high level of EFTu expression, up to 150mg/l compare to the usual level of 80mg/l. MRE600D is actually a deuteriophilic strain, preferring D_2O to H_2O. We have found it is very important to make sure that the selective agent (in this case ampicillin) remains in culture during cultivation. Slow growth rates on deuterated medium means that ampicillin is degraded (chemically and by β-lactamase) to a greater extent.

Considering the instability of expression level we checked the properties of the plasmid DNA from MRE600D cells and compared to the same plasmid isolated from *E.coli* strain JM109. For these studies we used the pJBDB02 plasmid (Fig.1) as well as pGEX-2T vector [Pharmacia]. For each plasmid these two strains were transformed with the same sample. Plasmid DNA from clones was isolated. The differences between undigested intact plasmid DNA from MRE600D and JM109 strains can be seen in Fig.2. Plasmid DNA from JM109 strain was as anticipated [8]. Fig.3 shows the comparative restriction analysis of the pJBDB02 plasmid isolated from the two strains. Three different enzymes were used: *EcoRI, HindIII* and *SmaI*. Again, the restriction pattern of plasmid from JM109 exactly corresponds to theoretically predicted whereas the same plasmid from MRE600D has extremely complex appearance. The most probable explanation of these interesting results is a high level

of plasmid rearrangements in MRE600D cells. This, in turn, can be a reason for instability of protein expression.

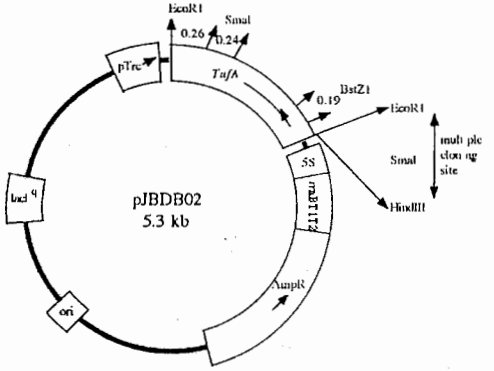

Fig.1. pJBDB02 plasmid map. pJBDB02 plasmid is a derivative o pTrc99A plasmid [Pharmacia] in which EFTu gene was inserted.

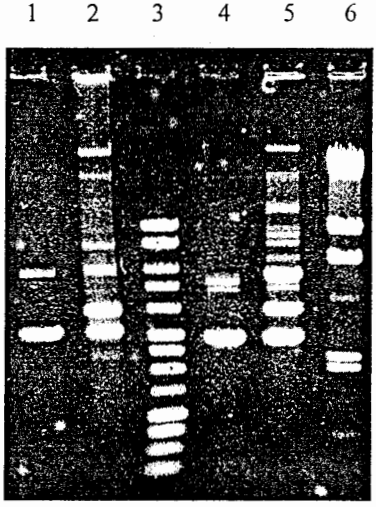

Fig.2. Influence of *E.coli* host strain on plasmid properties. 1 - JM109/pJBDB02 [*undigested*], 2 – MRE600D/pJBDB02 [*undigested*], 3 – 1kb DNA ladder, 4 – JM109/pGEX-2T [*undigested*], 5 – MRE600D/pGEX-2T [*undigested*], 6 – λ-DNA [*HindIII*].

Based on all these observations we decided to adapt two more *E.coli* strains along with MRE600. As alternative strains to wild-type MRE600 we chose JM109 and BLR[DE3] strains [Pharmacia]. Although they are disabled in terms of growth rate and tolerance of different conditions, they are extremely 'polite' to foreign DNA and allow overproduction of recombinant proteins. Both JM109 and BLR[DE3] strains have a recA$^-$ -genotype that prevent recombination and rearrangement of DNA. Besides which, both strains have mutations that confer resistance to nalidixic acid (gyrA96 mutation in JM109) and tetracycline (resistant gene in BLR transposon Tn10). This enables us to use these antibiotics as selective agents to prevent contamination of cultures.

Results of the first steps of this adaptation are presented in Fig.4. Unfortunately, BLR [DE3] strain was proved to be too disabled and did not grow on protiated succinate with 70% D_2O. As we predicted the growth rate of MRE600 was higher at every stage compared to JM109. Although JM109 grew fairly slowly and two subsequent cultivations were needed at every stage, it gradually became adapted to the new conditions.

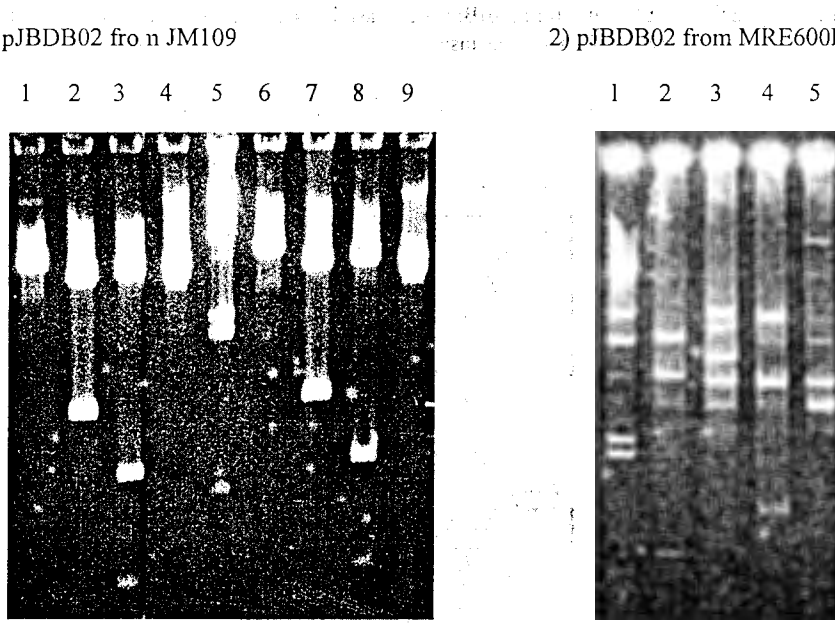

Fig.3. Restriction analysis of pJBDB02 plasmid from *E.coli* strains JM109 and MRE600D. 1st photo: 1,6 – pJBDB02 [*HindIII*], 2,7 - pJBDB02 [*EcoRI*], 3,8 - pJBDB02 [*SmaI*], 4,9 - pJBDB02 [*undigested*], 5 - λ-DNA [*HindIII*]. 2nd photo: 1 - λ-DNA [*HindIII*], 2 - pJBDB02 [*SmaI*], 3 - pJBDB02 [*HindIII*], 4 - pJBDB02 [*HindIII/EcoRI*], 5 - pJBDB02 [*undigested*].

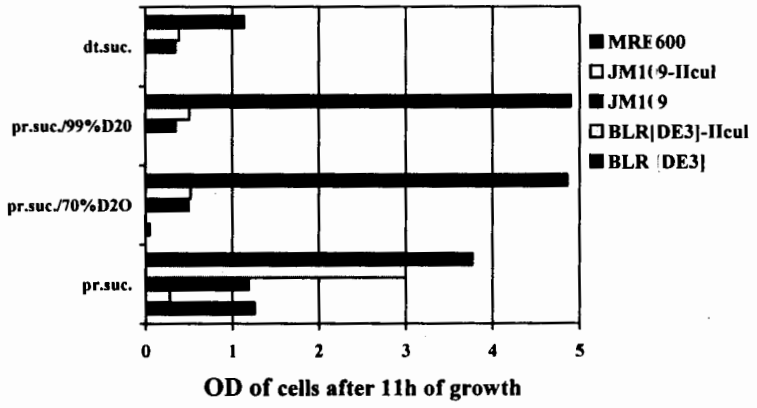

Fig.4. Adaptation of *E.coli* strains MRE600, JM109 and BLR[DE3] to deuterated succinate medium.

In conclusion:

E.coli MRE600D is very tolerant of deuterated media and gives levels of expression of perdeuterated protein comparable with those of protiated protein. However, it is unkind to plasmid DNA and this can result in poor expression. Pre iminary results suggest that it is feasible to prepare *E.coli* JM109D as an alternative host strain.

References:

[1] Moore, P.B. (1979) *Methods Enzymology* 59,639-653

[2] Nowotny, P., Nowotny, V., Voss, H. & Nierhaus, K.H. (988) *Methods Enzymology* 164, 131-145

[3] LeMaster, D.M. & Richards, F.M. (1988) *Biochemistry* 27, 142 150

[4] Derrick, J.P., Lian, L.-Y., Robrts, G.C.K. & Shaw, W.V. (199?) *Biochemistry* 31, 8191-8195

[5] Hsu, V.L. & Armitage, I.M. (1992) *Biochemistry* 31, 12778-127 84

[6] Gamble, T.R., Clauser, K.R. & A.A.Kossiakoff (1994) *Biophys Chemistry* 53, 15-26

[7] Bloor, D. (1992) *PhD thesis*, Manchester University, UK

[8] Johnson, P.H. & Grossman, L.I. (1977) *Biochemistry* 16, 4217-4224

Biological Structure Research with Spin Contrast Variation

R. Willumeit[1], N. Burkhardt[1], G. Diedrich[2], S. Forthmann[1], K.H. Nierhaus[2], H.B. Stuhrmann[1]
[1]GKSS Research Centre Geesthacht, Max-Planck-Str., 21502 Geesthacht, Germany
[2]MPI for Molecular Genetics, Ihnestr., 14195 Berlin, Germany

Abstract
Using sophisticated techniques for deuterating molecules, regions of interest in macromolecules can be labelled by isotopic substitution. In most cases the resulting contrast is sufficient to gain information about the structure. However, with very small labels or weakly contrasted molecules such as small proteins or RNA molecules in the 70S ribosome, the contrast generated by isotopic substitution is not high enough to allow characterisation of the *in situ* structure.
Help has come from the method of spin contrast variation. This method also relies on isotopic substitution, but, in addition takes into account the difference in the neutron scattering length arising from the dependence on the polarisation of the neutron and nuclear spins in the sample.
In recent years the spin contrast variation method has been used successfully to determine several structural features of the *E.coli* ribosome which will be discussed in this paper.

Introduction

Protein synthesis is one of the fundamental processes of life. Therefore ribosomes, which are the sites for the protein synthesis in each cell, are of great interest.
For a better understanding it is necessary to obtain the structure of the ribosome. One possible method is small angle neutron scattering (SANS). SANS combined with isotopic substitution and label triangulation led to a map of the positions of the proteins of the 30S subunit [1]. Seven proteins of the 50S subunit were also localised [2]. The next step towards biological structure investigations was nuclear polarisation dependent SANS, a method which was developed over the last few years.
First results of polarisation dependent SANS were obtained for the localisation of the proteins L3 (22.3 kDa) and L4 (22.1 kDa) in the 50S subunit (1.4 million Da) of the *E.coli* ribosome [3]. As markers inside the 70S ribosome (2.4 million Da) the proteins S6 (15.7 kDa) and S10 (11.7 kDa) were localised to determine distance changes in further investigations [4]. The most challenging task was undertaken when the *in situ* structure of tRNA and mRNA molecules was analysed [5-8].
The mapping of the protein positions of the 50S subunit of the *E.coli* ribosome was improved by two positions (proteins L1, 24.6 kDa and L2, 29.7 kDa) and preliminary results of the localisation of the proteins L14 (13.5 kDa) and L24 (11.2 kDa). Samples of five other proteins (L5 (20.2 kDa), L16 (15.3 kDa), L18 (12.8 kDa), L25 (10.7 kDa) and L35) are under processing. The aim will be a complete map of the large ribosomal subunit.

Method

Omitting magnetic scattering, the interaction of neutrons with matter arises from the interaction between incident neutron and the nucleus. The strength of this interaction is expressed by the scattering length. A pronounced change in the scattering lengths is found for the two isotopes of hydrogen. For ^1H (protons) the scattering length equals -0.374×10^{-12} cm, while it is $+0.667 \times 10^{-12}$ cm for ^2H (deuterons). If the spins of the neutrons and ^1H are parallel, the scattering length is equal to +1.08, in the antiparallel case it is equal to -1.83 (in

10^{-12} cm). The other nuclei which are present in a biological sample show very little change in the scattering length with spin polarisation [9].
^1H has a large incoherent scattering cross section of 79.9 barn, which is much smaller using ^2H (2 barn). Samples are therefore largely deuterated. For ribosomes, this means that only a small part of the ribosome remains protonated (e.g. the protein S6 in the deuterated 70S ribosome).
For experiments using nuclear spin contrast variation, an instrument for polarised neutron scattering, which is the small angle facility SANS1 and a special sample environment are required. The main parts of the SANS1 target station are a 2.5 Tesla electromagnet and a $^3He/^4He$ dilution refrigerator originally designed for high energy physics experiments by CERN, Geneva. Inside the sample cell temperatures of 130-150 mK can be reached [10].
To gain high nuclear spin polarisation in a short time the nuclear spins are polarised dynamically (Dynamic Nuclear Polarisation, DNP [11]). This technique requires that the sample is doped with paramagnetic centres (EHBA-Cr(V)) and the irradiation of microwaves. Although all nuclei with spin are affected by DNP, only the polarisation of ^1H and ^2H is significantly changed. The polarisation is determined by measuring the nuclear magnetic resonance (NMR) absorption signal. Since the data treatment is simplified if only one isotope has been polarised, the same NMR system is used to destroy any unwanted polarisation from the other isotope. Thus only ^1H spins (proton spin target) or only ^2H spins (deuteron spin target) are kept polarised in the sample during the measurements.

Data collection and data treatment

The measurements of the samples were performed over a week at three different detector-sample-distances (0.7 m, 1.8 m and 4.5 m). The samples were measured with unpolarised nuclear spins and polarised proton spins (proton spin target). The data were accrued up with respect to the detector-sample-distance, the polarisation of the sample and the neutron spin flipper state [8]. From the two dimensional scattering pattern after subtraction of solvent and incoherent scattering the three basic scattering functions [11] were derived. The data sets were corrected for the influence of wavelength distribution and collimation.
To determine the position of a label with respect to the ribosome the data analysis starts from an electron microscopy model [12, 13]. The calculated scattering curves obtained from the model are fitted to the measured data. The best least squares fit should give the position of the label. In this fit the parameter R

$$R = \sqrt{\frac{1}{N}\sum_{i=1}^{N}\left(\frac{I_{measured,i} - I_{calculated,i}}{\sigma_i}\right)^2}$$

is minimised for 38 intervals of Q in $0.015 < Q < 0.2$ and for all basic scattering functions.

Results and discussion

Localisation of proteins L1 and L2 in the 50S subunit of the E.coli ribosome

The nuclear spins of ^1H were in both cases polarised by DNP up to 66%. The polarisation decreased about 1 % per day during the measurements.
In the case of the protein L1 beside the 'proton spin target' also the 'deuteron spin target' was measured. Following the data analysis procedure described above the following positions were obtained for the proteins L1 and L2:

D50S(L1): The distance from the ribosomal centre of mass is measured to be $d = 115 \pm 3$ Å. The co-ordinates of the protein position are (x/y/z) = -104 ± 1 Å / 48 ± 4 Å / 18 ± 2 Å. This corresponds well with the result of immuno electron microscopy [14]. The determined radius of gyration is R_g = 23 ± 1 Å. The additional analysis of the deuteron spin target shifts the co-ordinates slightly within the error bar: (x/y/z) = -105 ± 1 Å / 50 ± 5 Å / 19 ± 3 Å. The solution found is a unique determination of the position as seen in figure 2 which shows a map of R-values with respect of the best fit solution.

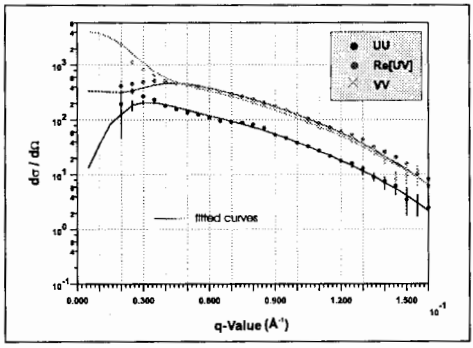

Figure 1: Basic scattering functions for the localisation of protein L1.

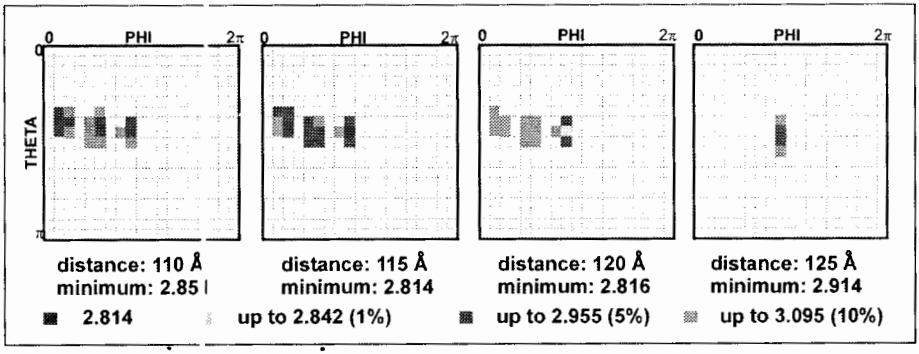

Figure 2: Minimum map for the position of protein L1.
Indicated are the R-values for the best fit (2.814) and R-values up to 10% higher than the best R-value. Even though three areas with reasonable small R-values show up only one definite minimum (distance 115 Å) can be found.

D50S(L2): The distance from the ribosomal centre of mass is measured to be $d = 57 \pm 5$ Å. The co-ordinates of the protein position are (x/y/z) = -48 ± 4 Å / 20 ± 2 Å / 24 ± 3 Å. This corresponds well with the result of immuno electron microscopy which obtained d = 56.7 Å and (x/y/z) = -53 Å / 17Å / 2 Å [14]. The determined radius of gyration is R_g = 21 ± 2 Å. The inter-protein distance d(L1-L2) = 63 ± 8 Å for the protein positions obtained by nuclear spin contrast variation and it is d(L1-L2) = 75 Å determined by [15].

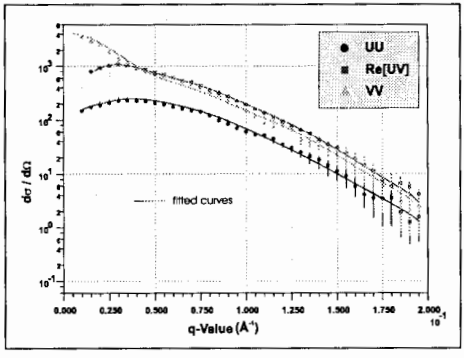

Figure 3: Basic scattering functions for the protein position of L2.

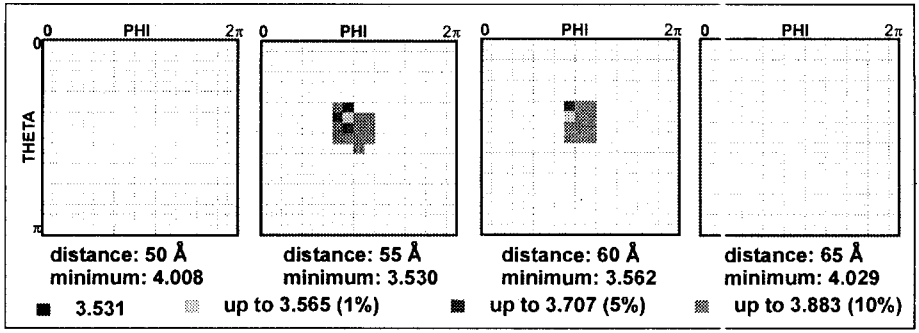

Figure 4: Minimum map for the position of protein L2.
Indicated are the R-values for the best fit (3.531) and R-values up to 10% higher than the best R-value. It is clearly seen that even for 10% deviation still only one position shows up.

Preliminary results for the localisation of proteins L14 and L24 in the 50S subunit of the E.coli ribosome

For the two proteins L14 and L24 so far two possible positions were calculated but the solution is not unique. Further data treatment will be necessary to present a final solution.

Still the present obtained results are within the limits of expectation: The preliminary position of L14 is close to the position which was determined by immuno electron microscopy [14]. Its distance to the centre of mass of the ribosome is in first approximation 56 ± 10 Å while its radius of gyration is determined to be $R_g = 17 \pm 1$ Å.

L24 is assumed to be found in a region where no other protein was located by immuno electron microscopy. The distance from the ribosomal centre of mass is measured to be $d = 45 \pm 4$ Å. The determined radius of gyration is $R_g = 22 \pm 2$ Å. Compared to the radius of gyration of 12 Å for a spherical particle with the mass of L24 (11.2 kDa) we conclude that L24 must be very elongated. This property was not taken into account for the here presented data treatment. Since this protein was not detected with other methods up to now, spin contrast variation will contribute the first information about the *in situ* structure of this protein. A more detailed discussion of the analysis of the protein data for L14 and L24 will be given elsewhere.

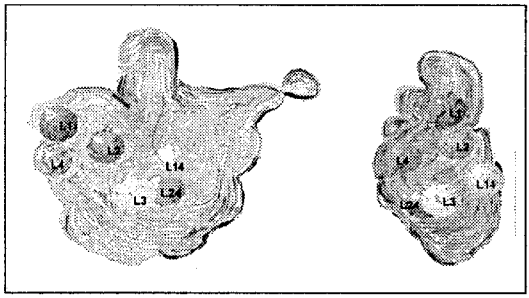

Figure 5: Protein positions in the 50S subunit of the *E.coli* ribosome.
The size of the spheres is not in scale. The positions for the proteins L14 and L24 are suggestions since the data treatment is still in progress. In the background the shape of the 50S subunit based on data from electron microscopy [12] is seen.

Conclusion

The method of spin contrast variation was successfully used to localise further protein positions in the 50S subunit of the *E.coli* bacteria. Thus the mapping of the 50S subunit now includes the positions for the proteins L1, L2, L3 and L4 while preliminary co-ordinates for the positions of L14 and L24 are suggested. To improve the data analysis in further investigations the shape of the proteins will also be taken into account.

Acknowledgements

A complicated experiment such as spin dependent neutron scattering of highly complex biological samples can only be achieved with the co-operation of many people. Therefore we would like to thank everyone who was involved, especially W. Müller (GKSS, Geesthacht).

Literature

[1] Capel, M.S., Engelman, D.M., Freeborn, B.R., Kjieldgaard, M., Langer, J.A., Ramakrishnan, V., Schindler, D.G., Schneider, D.K., Schoenborn, B.P., Sillers, I.Y. & Moore, P.B. (1987) Science Vol. 238, 1403-1406.

[2] May, R.P., Nowotny, V., Nowotny, P., Voss, H. & Nierhaus, K.H. (1992). EMBO J. 11, 373-378.

[3] J. Zhao and H.B. Stuhrmann (1993) J. de Physique I 3, 233 - 236.

[4] R. Willumeit, M. Schmitt, N. Burkhardt, R. Jünemann, J. Wadzack, K.H. Nierhaus, H.B. Stuhrmann (1997) Physica B 234, 202 - 204.

[5] J. Wadzack, N. Burkhardt, R. Jünemann, G. Diedrich, K.H. Nierhaus, J. Frank, P. Penczek, W. Meerwinck, M. Schmitt, R. Willumeit, H.B. Stuhrmann (1997) J. Mol. Biol. 266, 343-356.

[6] Knud H. Nierhaus, Heinrich B. Stuhrmann and Dmitri Svergun (1998) Prog. Nucl. Acid Res. Mol. Biol. 59, 177-204.

[7] Knud H. Nierhaus, Jörg Wadzack, Nils Burkhardt, Ralf Jünemann, Wolf Meerwinck, Regine Willumeit and Heinrich B. Stuhrmann (1998) PNAS 95, 945-950.

[8] R. Willumeit, N. Burkhardt, J.Wadzack, K. H. Nierhaus, H. B. Stuhrmann (1997) J. Appl. Cryst. 30, 1125-1131.

[9] Knop, W., Hirai, M., Olah, G., Meerwinck, W., Schink, H.J., Stuhrmann, H.B., Wagner, R., Wenkow-EsSouni, M., Zhao, J., Schärpf, O., Crichton, R.R., Krumpolc, M., Nierhaus, K H., Niinikoski, T.O. & Rijllart, A. (1991). Physica B 174, 275-290.

[10] J. Zhao, W. Meerwinck, T. Niinikoski, A. Rijllart, M. Schmitt, R. Willumeit, H. B. Stuhrmann (1995) Nucl. Instr. Meth. A 356, 133-137.

[11] Abragam, A & Goldman, M. (1982). Nuclear Magnetism, Order and Disorder, Oxford: Clarendon Press.

[12] Wagenknecht, T., Grassucci, R. & Frank, J. (1988). J. Mol. Biol. 199, 137-147.

[13] Frank, J., Penczek, P., Grassucci, R. & Srivastava, S. (1991). J. Cell Biology 115, 597-605.

[14] Stöffler-Meilicke, M. & Stöffler, G. (1990). The Ribosome Structure, Function and Evolution, edited by Hill, W.E., Dahlberg, A., Garrett, R.A., Moore, P.B., Schlessinger, D. & Warner, J.R., Washington D.C.: American Society for Microbiology, 123-133.

[15] Walleczek, J., Schüler, D., Stöffler-Meilicke, M., Brimacombe, R., Stöffler, G. (1988). EMBO J. vol. 7, no. 11, 3571-3576.

STRUCTURAL MODEL OF THE 30S SUBUNIT OF RIBOSOMES *THERMUS THERMOPHILUS* FROM SOLUTION SCATTERING

Fan Lixin [1], Aksenov V. L.[1], Algalarov C. Ch.[2], Gilles R.[3], Koch M.[4], May R.[5], Selivanova O. M.[2], Serdyuk I. N.[1,2], Shcherbakova I.V[2]., Svergun D. I[4,6], Volkov V. V.[6], Wiedenmann A.[3]

[1] *Frank Laboratory of Neutron Physics, Joint Institute for Nuclear Research, 141980 Dubna, Moscow Region, Russia*
[2] *Institute of Protein Research, Russian Academy of Sciences 142292 Pushchino, Moscow region, Russia*
[3] *Berlin Neutron Scattering Center, Glienicker Str.100, D-14109 Berlin-Wannsee, Germany*
[4] *EMBL, Hamburg Outstation, NotkestraЯe 85, D-22603 Hamburg, Germany*
[5] *Institute Laue - Langevin, Grenoble, France*
[6] *Institute of Crystallography, Russian Academy of Sciences, Leninsky pr. 59, 117333 Moscow, Russia*

Summary

The method of spherical harmonics was applied for studying the 30S ribosomal subunit from *Thermus thermophilus* in solution using neutron contrast variation. A two-phase structural model of the 30S ribosomal subunit from *Thermus thermophilus* with the resolution 35Å was built from the envelope functions of the 30S and its RNA -rich core. The initial approximation for the envelopes of the 30S ribosomal subunit from *Thermus thermophilus* was taken from two-phase model of the 30S E.coli. A comparison of the 30S *Thermus thermophilus* and 30S E.coli models shows that primary difference between them consists in the special distributions of the protein component whereas the special distributions of the RNA component coincide completely in both models.

Introduction

Construction of a high resolution three-dimensional model of the ribosome and an adequate structural description of the mechanism of protein synthesis are impossible without clear distinction between the protein and RNA molecules in the ribosomal structure. With recent achievements in cryoelectron microscopy and X ray crystallography, modern structural ribosomology approached a resolution of 15-20 Å [Frank et al.,1995; Stark et al.,1995; Schluzen et al.,1995]. However, both X-ray crystallography and electron microscopy do not suite well to make such distinction, since in this case the contrast between RNA and the protein is rather low. Contrast variation in neutron scattering is the method of choice allowing clear separation between the two main ribosomal components and its possibilities are enhanced by their selective deuteration. Recently a direct method of small angle scattering data interpretation using spherical harmonics was developed [Svergun 1993; Svergun et al., 1996]. The application of this method to the 50S [Svergun et al., 1994.a,b] and 70S *E.coli* ribosomes [Svergun et al., 1997.a,b] allowed to construct reliable spatial models of these particles and their

RNA moieties at a resolution 30-35 Å. The main advantage of this method consists in the possibility to directly visualise the position of RNA in the ribosome without using *a priori* information.

Until the recent time these models have been mainly constructed for *E.coli*. However, most current structural research is performed on ribosomes from the heat-loving bacterium T. thermophilus for following reasons. First, ribosomal particles from this bacterium and their components are much more stable and crystallize more readily and second, the structure of a number of its protein have already been elucidated at the atomic level[Liljas and Garber,1995; Liljas and Garber, 1995; Ramakrishnan et al; 1995]. The main goal of this work is to use new method of data analysis and to apply them to obtain a low resolution model of the 30S subunits of the *Thermus thermophilus* ribosomes, which in the near future can serve as a basis for localisation of some ribosome proteins in this subunit.

Materials and Methods

Preparation of ribosomes

The cells of T. thermophilus were grown in synthetic medium containing glycerol and succinate as a carbon source according to protocol [Fan et al.,1997]. Two types of ribosomal particles were obtained. The first type, protonated particle, was grown on a medium containing H_2O, H- glycerol and H- succinate. The second type, deuterated particle, was grown on a medium containing 98% D_2O, D- glycerol and D- succinate.

The ribosomes were isolated from the *T. thermophilus* biomass immediately after the yield. The washed biomass was ground with a double amount of aluminum oxide at gradual addition of 2 vol. of the buffer 150/500 (50 mM Tris HCl, pH 7.5, 150 mM $MgCl_2$, 500 mM NH_4Cl, 0.1 mM EDTA, 1 mM DTT). Phenylmethylsulfonylfluoride (20 mg/l) dissolved in acetone, and DNase (0.1 mg/l) were added to the obtained suspension, and incubated for 30 min at 4°C. Aluminum oxide and cell debris were removed by centrifugation at 14000 rpm for 40 min in a JA-14 rotor. The supernatant was gathered and the ribosomes were precipitated by centrifugation for 3 h at 50000 rpm in a Ti60 rotor. The sediments of the ribosomes were suspended in the buffer 150/500 and clarified at 20000 g for 30 min.

The ribosomes were purified by centrifugation through the CsCl-sucrose cushion[Gogia et al., 1986). The ribosomes (30ml) were laminated to the cushion (7 ml), containing 20 mM Tris HCl, pH 7.5, 1.8 M sucrose, 0.8 M CsCl, 0.15 M $MgCl_2$, 0.1 mM EDTA, 5 mM 2-mercaptoethanol in the test-tubes of the SW28 rotor. They were centrifuged at 25000 rpm for 20 h. The cushion below the dyed zone of the membranes was extracted by the capillary and dialysed against the buffer 50/150 (20 mM Tris HCl, pH 7.5, 50 mM $MgCl_2$, 150 mM NH_4Cl, 0.1 mM EDTA, 1 mM DTT).

The fractions containing 70S ribosomes were pooled, concentrated and dialysed against the buffer 1/300 (20mM tris-HCl pH 7.5,1 mM $MgCl_2$, 300 mM NH_4Cl, 0.1 mM EDTA, 1 mM DTT). The quality of the obtained preparations was evaluated by analytical centrifugation.

Separation of 30S subunits

The 30S ribosomal subunits were separated by centrifugation in the sucrose gradient (SW-28, 25000 rpm, 20 h). Factions of the 30S subunits were pooled and

dialysed against the buffer 50/150, and then dry ammonium sulphate was added up to 1.5 M. The preparations were concentrated by the hydrophobic chromatography with the Buty-ToyoPearl 650M column of small volume. The ribosomal subunits were eluted by the buffer 50/150.

Preparation of samples for neutron scattering

Before measurements the preparations were dialysed against a buffer containing 20 mM Tris-HCl (pH 7.6), 0.5 mM $MgCl_2$, 100 mM KCl. Buffers containing 0, 20, 35, 40, 80, 98% D_2O were used for contrast variation. The sample with the highest D_2O concentration was prepared by dialysis. The D_2O content was controlled by density and transmission measurements.

Scattering experiments and data treatment

Neutron scattering measurements were carried out with three SANA facilities: "YUMO" (JINR, Dubna), "V4"(HMI, Berlin) and "D11"(ILL, Grenoble). Two series of neutron scattering data for first type of ribosomal particles ((H)-30S) were obtained using the V4 small angle spectrometer [Keiderling *et al.*, 1992]. The mechanical velocity selector giving a wavelength distribution with full-width-half-maximum $\Delta\lambda/\lambda$=0.105 filters out neutrons with a wavelength of 8.0 Å and 6.02 Å for the first and second series, respectively. The samples were measured in buffers containing 0, 20, 40, 98% D_2O and 0,35, 80, 98% D_2O at four sample-detector distances(8 m, 4 m, 2 m, 1.16 m) for first and second series, respectively. The concentrations of preparates were 18.5, 23.2, 24.9, 15.0 mg/ml in H_2O, 20, 40, 98% D_2O for the first series and 34.1, 36.9, 37.8, 33.0 mg/ml in H_2O, 35, 80 and 98% D_2O buffer for the second series, respectively. The total range of momentum transfer extends from 0.0068 to 0.18 $Å^{-1}$. The third seri of neutron scattering data for two types of ribosomal particles ((H)-30S and (D)-30S) was obtained using the D11 small angle spectrometer [Ibel, 1976; Lindner et al., 1992].Three experimental settings were used with sample-detector distances of 10m, 3.6m and 1.2m at the average wavelength of 6.0 Å and $\Delta\lambda/\lambda$=0.09. The total range of momentum transfer extends from 0.0075 to 0.20 $Å^{-1}$. The first type of ribosomal particle was measuremented at four contrasts ((H_2O, 32%, 72% и 98% D_2O) and high concentrations (17,1; 7,7; 15,7 и 14,8 mg/ml) and low concentrations (1,3; 0,3; 1,72 и 1,12 mg/ml). The second type of ribosomal particle was measuremented at one contrast (H_2O) and two concentrations (29,6 and 1,59 mg/ml). All measurements were done at 10°C. The fourth seri of neutron scattering data for first types of ribosomal particles was obtained using the YUMO small angle spectrometer[Ostanevich, 1988]. The sample-detector distance was 10.52m. The range of momentum transfer was 0.007 - 0.12 $Å^{-1}$. The first type of ribosomal particle was measuremented at four contrasts (H_2O, 35%, 80% и 98% D_2O) and low concentrations (~4mg/ml).

The synchrotron radiation X-ray scattering data were collected following standard procedures using the X33 camera [Koch & Bordas, 1983; Boulin *et al.*, 1986, 1988] of the EMBL on the storage ring DORIS III of the Deutsches Elektronen Synchrotron (DESY) and multiwire proportional chambers with delay line readout [Gabriel & Dauvergne, 1982]. At the sample-detector distance of 4.2 m and the wavelength λ=0.15 nm, the range of momentum transfer is $0.08 < s < 1.5$ nm^{-1}. Samples with concentrations of 4-20 mg/ml were used. The data were normalised to the intensity of the incident beam, corrected for the detector response, the scattering of the buffer was

subtracted and the difference curves were scaled for concentration. All procedures involve statistical errors propagation using the program SAPOKO [Svergun & Koch, unpublished].

The maximum diameter of the 30S subunit was estimated from the X-ray scattering curve using the orthogonal expansion program ORTOGNOM [Svergun, 1993]. The values of the forward scattering and the radii of gyration for individual scattering curves were evaluated using the Guinier approximation [Feigin & Svergun, 1987] and also by the indirect transform program GNOM [Svergun *et al.*, 1988; Svergun, 1992]. GNOM was also used to refine the merging coefficients between the neutron data sets recorded for the same particle with different smearing conditions [Svergun, 1991].

SAS invariants as functions of contrast

The solution scattering intensity I(s) from a particle with a scattering length density distribution $\rho(\mathbf{r})$ in a solvent of average scattering density ρ_s is the square of the Fourier transform of the excess scattering length density $\rho(\mathbf{r})$ - ρ_s averaged over all particle orientations. The particle contrast is

$$\overline{\Delta\rho} = \int [\rho(\mathbf{r}) - \rho_s] \, dV = \overline{\rho} - \rho_s V \qquad (1)$$

where integration is performed over the excluded volume V of the particle. The forward scattering I(0) is proportional to $(\overline{\Delta\rho}\ V)^2$ and the contrast dependence of $\sqrt{I(0)}$ should be a straight line crossing the abscissa at the matching point, where the average particle density is equal to that of the solvent [Stuhrmann & Kirste, 1965].

The radius of gyration of the particle as a function of contrast is written as

$$R_g^2(\overline{\Delta\rho}) = R_c^2 + \alpha/\overline{\Delta\rho} - \beta/\overline{\Delta\rho}^2 \qquad (2)$$

where R_c is the radius of gyration at infinite contrast, and the constants α and β are defined by [Ibel & Stuhrmann, 1975]. As the 30S subunit consists of two distinct components, RNA and protein moieties, its radius of gyration can also be expressed in terms of their radii of gyration, R_{pro} and R_{rna} as

$$R_g^2(\overline{\Delta\rho}) = x_1 R_{pro}^2 + (1-x_1)R_{rna}^2 + x_1(1-x_1)L^2 \qquad (3)$$

where $x_1 = \overline{\Delta\rho}_{pro} v_1 / (\overline{\Delta\rho}_{pro} v_1 + \overline{\Delta\rho}_{rna}(1 - v_1))$, v_1 is the volume fraction of the protein moiety, $\overline{\Delta\rho}_{pro}$ and $\overline{\Delta\rho}_{rna}$ are the contrasts of the two components, and L is the distance between their centres of mass [Serdyuk, 1979].

Scattering from the model of the 30S subunit

As the 30S ribosomal subunit is a two-component particle containing ribosomal RNA and 19 proteins its scattering intensity from this particle can be written as[Koch&Stuhrmann 1979; Serdyuk,1979; Tardieu & Vachette, 1982]

$$I(s) = \Delta\rho_{rna}^2 I_{rna}(s) + \Delta\rho_{pro}^2 I_{pro}(s) + \Delta\rho_{rna}\Delta\rho_{pro} I_{cross}(s) \qquad (4)$$

where $\Delta\rho_{PRO}$ and $\Delta\rho_{rna}$, $I_{rna}(s)$ and $I_{pro}(s)$ are the contrasts and the scattering intensities of the RNA and protein moieties, respectively, and $I_{cross}(s)$ is a cross term. The scattering amplitude of the protein moiety is represented by a difference between that of the entire subunit and of its rRNA. The contrasts of the ribosomal components (Table 1) are evaluated from their chemical compositions as described in paper [Svergun *et al.*, 1997a]. The contrast of the entire hydrated subunit is calculated using the volume fractions of the components as $\overline{\Delta\rho}_{30S} = v_1\,\overline{\Delta\rho}_{pro} + (1\text{-}v_1)\,\overline{\Delta\rho}_{rna}$, where the volume fraction of hydrated protein is 0.31.

At a low resolution the structure of 30S subunit can be presented using a two-phase model described by the outer and inner envelope functions representing the entire subunit and its RNA moiety, respectively

Each envelope functions can be described by the angular function $F(\omega)$ which is parametrized using the multipole expansion:

$$F(\omega) \approx \sum_{l=0}^{L} \sum_{m=-l}^{l} f_{lm}\, Y_{lm}(\omega) \qquad (5)$$

where the truncation value L describes the resolution: $(5/3)^{1/2}\,\pi R_g/(L+1)$ and number of independent parameters of model: $(L+1)^2$-6, f_{lm} are complex numbers, $Y_{lm}(\omega)$ - spherical harmonics and (r, ω) are spherical coordinates[Stuhrmann,1970].. The scattering amplitudes of the ribosomal component is expressed as

$$A(s) = \sum_{l=0}^{\infty} \sum_{m=-l}^{l} A_{lm}(s)\, Y_{lm}(\omega) \qquad (6)$$

where the partial amplitudes $A_{lm}(s)$ are a non-linear combination of the coefficients f_{lm}

Then the scattering intensity from a two-phase model for the given contrasts can been whiten as[Stuhrmann,1970; Harrison,1969]

$$I(s,\Delta\rho) = \sum_{l=0}^{\infty} \sum_{m=-l}^{l} \left[A_{lm}^{total}(s)\right]^2 \qquad (7)$$

where $A_{lm}^{total}(s) = \Delta\rho_{pro} A_{lm}^{30S}(s) + (\Delta\rho_{rna} - \Delta\rho_{pro}) A_{lm}^{rna}(s)$

The parameters describing the structures of the components can be determined so as to minimize the overall discrepancy

$$R_I^2 = \frac{1}{M}\sum_{i=1}^{M} R_{Ik}^2 = \frac{1}{M}\sum_{k=1}^{M} \frac{\sum_j \left[(I_{exp}^{(k)}(s_j) - I_{calc}^{(k)}(s_j))/\sigma(s_j) \right]^2}{\sum_j \left[I_{exp}^{(k)}(s_j)/\sigma(s_j) \right]^2} \quad (8)$$

where M is the total number of curves, $I_{exp}^{(k)}(s_j)$ and $\sigma(s_j)$ are measured scattering intensity and its standard deviation, respectively, in the j-th experimental point of the k-th curve, $I_{calc}^{(k)}(s_j)$ is the corresponding scattering from the model evaluated using equation(7) for contrasts of the components corresponding to the k-th curve.

A program MONSTER was used to perform a non-linear search of the multipole coefficients describing the two shapes. The detail of this program can be found in [Svergun et al.1997b; Svergun,1991, 1994,1997].

Results and Discussion

Figure 1 represents the normalized forward scattering as a function of the D_2O concentration in the solvent for the 30S samples measured at HMI and ILL which yields the matching point of 59% D_2O in good agreement with the results for *E.coli* reported earlier [Serdyuk *et al.*, 1979]. The molecular mass of the 30S subunit calculated using the scattering of water as a standard for the abslute calibration [Koch & Stuhrmann, 1979] is equal to 860 kDa which agrees with the value 850 kDa predicted from the chemical composition [Agalazov, unpublished results].

Table 1 summarises the contrasts of the ribosomal components in solutions with different D_2O concentrations evaluated as described in Materials and Methods (the contrasts are given in units of 10^{10} cm^{-2}) and the individual R_{Ik} factors (eq.(8)).

The plot of the squared radius of gyration *versus* reciprocal contrast for 30S ribosomal subunit is presented in Figure 2.

The structural parameters evaluated from the experimental data using Eqs (2-3) in Materials and Methods are given in Table 2 along with those of the 30S in the four-phase model[Svergun et al. 1997a]. The maximum diameters D_{max} of the 30S subunit has been evaluated to be 25nm from the X-ray scattering curves using program ORTOGNOM.

Good agreement of the integral parameters for the 30S subunit *E.coli* and *Thermus thermophilus* allows us to suggest that their structures at low resolution are similar. To verify this hypothesis, we have calculated theoretical scattering curves of the 30S subunit of *E coli* taken from the four-phase model of the 70S ribosome [Svergun et al.1997a,b], for the all experimental scattering curves at different contrasts presented in Table 1. On the whole, the model of the 30S subunit *E.coli* gives reasonable agreement with 14 experimental scattering curves of 30S *Thermus thermophilus*: the averaged R-factor (8) is 8.3%. However, significantly worse agreement between the experimental and theoretical data for neutron curves with increased (more than 70%) concentration of D_2O (Table 2) has engaged our attention. Since the matching points of the protein and RNA are 40% and 70%, respectively, at a high content of D_2O the protein component makes the predominant contribution into scattering. It permits to conclude that primary difference between two types of the 30S subunits consists in the special distributions of the protein component, whereas the conformations of the RNA molecules differ little at low resolution.

Tab.1. Contrasts and individual R_{lk} factors

Spectrometer	Particles	% D_2O in H_2O/ D_2O mixture	ρ_{pro} (10^{10} cm^{-2})	ρ_{RNA}	R_{lk} ($\times 10^{-2}$)	
					E.coli	T.therm.
		0	1.79	2.27	2.45	2.19
V4		35	0.293	1.18	3.46	2.17
	(H)-30S	80	-1.41	-0.069	17.6	7.40
		98	-2.48	-0.848	7.75	7.34
		0	1.83	2.27	3.57	2.96
V4		20	0.972	1.64	4.25	3.57
	(H)-30S	40	0.11	1.02	9.05	8.09
		98	-2.37	-0.78	3.87	3.16
		0	1.8295	2.2646	5.35	3.79
		32	0.4577	1.2690	3.36	3.07
D11		72	-1.2571	0.0246	13.7	10.1
		99	-2.3716	-0.7843	9.71	8.22
	(D)-30S	0	5.52	3.82	8.79	7.23
X33	(H)-30S (D)-30S	X-ray	2.26.	4.23.	5.88	6.46

Tab.2. Integral parameters of the 30S ribosomal subunit

Particles	Parameters	Neutron scattering	Optimized two-phase model
	R_c(Å)	72±2	71.70
	R_{pro}(Å)	79±3	77.54
E.coli	R_{rna}(Å)	66±2	67.21
	$V(\times 10^3 Å^3)$	1400±200	1570
	average R-factor		0.0823
	R_c(Å)	71±3	73.89
T.thermophilus	R_{pro}(Å)	80±2	81.97
	R_{rna}(Å)	66±2	66.85
	$V(\times 10^3 Å^3)$	1470±200	1601
	average R-factor		0.0599

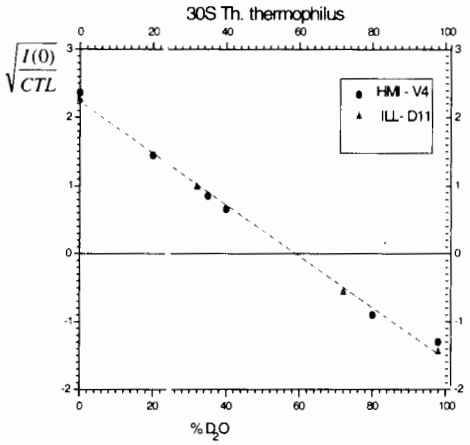

Figure 1. Normalized forward scattering of the 30S subunit T. termophilus as a function of the D_2O concentration of the solvent. C- sample concentration;d- sample thickness; T- transmission.

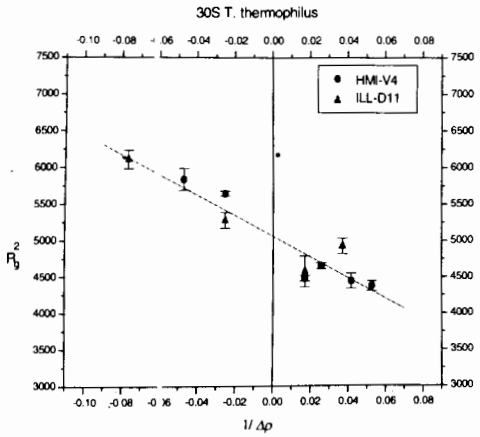

Figure 2. Square of the radii of gyration of the 30S subunit T. termophilus as a function of the reciprocal contrast.

The two-phase model of the 30S *Thermus thermophilus* was refined using the MONSTER program, and the model of the 30S subunit *E.coli* was taken as an initial approximation. The shape of the envelope of the 30S subunit and of the RNA moiety are evaluated with a multiple resolution up to L=7 that corresponds to a spatial resolution of about 35 Å. For the refinement the range $0 < s < 0.18 Å^{-1}$ is used, where the scattering by inhomogeneities within each phase [Svergun,1994; Svergun et al.1997a,b] was negligibly small and was not taken into account. The display of the three-dimensional model was done using the ASSA program [Kozin et al.,1997]. The model obtained as a result of the refinement (Fig.4) gives significantly better agreement with the experimental data than the initial approximation: the averaged R-factor is 6.1%. Scattering curves were evaluated with the contrasts of the components in Table 1. Some of the obtained fits are displayed in Figure 3 (a-d).

If we evaluate the deviation between two shapes $F_1(\omega)$ and $F_2(\omega)$ using the root-mean-square,

$$R_{\omega}^2 = \frac{\int \left[F_1(\omega) - F_2(\omega)\right]^2 d\omega}{\int \left[F_1(\omega)\right]^2 d\omega} \qquad (9)$$

it emerges that the overall shape of the 30S subunit has undergone greater changes compared to the starting model: R_ω between the shapes of the regions occupied by RNA, for the models of *E.coli* and *Thermus thermophilus* is 3.6%, whereas this value for the outer shapes is significantly higher (6.2%). This confirms the assumption as to the differences in the special distributions of the protein component in these units. A comparison of the models of *E.coli* and *Thermus thermophilus* is presented in Figure 5.

It is also necessary to point out the limitations of the obtained model. First of all, according to the Kotelnikov theorem [Kotelnikov&Nikolaev,1950] the number of Shannon channels in the experimental curve is $N_s = s_{max}D_{max}/\pi$, and in our case a single curve provides $N_s \sim 15$. The contrast variation data set (14 curves in total) in the case of the two-phase system allows to determine three basic scattering functions (see eq. (4)), This data set thus provides three times more information then a single scattering curve and the entire data set contains 45 channels. The number of independent parameters in the model is kept lower then 1.5 times this number of channels. At the same time, the two-phase model with the use of harmonics up to L=7 requires 128 parameters. The information content of the experimental data is inadequate for the reconstruction of the model *ab initio*. Therefore, the availability of the two-phase model of the 30S subunit of *E.coli* was a necessary condition to construct the model of *Thermus thermophilus*.

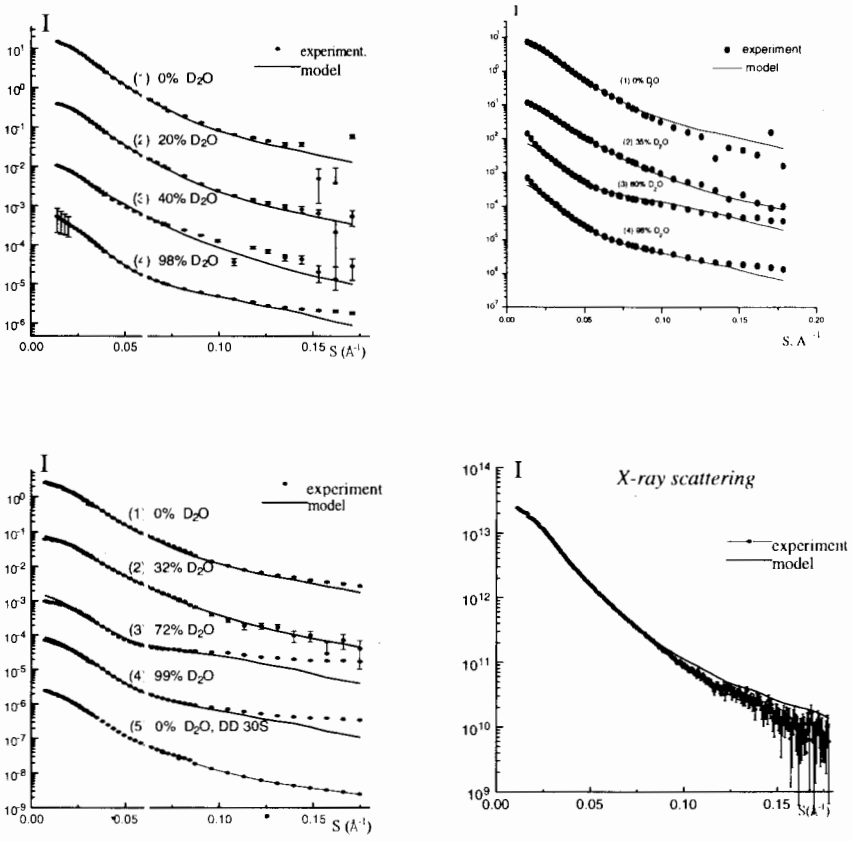

Fig.3. Fitting of the neutron ((a) to ©) and X-ray (d) solution scattering data of the 30S subunit of the *Thermus thermophilus* ribosomes with the refined two-phase model (solid lines) shown in fig.4. Each curve is shifted down by one logarithmic unit for clarity. (a), (b) - data obtained in HMI, (c) - ILL, (d) - DESY

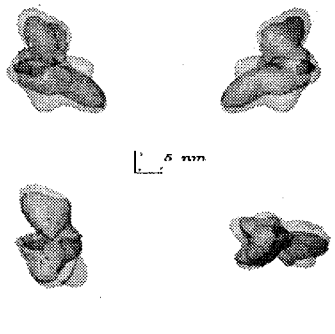

Fig. 4. Two-phase model with the resolution 35Å for the subunit of the ribosome T. thermophilus and its RNA (in side). The 30S subunit is displayed in dark gray and its RNA in litter gray.

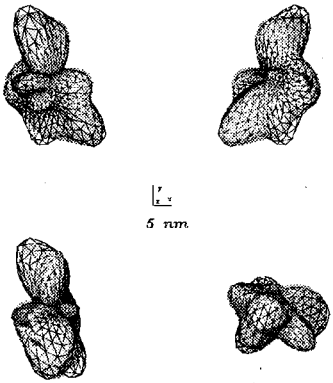

Fig. 5. Comparison of the 30S ribosome T. thermophilus and 30S E. coli models. The 30S ribosome 30S E.coli is displayed in solid body.

Conclusions

In spite of the above limitations, the obtained two-phase model for the 30S ribosomal subunit from *Thermus thermophilus* gives an adequate description of the structure at the low resolution. and it fits a large set of experimental neutron and X-ray scattering data. The *Thermus thermophilus* species are extensively used to grow ribosomal crystals. Our results open the possibility to use this model to phase the low resolution reflections in ribosomal crystallography. Moreover, our model in the near future can serve as a basis for localisation of some ribosome proteins in this subuni .

References

1. Boulin C. et al.// *Nucl. Instrum. Meth.* 1986. **A249**. 399-407.
2. Boulin C.J et al. // *Nucl. Instrum. Methods*. 1988. **A269**. 312-320.
3. Fan L. et al.// J. Appl. Cryst. 1997. 30. 59-64
4. Feigin L. A. & Svergun D. I. // Structure analysis by small-angle X-ray and neutron scattering. Plenum Press. 1987. New York.
5. Frank J. et al.// *Nature*. 1995. **376**. 441-444.
6. Koch M. H. J. & Bordas J.// *Nucl. Instrum. Meth.* 1983. **208**. 461-469

7. Kotelnikov V.A.& Nikolaev A.M. *Основы радиотехники.* M.: Связьтехиздат, 1950(in russian)
8. Kozin M. B et al.// *J. Appl. Cryst.* 1997. **30**. 811-815.
9. Gabriel A. & Dauvergne F. // *Nucl. Instrum. Meth.* 1982. **201**. 223-224.
10. Gogia Z. et al.// 1986. **20**.519-526.
11. Harrison B.C. / J. Mol. Biol. 1969. **42**. 457-462.
12. Ibel K. & Stuhrmann, H.B.//J.Mol.Biol. 1975.93.255-265.
13. Ibel K.// J.Appl. Cryst. 1976. 9. 630-643.
14. Keiderling U. et al. // Proceedings of Intern. Seminar on Structural Investigation on Pulsed Neutror Source. Dubna. 1-4 September 1992.
15. Koch M. H. J. & Stuhrmann H. B. // *Meth. Enzymol.* 1979. **59**. 670-706.
16. Liljas A. & Garber M.// Curr. Opin. Struct. Biol. 1995. 5. 721-727
17. Lindner P.et al // Physica B. 1992. 180&181. 967-972
18. Ostanevich Yu //Macromol. Chem. Macromol. Symp.1988. 15. 91-103.
19. Ramakrishnan V. et al.// Biochem. Cell. Biol. 1995. 73. 979-986.
20. Schluzen F. et al.//Biochem. Cell. Biol. 1995. 73. 739-749.
21. Serdyuk I.N.// *Meth. Enzymol.* 1979. 59. 750-775.
22. Stark H.et al. // Structure. 1995. v.3. p.815-821
23. Svergun D.I. et al. // J. Mol. Biol. 1994. v.240. N1.-p.66-77.(a)
24. Svergun D.I.,. et al. // J. Mol. Biol. 1994. v.240. N1.-p.78-86(b)
25. Svergun D.I.// Acta Cryst. 1994. v. A50. N3.-p.391-402.
26. Svergun D. I et al. // *J. Mol. Biol.* 1997. **271**. 588-601.(a)
27. Svergun D. I et al. // *J. Mol. Biol.* 1997. **271**. 602-618.(b)
28. Svergun D. I. // *J. Appl. Cryst.* 1993. **26**. 258-267.
29. Svergun D. I., Semenyuk A. V. & Feigin L. A. // *Acta Cryst.* 1988. **A44**. 244-250.
30. Svergun D. I. // *J. Appl. Cryst.* 1992. **25**. 495-503.
31. Svergun D. I. // *J. Appl. Cryst.* 1991. **24**. 485-492.
32. Svergun D.I.at al. //Acta Cryst. 1996. A52. 419-426.
33. Svergun D.I. // *J. Appl. Crystallogr.* 1997. **30**. 792-797.
34. Stuhrmann H. B. & Kirste R. G.// *Zeitschr. Physik. Chem. Neue Folge* 1965. **46**. 247-250.
35. Stuhrmann H.B.// Acta Cryst. A26. 297-300; Z. Phys. Chem. Frankfurt. 1970. 72. 177-183.
36. Tardieu A & Vachette P. // EMBO J. 1982. V.1. 35-42.

NUCLEAR SPIN DIFFUSION IN DEUTERATED SOLVENTS FROM NMR AND POLARISED NEUTRON SCATTERING.

Ben van den Brandt[†], Eric Fanchon*, Patrick Hautle[†], Jacques Gai lard[#], Hélène Jouve*, Richard Kahn*, J. Antoon Konter[†], Salvatore Mango[†], Thomas Müller[+], Heinrich B. Stuhrmann*[&], Oliver Zimmer[+]

*) Institut de Biologie Structurale, 41 Avenue des Martyrs, F-38027 Grenoble
[#]) CEA Grenoble , 17 Avenue des Martyrs, F- Grenoble
[+]) Institut Laue Langevin, BP. 156, F-38042 Grenoble
[†]) Paul-Scherrer-Institut, CH-5232 Villigen
[&]) on leave from GKSS, Geesthacht

Abstract
Both dynamic nuclear spin polarisation (DNP) and selective nuclear spin depolarisation by NMR saturation including selective inversion of the nuclear spin polarisation by the method of adiabatic fast passage (AFP) create gradients of polarisation near paramagnetic centres (organic radicals). Their lifetime changes from a couple of hours to some ten seconds depending on the isotopic composition, i.e. deuteration, and the concentration of the paramagnetic centres. This has been observed with sodium bis[2-ethyl-hydroxybutyrate]-oxochromate(V), $Na[C_{12}H_{20}O_7Cr^V]$ which is often used both in experiments of high energy physics and in studies of nuclear spin contrast variation with ribosomes. The number of selectively polarised proton spins is about 20. This means that the magnetic diffusion barrier roughly coincides with the radius (r= 5 Å) of the Cr(V)-complex. The possible spin off for biological structure research is considerable. A large amplitude of selectively polarised proton spins equal to that of a heavy atom in X-ray scattering is added to that of magnetic neutron scattering from an unpaired electron. Hence, there is a gain in the amplitude of coherent scattering at the site of the radical by two orders of magnitude. Radical densities could then be observed even in very dilute paramagnets, like in enzymes containing protein radicals. We report results from polarised neutron scattering and NMR studies from differently deuterated solutions of the Cr(V)-complex and some preliminary results from free tyrosyl radical.

Introduction.
The replacement of the hydogen isotope ^1H (=H) by its heavier isotope ^2H (=D), i.e. the deuteration, has played an outstanding role in neutron scattering studies on

biological structures ever since. This is also true for quite some applications of nuclear magnetic resonance (NMR). Surprisingly, deuteration appears to be less necessary for a method which makes use of both polarised scattering and NMR simultaneously. It is the aim of this paper to explain this statement.

Nuclear polarisation dependent cross sections of polarised neutron scattering.
The length b of coherent neutron scattering of both hydrogen isotopes, H and D, depends on the nuclear polarisation P. Using a completely polarised neutron beam we have

$$b_H = (-0.374 \pm 1.456 P_H)10^{-12}\,cm$$
$$b_D = (+0.667 \pm 0.280 P_D)10^{-12}\,cm \qquad (1)$$

The '+' sign of '±' holds of the direction of both nuclear spin polarisation und neutron spin polarisation point into the same direction. The '–' sign applies if the nuclear spins point into a direction opposite to that of the neutron spins. There is a huge variation of the scattering length b_H of the protons with P_H from -1.83×10^{-12} cm to $+1.082 \times 10^{-12}$ cm. A considerably smaller variation is observed with polarised deuterons.

Similarly the cross section of incoherent scattering varies with nuclear polarisation. Usually, it is the dominant part of neutron scattering by protons:

$$\sigma_{inc.} = 106.5[(3/4 \pm (-1/2 P_H) - 1/4 P_H^2)]10^{-24}\,cm^2 \qquad (2)$$

If, however, the '+' sign of '±' holds, i.e if both nuclear spin and neutron spin point into the same direction, then there is no incoherent scattering. There is a strong dependence of neutron beam transmission on polarised proton spin targets[1]. Hence, polarised hydrogenous materials are excellent spin filters.

Low incoherent scattering as achieved by 'positive' proton spin polarisation is highly beneficial to structural studies, e.g. in protein crystallography. This method presents an alternative to the suppresion of incoherent scattering scattering from protons by perdeuteration of proteins. The cross section of incoherent scattering from deuterons is 2 barns ($=2 \times 10^{-24}$ cm^2) only.

Nuclear spin contrast variation
Hydrogenous substances are more readily amenable to structural studies by neutron scattering after suppression of incoherent scattering by massive deuteration. Ideally, protons should be left only in those parts of complex structures which are of interest. All residual protons should be substituted by deuterons. This is done in

[1] Following a usage in nuclear and particle physics we call samples with polarised nuclear spins **polarised targets**. A sample containing protons and deuterons is called a **proton spin target**, if only its proton spins are polarised, and it is called a **deuteron spin target** if only its deuteron spins are polarised.

nearly all experiments of nuclear spin contrast variation. Fig. 1 shows the variation of the scattering length density of proteins and RNA with proton spin polarisation in the light of polarised neutron scattering. Using a deuterated solvent, the contrast of these materials increase considerably with more negative P_H, whereas both protein and RNA have scattering densities equal to that of the deuterated solvent at P_H slightly below +0.7. We note that proton spin polarisation strongly varies the contrast of the solute, but it does not discrimanate between proteins and RNA. This is different from what we know from contrast variation in H_2O/D_2O mixtures.

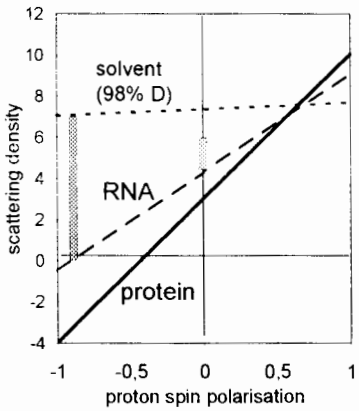

Fig. 1. The scattering density of RNA, protein and a mixture of perdeuterated glycerol and D_2O in units of 10^{10} cm^{-2} versus the proton spin polarisation P_H. The bar at $P_H = 0$ is the contrast of RNA in D_2O. A much larger contrast of RNA is obtained at $P_H = -0.9$ using the deuterated solvent mixture.

In structural studies on ribosomes deuterated particles are used. It is very fortunate that the scattering density of the deuterated ribosome is close to that of the deuterated solvent. As the ribosome is nearly transparent to coherent neutron scattering, even very small parts of it (< 0.01), e.g. details of the translational apparatus which have been left protonated, can be rendered visible by proton spin polarisation.

Dynamic nuclear spin polarisation.

Experiments of nuclear spin contrast variation require a polarised neutron beam and the polarisation of nuclear spins of the sample.

Polarised neutron are obtained by total reflection from smooth magnetised surfaces (Schärpf). The polarisation of nuclear spins requires extreme conditions as shown in Fig.2. Even if these would be realised the time to obtain a modest proton spin polarisation would be prohibitively long.

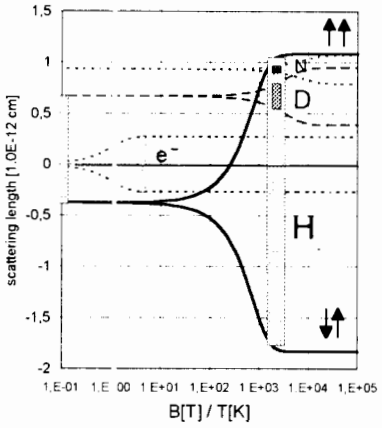

Fig. 2. With increasing magnetic field B and decreasing temperature the polarisation increases according to the magnetic momentum of the particles. In a completely polarised neutron beam the scattering lengths develop as described in (1). The magnetic scattering amplitude of an unpaired electron is given for comparison.

This is the necessary prerequisite for dynamic nuclear spin polarisation. We outline the practical procedure: The sample is doped by a small amount of paramagnetic centres with concentrations less than 10^{-4} to 10^{-5} per atom. Very often this is done by adding a stable organic radical, such as EHBA-Cr(V), $Na(C_{12}H_{20}O_7Cr^{V}$ .D2O. Alternatively, radicals can be created by irradiation of the frozen sample wi h high energy particles or by UV light. The solvent must be a good glass former unde r conditions of rapid freezing. For biological macromolecules a mixture of glycer ol and water (11/9) turned out to be most useful.

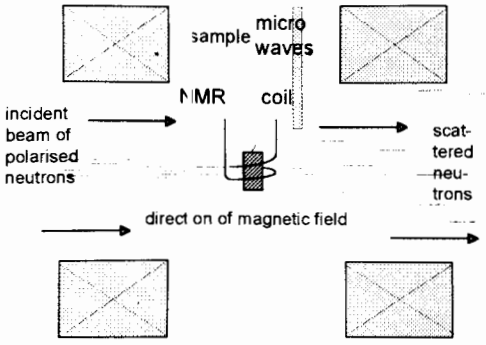

Fig. 3. The facility for dynamic nuclear spin polarisation. A strong magnetic field is created by superconducting magnets (cross section of coils in each corner). The sample is kept at temperatures below 1 K. The refrigerator is not shown. Irradiation by microwaves polarises the proton spins (see text). The NMR signal is a measure of the nuclear spin polarisation. The beam of polarised neutrons is entering the target station left side. This set up is similar to that used by one of us (O. Z.) at the ILL.

At T = 1K and B = 2.5 T the spins of the unpaired electrons are nearly completely polarised wherea s those of the nuclear spins are not (Fig. 2). The method of DNP makes it possible to impart to the nuclear spins a polarisation whose magnitude is comparable with the thermal equilibrium polarisation of the electrons and whose

orientation can be chosen at will parallel or antiparallel to the external field (Glättli & Goldman, 1987) . Irradiation by 4 mm microwaves slightly below the Larmor frequency of the unpaired electrons (69.1 – 0.15 GHz approximate y) aligns the nuclear spins in the direction of the external magnetic field. Using microwaves slightly above the electronic Larmor frequency (69.1 + 0.15 GHz approximately) aligns the nuclear spins in the direction *opposite* to the external field (Fig. 3). For proton spins, under favourable conditions a polarisation of more than 95% can be obtained after a fraction of an hour to several days. For deuterons, because of the smaller magnetic momentum the present practical limit is $P_D = 45\%$ (Fig. 2).

Measurement and control of nuclear polarisation by NMR.

The proton spin polarisation is determined by comparing the enhanced nuclear magnetic resonance (NMR) signal with the thermal equilibrium signal (Fig.4,7). In order to measure the absorption function due to NMR a coil is put in close contact to the sample (Fig. 3). Through the inductive coupling between the spins and the coil the impedance will vary with the frequency of the resonant circuit. The change of the impedance is detected by a continuous-wave constant current Q-meter.

Selective nuclear depolarisation is achieved by a radio frequency sweep across the NMR peak at a power rate which is about a hundred times higher than in the measurement of nuclear polarisation (Fig 4, top, left). In the case of specifically deuterated biomolecules or polymers two options may be envisaged:

- selective depolarisation of the deuteron spins ⇒
  ⇒ for proton spin contrast variation
- selective depolarisation of the proton spins
  ⇒ for deuteron spin contrast variation

In the case of deuterated samples, this technique facilitates the analysis of the data.

Creation of polarisation gradients by reversal of nuclear of nuclear spin polarisation.

The method of adiabatic fast passage (AFP) is used to reverse selectively the polarisation of an isotope. The efficiency of this method is quite high: after a radio frequency sweep across the NMR profile obeying certain criteria (Hautle et al. 1992) typically more than 80% of the nuclear spins can be reversed. We report on experiments performed on mixtures of glycerol/water at two different degrees of deuteration, 97.8% (sample A) and 83% (sample B). Both solutions contained 7 mg/ml of EHBA-Cr(V), $Na[C_{12}H_{20}O_7Cr^V]$, which corresponds to 1.3×10^{19} unpaired electrons per cm^3.

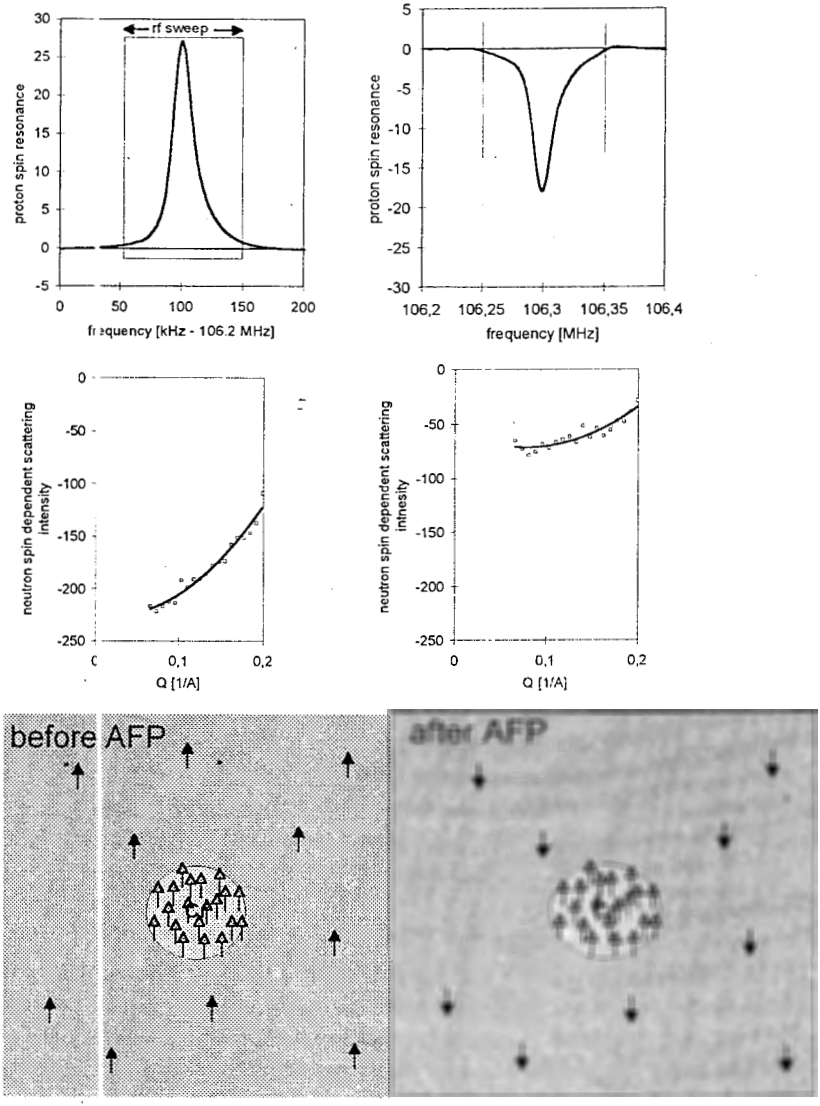

Fig. 4. The influence of proton spin reversal by AFP on proton NMR (upper part) neutron spin dependent scattering (central part) and its interpretation (lower part). Left side: before AFP. Right side: after AFP. There is no change of the deuteron NMR.
The diameter of the selectively polarised proton cluster as obtained from neutron scattering is 9Å. This is the volume of EHBA-Cr(V) molecule which contains 20 protons.

Sample A: This sample has the very low content of 2.2% protons out of the total number of hydrogen atoms. More than 1/3 of its protons are those of EHBA-Cr(V). The others are mainly those of the deuterated glycerol (98.4%). Proton spin reversal by AFP has an influence on the protons in the bulk as these are supposed to contribute to the inverted proton NMR. Polarised neutron scattering indicates that one third of the proton spins kept their original position. Following the above hypothesis, these protons must be close to Cr(V). As they give rise to an NMR spectrum which has a width close to 1 MHz, they are hardly influenced by the rf sweep of 100 kHz. The lower part of Fig. 4 summarises the state of the sample before and immediately after AFP. After the rf sweep of 2s duration the proton polarisation varies across the boarder of the Cr(V)-complex from $P_H = +0.32$ to $P_H = -0.30$ in the solvent. The gradient of proton spin polarisation is remarkably stable (Zhao et al. 1995). The internal equilibrium is reached in a complicated process which formally can be described by at least two relaxation times of $t_1 = 2.2$ h and $t_2 = 0.6$ h and They apply to the convergence of both proton NMR and polarised neutron scattering towards the internal equilibrium (Fig. 5,6). During the period of half a day both the *average* proton polarisation and the deuteron polarisation vary by hardly more than 10%. At T=0.15 K, the internal relaxation time between the deuterons with positive polarisation and the protons with a uniformly negative proton polarisation at 10 h after AFP takes several days. The spin lattice relaxation time T_1 of this target is typically 2 weeks.

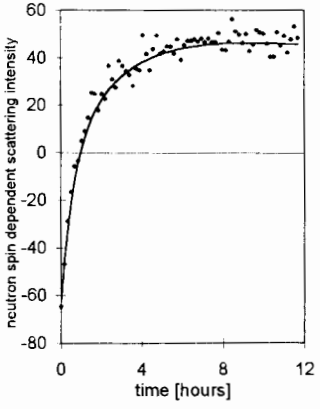

Fig. 5. $I(\uparrow\uparrow) - I(\downarrow\uparrow)$ of polarised neutron scattering.

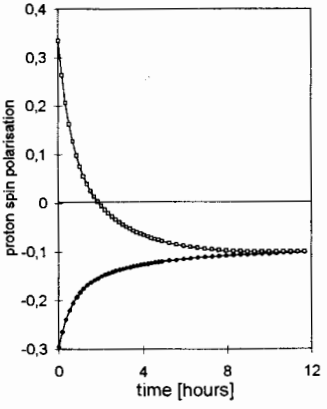

Fig.6. Proton polarisation near Cr(V) (□) and in the bulk (solvent) (◆).

Sample B: Its higher proton content of 13% gives rise to a faster approach to internal equilibrium of proton polarisation. The relaxation times t_1 and t_2 obtained

from proton NMR are reduced by an order of magnitude to 800s and 90s respectively. This trend is expected from a spin diffusion controlled internal relaxation. The extrapolation to vanishing deuteration yields t_1 = 120s and t_2= 10s.

Dynamic nuclear spin polarisation with the tyrosyl radical.

Recent experiments have shown that tyrosyl radicals support dynamic nuclear spin polarisation (Fig. 7). This result is relevant for structural studies on radicals in proteins. As the radical concentration was slightly less than 10^{18} per cm^3, the proton polarisation by DNP was very slow (1% per hour).

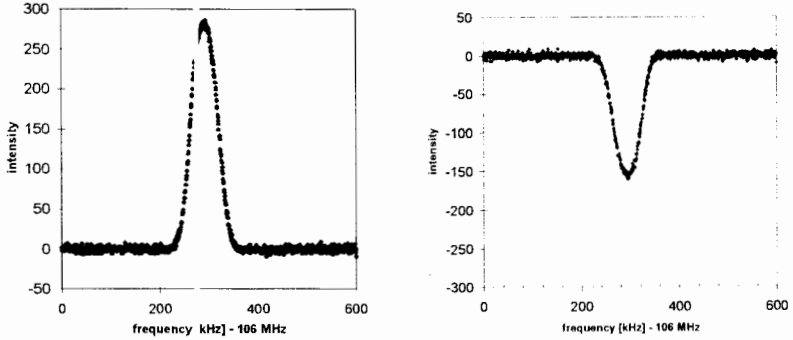

Fig. 7.Proton NMR from a frozen solution of tyrosyl radicals.

Conclusion.

Gradients of proton spin polarisation occur during DNP and they can be modified by NMR techniques. The creation of a local contrast is facilitated by magnetic spin diffusion barrier surrounding the paramagnetic centres. The selective polarisation of the protons within this confinement adds am amplitude of polarised neutron scattering which is a 100 times stronger than that of magnetic scattering from an unpaired electron. This opens the way to the study of the spin density in dilute paramagnets like radicals in proteins. There is no need for the deuteration of the protein itself, though the use of deuterated solvents still remains a useful way to improve neutron diffraction data.

References

H. Glättli & M. Goldman (1987) Methods of Exp. Physics, 23C, 241-286

P. Hautle, W. Gruebler, B. van den Brandt, J.A. Konter, S. Mango, M. Wessler (1992) Phys. Rev. Lett. 33, 696-699

J. Zhao, W. Meerwinck, T.O. Niinikoski, A. Rijllart, M. Schmitt, R. Willumeit, H.B. Stuhrmann (1995) Nucl. Instr. Methods Phys. Res. A, 356, 133-137

A PARTIALLY UNFOLDED STATE OF LYSOZYME WITH A DEVELOPED SECONDARY STRUCTURE IN DIMETHYLSULFOXIDE H_2O/D_2O MIXTURES

A.A.Timchenko, M.D.Kirkitadze, D.A.Prokhorov, S.A.Potekhin, I.N.Serdyuk

Institute of Protein Research, RAS, 142292 Moscow Region, Pushchino, Russia

Summary: The conformation of a chicken egg-white lysozyme molecule (dimensions, stoichiometry of its associates, and the degree of helicity) in DMSO was studied by small-angle neutron scattering, dynamic light scattering, and optical rotatory dispersion in the visible region of the spectrum. It was found that a lysozyme molecule in 60% DMSO (pH 2.5) has a partially unfolded structure with a well developed secondary structure and has a tendency to associate. Increasing the DMSO concentration to 70% causes further association and monomers in the associates have a partially unfolded structure with a well developed secondary structure. Decreasing pH to 2.0 at 70% DMSO causes the formation of gel with the ordered structure. The H_2O-D_2O contrast variation technique in DMSO solutions did not reveal noticeable DMSO binding to protein.

Structural description of protein folding intermediates is very important for the understanding of the self-organization mechanism. However, kinetic intermediates are difficult to detect due to the short time of folding. Therefore, more fruitful might be attempts to find experimental conditions where these intermediates are more stable. Some investigations have shown (see, e.g.[1]) that partially folded states can be formed after addition of some organic compounds (alcohols, DMSO). Proteins in these conditions are characterized by a native-like secondary structure and sufficiently small dimensions in comparison with those for the fully unfolded state. Here we have investigated the conformation of lysozyme at different concentrations of DMSO by the joint application of neutron scattering, dynamic light scattering and optical rotatory dispersion (ORD).

Materials and Methods. Lysozyme was dissolved in 20 mM Gly-HCl buffer containing 40 mM KCl at pH 2.5 and pH 2.0. DMSO was added to the protein solutions in 60%(v/v) and 70%(v/v) concentrations. Binding of DMSO to the protein was investigated at 25%(v/v) DMSO and 0.0, 0.1, 0.2 and 0.98 D_2O/H_2O ratios in the protein solutions without DMSO. ORD measurements were carried out on a Perkin-Elmer 141 spectropolarimeter in the range of wavelengths 364-579 nm. Dynamic light scattering experiments were performed on the spectrometer described in [2]. Neutron scattering experiments were done on the spectrometer YUMO (IBR-2) described in [3]. The acquisition time for one scattering pattern was about 2 h.

Results and Discussion. In the previous paper [1] the dependence of ORD spectra of lysozyme on DMSO concentration at pH 2.5 was studied. It was shown that at the DMSO concentration more than 45% the denatured transition with increasing protein helicity is observed (see Fig.1). Such high helicity of the denatured protein is likely

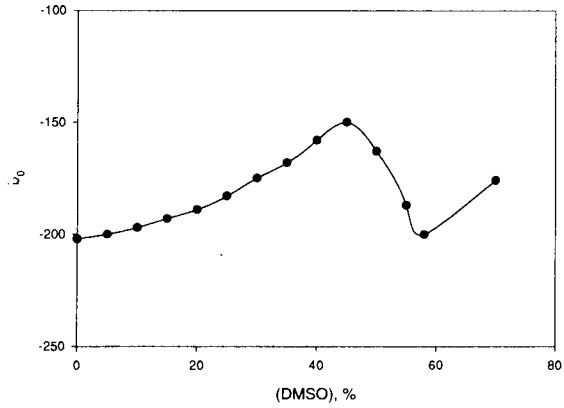

Fig.1. The dependence of Moffit-Yang parameter b_0 on the DMSO concentration. at 70% DMSO causes the Moffit-Yang parameter b_0 to be positive and can be interpreted as the appearance of definite structure in solution, maybe a liquid crystal like one.

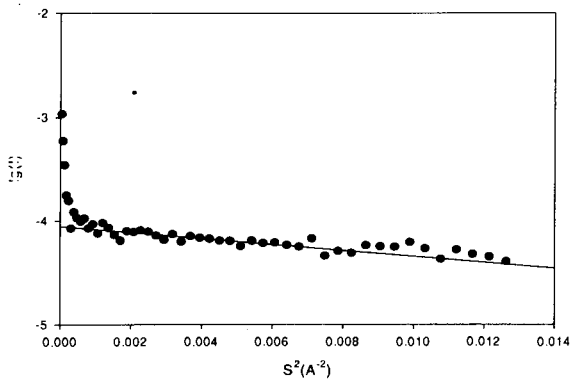

Fig.2. The Guinier plot of neutron scattering data for lysozyme in 60% DMSO. $S=4\pi/\lambda*\sin(\theta/2)$ is the module of the scattering vector, where λ is the neutron wavelength, θ is the scattering angle.

Table 1. Values of molecular mass (M), radius of gyration (Rg) and translational diffusion coefficient (D) in Fick's units (1u.F.=10^{-7}cm^2/s) for lysozyme at different concentrations of DMSO.

DMSO(%)	0	60	70
Rg(A)	14.7+/-1.0	18.0+/-1.0	38.5+/-1.0
M(kD)	11.5+/-2.0	11.5+/-2.0	73.5+/-1.0
D(u.F)	10.5+/-0.2	6.5+/-0.1	3.1+/-0.1

connected with decreasing the dielectric constant of solution and increasing the interaction between peptide dipoles and the nearest side chain charges. Moreover, decreasing pH to 2.0 at 70% DMSO causes the Moffit Yang parameter b_0 to be positive and can be interpreted as the appearance of definite structure in solution, maybe a liquid crystal-like one.

The Guinier plot for lysozyme in 60% DMSO is shown in Fig.2. The values of molecular mass (M) and radius of gyration (Rg) calculated from this plot are presented in Table 1 in comparison with those for native lysozyme. One can see that the Rg value is noticeably higher than that for native molecule. Moreover, the comparison of corresponding Kratky plots (Fig.3) shows systematically low values for lysozyme in 60% DMSO. This means that protein molecules are partially unfolded. At the same time there is a tendency of lysozyme molecules to associate (see the initial part of the Guinier plot in Fig.2). Dynamic light scattering experiments have shown noticeably low values of the translational diffusion coefficient (see Table 1) and the evaluation of molecular mass from the static light scattering data gave a double molecular mass of lysozyme. This is not surprising because much lower scattering vector values are presented in the light scattering experiments. Most likely such association is not specific because there is an influence only on the initial part of the scattering curve (see Fig.2 and Table 1). For compact associates, approximately a double decrease in the value of the diffusion coefficient (see Table 1) upon the double increase of the molecular mass means that the lysozyme molecule has a partially unfolded structure.

The increase of the DMSO concentration to 70% causes further association of protein molecules as one can seen from Table 1. The averaged molecular mass corresponds to that of a hexamer. At the same time the radius of gyration increases more than can be expected for the hexamer consisting of molecules in the native state. The same is valid for the diffusion coefficient from dynamic light scattering (see Table 1). Moreover, the Kratky plot presented in Fig.4 clearly shows non-globular behavior and witnesses for a partially unfolded structure of protein molecule. Thus, monomers in the associates have a partially unfolded structure with a well-developed secondary structure (see Fig.1). Decrease of pH from 2.5 to 2.0 causes the formation of gel with the ordered structure as can be seen from the Kratky plot in Fig.4 (the well-developed maximum appears).

To evaluate the influence of possible binding of DMSO to lysozyme molecules on the above results, we have checked such binding by using the contrast variation technique. Namely, neutron scattering experiments have been carried out at a different ratio of D_2O/H_2O. If one supposes that the density of DMSO bound to protein is about

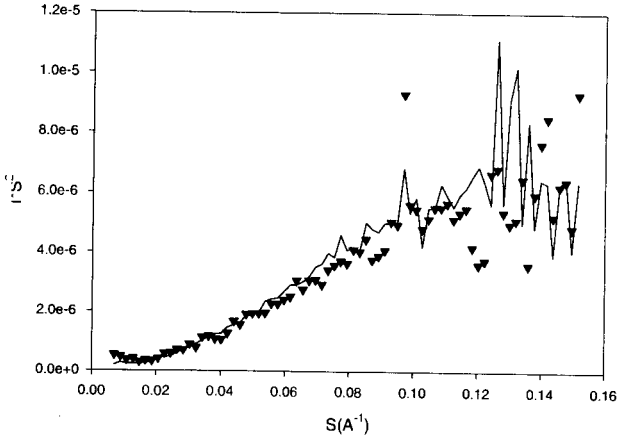

Fig.3.The Kratky plot of neutron scattering data for native lysozyme (--) and for that in 60% DMSO (▼).

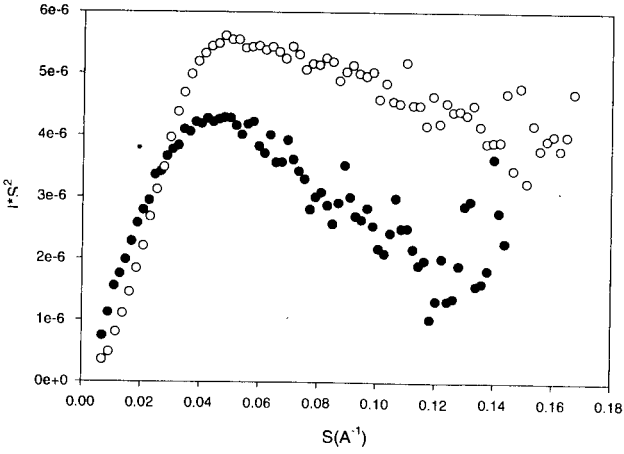

Fig.4.The Kratky plot of neutron scattering data for lysozyme in 70% DMSO pH 2.5 (o) and pH 2.0(•).

the same as that for pure DMSO then the coherent scattering-length dens ty of protein with known composition can be calculated according to:

$$\mathbf{b_{prot}=(b_h+(1-r)*A*(b_d- b_h)+b_s*x)/(1+x)} \quad \textbf{(1),}$$

where $\mathbf{b_h}$ is the scattering-length density of fully protonated proteir, $\mathbf{b_d}$ is the scattering-length density of fully deuterated protein, $\mathbf{b_s}$ is the scattering-length density of substance to be absorbed (e.g. DMSO), **A** is the part of D_2O in the protein solution without DMSO, **x** is the ratio of absorbed substance volume to that of the protein, **r** is the part of not-exchangeable labile protons (usually this value is about 0.2). For the, solvent the scattering-length density can be calculated according to:

$$\mathbf{b_{solv}= B* b_s+(1-B)*B_H+(1-B)*A*(B_D-B_H)} \quad \textbf{(2),}$$

where $\mathbf{B_H}$, $\mathbf{B_D}$ are the scattering-length densities of H_2O and D_2O, respectively, **B** is the part of substance (DMSO) in a solution. At the matching point $\mathbf{b_{prot}= b_{solv}}$. For 25% DMSO at **x**=0 the matching point corresponds to 60% of D_2O in the solution without DMSO, at **x**=0.2 it corresponds to 50% of D_2O. Fig.5 shows the experimental dependence of square-root of normalized intensity on the percentage of D_2O in the solution without DMSO. From this plot the experimental value of the matching point

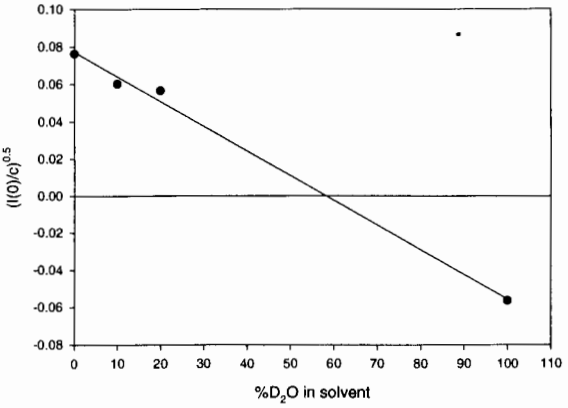

Fig.5.The dependence of square-root of normalized neutron scattering in ensity on the percentage of D_2O in lysozyme solution 1 without DMSO. The concentration of DMSO is 25% (v/v).

Acknowledgments:

The authors express their gratitude to M.V.Avdeev for his help in the performing neutron scattering experiments.

Conclusion:

1) It was found that a lysozyme molecule in 60% DMSO (pH 2.5) has a partially unfolded structure with a well developed secondary structure and has a tendency to associate.

2) Increasing the DMSO concentration to 70% causes further association of lysozyme molecules, and monomers in the associates have a partially unfolded structure with a well developed secondary structure.

3) Decreasing pH to 2.0 at 70% DMSO causes the formation of gel with the ordered structure.

4) The H_2O-D_2O contrast variation technique in DMSO solutions did not reveal noticeable DMSO binding to the protein.

References.

1) Kirkitadze M.D., Surin A.S., Potekhin S.A. Bioorg.Khimiya (1996), v.22, pp.21-24

2) Timchenko A.A., Griko N.B., Serdyuk I.N. Optika & Spektroskopiya (1988), v.64, pp.343-349

3) Serdyuk I.N. Physica B. (1995), v.213, pp. 892-894

BIOLOGICAL MEMBRANES: SOLID STATE ^{2}H-NMR OF LIPIDS AND PROTEINS, COMPLEMENTED BY NEUTRON DIFFRACTION

Anne S. Ulrich* & Anthony Watts$
* Institute of Molecular Biology, University of Jena, Winzerlaer Str. 10, 07745 Jena, Germany; ulrich@molebio.uni-jena.de.
$ Oxford Biomembrane Structure Unit, Biochemistry Department, University of Oxford, South Parks Road, Oxford OX1 3QU, UK.

Biological membranes are complex assemblies of lipids and proteins, whose structure and dynamics cannot usually be probed by conventional crystallographic or high-resolution NMR approaches. Instead, "solid state" NMR is used to observe isotope labels that are selectively incorporated into a specific site of the membrane-bound molecule [1]. That way, local dynamics and the molecular geometry of the specifically labelled segment can be characterized [2]. The advantage of using the deuterium nucleus as a reporter lies in the unique possibility of complementing the NMR data with neutron diffraction experiments on the same labelled sample. Solid state ^{2}H-NMR can provide the vectorial alignment of a labelled group (for example a C-CD_3 bond direction) with respect to the membrane normal [3, 4], while neutron diffraction is able to localize the depth of the deuterated site in the lipid bilayer.

Several different applications of ^{2}H-NMR and neutron diffraction will be discussed here in a broad overview, to illustrate the kind of structural and dynamic information that can be obtained about lipids, membrane-bound peptides, and integral membrane proteins. The interested reader is referred to the original literature and the numerous references cited therein.

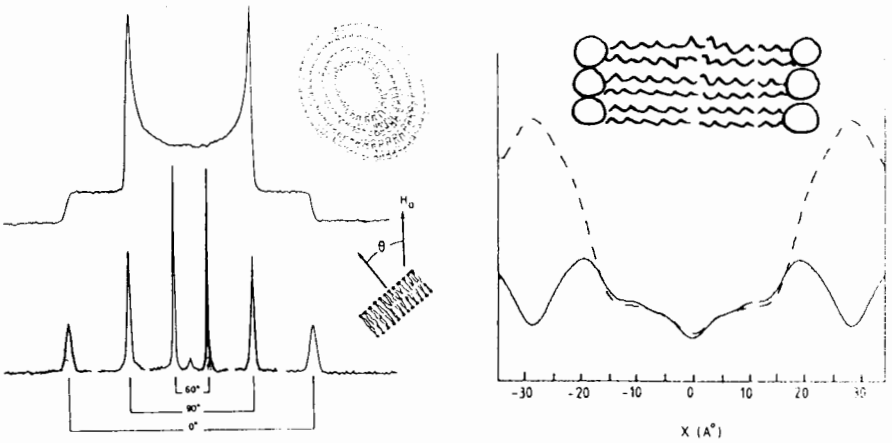

Fig. 1. Characteristic ^{2}H-NMR lineshapes (left) and neutron scattering density profiles (right) of lipid bilayers, used as membrane models.

The deuterium nucleus possesses a spin of I=1, and the quadrupolar interaction dominates the wideline ^{2}H-NMR spectrum (Fig. 1, left). To a good approximation the symmetry axis of this interaction is aligned along the C-^{2}H bond. A selectively deuterium-labelled sample of non-oriented membranes gives rise to a powder spectrum (top), consisting of the weighted contributions from all molecular orientations in space. A uniaxially oriented sample, on the other hand, gives rise to a pair of narrow lines (bottom), which are separated by an orientation-dependent quadrupole splitting $\Delta\nu_Q \propto 3(\cos^2\theta - 1)/2$.

The neutron scattering density profile of an oriented, protonated sample (Fig. 1, right) corresponds to a "cross-section" through the lipid bilayer, which has a maximum near the headgroups (full line) [5]. When exchanging H_2O for D_2O to generate a contrast (dotted line), the difference in intensity reveals the location of the deuterons relative to the bilayer [6]. For example, in an earlier application the repeat distance of a multilamellar lipid sample was monitored as a function of bilayer hydration [7]. A stepwise swelling was observed, suggesting that the bilayer dimensions changed discontinually with the addition of water. To provide a complementary picture, ^{2}H-NMR measurements were carried out on synthetic lipids with specific deuterium labels in the headgroup. The quadrupole splittings and relaxation times showed that, at a molecular level, the headgroup orientation and mobility change smoothly up to a saturating hydration [8-10]. From this data it was also possible to determine the hydration force parameters of the lipid, which was further supported by a ^{2}H-NMR study on D_2O [11,12].

The response of a deuterated lipid segment to a perturbation in the bilayer offers the potential to describe lipid-peptide and lipid-protein interactions in terms of electrostatics or hydrophobic penetration. For example, the membrane-binding mode of the hemolytic peptide, melittin, from bee venom was investigated by a combination of ^{2}H-NMR and neutron scattering. Using headgroup-deuterated lipids, the disruption of a lipid bilayer into small isotropic fragments could be demonstrated by the collapse of the NMR lineshape [13]. Deuterium labels have also been placed directly onto the melittin peptide, for example by deuteromethylation of lysine residues. A pH titration, by simply monitoring the changes in deuterium quadrupole splitting, yielded a pK_a value which suggests that these side chains are located at the polar membrane surface [14]. More subtle changes with pH, which affected the localization of the whole molecule, were attributed to a protonation of the N-terminal amino group of melittin. Here, neutron diffraction was used to locate the depth of a deuterated alanine that had been incorporated into the synthetic peptide [15]. This central segment appeared to reflect a dynamic equilibrium, where the N-terminal part of melittin would insert relatively deep into the hydrophobic bilayer at high pH, but move out when acquiring a positive charge by protonation.

Also in the structure analysis of integral membrane proteins, the combination of ^{2}H-NMR and neutron diffraction has been applied to much mutual benefit. The active site of bacteriorhodopsin has been investigated in considerable detail, since the retinal chromophore can be readily removed and replaced by synthetic analogues with deuterons at any position. This particular membrane protein had already been well resolved by electron microscopy, because of its intrinsic hexagonal packing in the purple membrane. However, it still remained unclear how the chromophore is aligned in the binding pocked, and how it moves during the photocycle of the proton pump.

A series of selectively deuterated retinals were incorporated into the protein and examined by neutron diffraction, to determine not only the depth of each labelled segment within the bilayer, but also each position in a projection map of the protein, as shown in Fig. 2 on the left [16,17]. The deuterated methyl groups of retinal were also examined by ^{2}H-NMR, one by one, to determine the orientation of each C-CD_3 bond vector with respect to the membrane plane. The three-dimensional structure of the whole chromophore could thus be modelled from these individual angles with high accuracy, as summarized in Fig. 2 on the right [18-20]. The light-induced isomerization of retinal was investigated the same way by neutron diffraction and ^{2}H-NMR [21, 22]. A comparison of the ground state and M-intermediate suggests that the deprotonated chromophore moves upward by a few degree, presumably to allow the Schiff-base end to open up the pathway for proton translocation through the membrane.

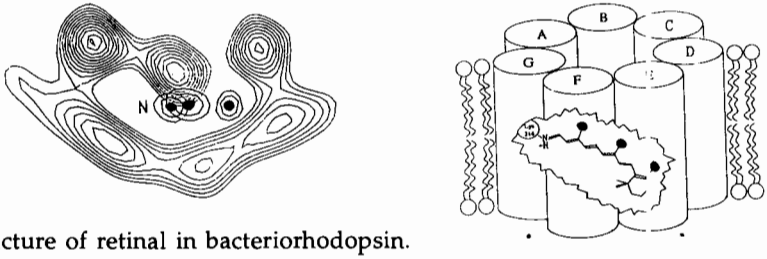

Fig. 2. Structure of retinal in bacteriorhodopsin.

For an "inverse" approach, finally, a fully deuterated bacteriorhodopsin was prepared with a protonated retinal, so that only the ^{1}H-NMR signals of retinal would be observed [23]. This study was carried out by high resolution NMR in detergent micelles, rather than using solid state methods on the membrane embedded protein. Indeed, selected NOE cross-peaks were observed between retinal protons, as well as to neighbouring aromatic residues which had also been protonated biosynthetically in a different set of samples. This high-resolution NMR study demonstrates that it is possible to detect intramolecular contacts even within a large membrane protein, provided it is suitably labelled.

1. Watts, A., A.S. Ulrich & D.A. Middleton (1995) Solid-state NMR studies of membrane proteins (Review). *Mol. Membr. Biol.* 12: 233-246
2. Ulrich, A.S. & S.L. Grage (1998) Solid state ^{2}H-NMR. In *Solid state NMR of polymers* (Eds. I. Ando & T. Asakura). Elsevier Science, In press.
3. Ulrich. A.S. (1996) NMR studies of oriented membranes to determine single bond orientations. *Macromol. Symp.* 101: 81-89
4. Asakura, T., M. Minami, R. Shimada, M. Demura, M. Osanai, T. Fujito, M. Imanari & A.S. Ulrich (1997) ^{2}H-labeling of bombyx mori silk fibers and their structural characterization by solid state ^{2}H-NMR. *Macromol.* 30: 2429-2435
5. Wiener M. C. & S. H. White (1992) Structure of a fluid DOPC bilayer determined by joint refinement of X-ray and neutron diffraction data. *Biophys. J.* 61: 434-447.
6. Knott, R. B. & B. T. Schönborn (1986) Quantitation of water in membranes by neutron diffraction and X-ray techniques. *Meth. Emzymol.* 127: 217-229.
7. Klose, G. S. Brückner, V. Yu. Bezzabontnov, S. Borbely, & Yu. M. Ostanevich

(1986) Hydration and swelling of the total lipid fraction of egg yolk and the influence of some additives studied by small-angle neutron scattering. *Chem. Phys. Lipids* 41: 293-307.
8. Ulrich, A.S. & A. Watts (1994) Molecular response of the lipid headgroup to bilayer hydration as monitored by ^{2}H-NMR. *Biophys. J.* 66: 1441-1449.
9. Ulrich, A.S. & A. Watts (1994) Lipid headgroup hydration studied by ^{2}H-NMR: a link between spectroscopy and thermodynamics. *Biophys. Chem.* 49: 39-50.
10. Ulrich, A.S., F. Volke & A. Watts (1990) The dependence of phospholipid headgroup mobility on hydration as studied by ^{2}H-NMR spin lattice relaxation time measurements. *Chem. Phys. Lipids* 55: 61-66.
11. Volke, F., S. Eisenblätter, & G. Klose (1994) Hydration force parameters of phosphytidylcholine lipid bilayers determined from ^{2}H-NMR of deuterated water. *Biophys. J.* 67: 1-7.
12. Ulrich, A.S., M. Sami & A. Watts (1994) Hydration of DOPC bilayers by differential scanning calorimetry. *Biochim. Biophys. Acta* 1191: 225-230.
13. Dempsey, C.E. & A. Watts (1987) A ^{2}H- and ^{31}P-NMR study of the interaction of melittin with DMPC bilayers and the effects of contaminating phospholipase A_2. *Biochem.* 26: 5803-5811.
14. Dempsey, C.E., G.D. Cryer & A. Watts (1987) The interaction of amino-deuteromethylated melittin with phospholipid membranes studied by ^{2}H-NMR. *FEBS Lett.* 218: 173-177
15. Bradshaw, J.P., C.E. Dempsey & A. Watts (1994) A combined X-ray and neutron diffraction study of selectively deuterated melittin in phospholipid bilayers: effect of pH. *Mol. Membr. Biol.* 11: 79-86.
16. Heyn, M.P., J. Westerhausen, I. Wallat & F. Seiff (1988) High-sensitivity neutron diffraction of membranes: location of the Schiff base end of the chromophore of bacteriorhodopsin. *Proc. Natl. Acad. Sci. USA.* 85: 2146-2150.
17. Hauss, T., S. Grzesiek, H. Otto, J. Westerhausen & M.P. Heyn (1990) Transmembrane location of retinal in bacteriorhodopsin by neutron diffraction. *Biochem.* 29: 4904-4913.
18. Ulrich, A.S., A. Watts, I. Wallat & M.P. Heyn (1994) Distorted structure of the retinal chromophore in bacteriorhodopsin resolved by ^{2}H-NMR. *Biochem.* 33: 5370-5375
19. Ulrich, A.S. & A. Watts (1993) ^{2}H-NMR lineshapes of immobilized uniaxially oriented membrane proteins. *Solid State Magn. Reson.* 2: 21-36.
20. Ulrich, A.S., M.P. Heyn & A. Watts (1992) Structure determination of the cyclohexene-ring of retinal in bacteriorhodopsin by solid-state ^{2}H-NMR. *Biochem.* 31: 10390-10399.
21. T. Hauss, G. Büldt, M.P. Heyn & N.A. Dencher (1994) Light-induced isomerization causes an increase in the chromophore tilt in he M intermediate of bacteriorhodopsin: a neutron diffratvcion study. *Proc. Natl. Acad. Sci. USA* 91: 11854-11858.
22. Ulrich, A.S , I. Wallat, M.P. Heyn & A. Watts (1995) Re-alignment of the retinal chromophore in the M-state of bacteriorhodopsin. *Nature Struct. Biol.* 2: 190-192
23. Patzelt, H., A.S. Ulrich, P. Düx, H. Egbringhoff, J. Ashurst, H. Oschkinat & D. Oesterhelt (1997) Structural investigations on native bacteriorhodopsin in detergent micelles by NMR spectroscopy. *J. Biomol. NMR* 10: 95-106

DEUTERATION OF BACTERIORHODOPSIN AND LIPIDS FOR NEUTRON STUDIES OF PURPLE MEMBRANE

Claude Pfister

Institut de Biologie Structurale and University of Grenoble
41 avenue des Martyrs, 38027 Grenoble Cedex 1, France.

1 - Introduction

The plasma membrane of the archaeon *Halobacterium salinarum* (previously named *Halobacterium halobium*) contains purple patches (Purple Membrane, PM) made up of a 26000 molecular weight protein, bacteriorhodopsin (BR), and lipids, with respective proportions of 75% / 25% by weight. The colour is due to a molecule of retinal, covalently bound to a lysine residue in the protein. It was quickly discovered that, for each photon absorbed by retinal, a photocycle of colour changes occurs in retinal, associated with transfer of one proton across the membrane, from the cytoplasmic side to the exterior.

The extraordinary opportunity for structural studies on BR arises from the natural two-dimensional organisation of the protein in the membrane purple patches, and the consequent feasibility of diffraction experiments on the native system. Electron diffraction patterns, since more than 20 years ago and up to recent investigations (Henderson and Unwin, 1975; Grigorieff et al., 1996), revealed that each molecule of BR consists of 7 alpha-helices spanning the membrane, that 3 BR molecules formed a trimer in the plane of the membrane, and that lipids and protein formed a 2D array with little or no lateral diffusion at low temperatures. It is only recently that a high-resolution X-ray 3D structure has been obtained, confirming the major features proposed earlier (Pebay-Peyroula et al., 1997).

Because BR is very abundant in PM, and because its function is particularily simple (light-driven proton pump), an enormous amount of biochemical investigations have been carried out, dealing with wild type BR, mutants and BR reconstituted and refolded from proteolytic fragments, using native patches as well as reconstituted systems. BR has become a paradigm to develop and test membrane protein structural methods

Neutron diffraction has played an essential role for further structural investigations on this protein. Deuteration of selected parts of PM (BR, retinal, lipids, see below) was largely used in these studies, to take advantage of the 4-fold lower coherent scattering cross section of ^{2}H with respect to ^{1}H. *H. salinarum* lends itself very well to *in vivo* ^{2}H-labelling, because it incorporates many nutrients with very few metabolic steps. The first part of the review below summarizes the major results of studies designed to localise the label by differential diffraction studies.

To function as a light-driven proton pump, PM needs to be hydrated and kept in a warm environment, and this has been related to the presence in BR of movements in the pico-nanosecond time range, detected by incoherent neutron scattering (Ferrand et al., 1993). To localize these movements, selective deuteration has also been used (Reat et al., 1998), taking advantage of the 40-fold lower incoherent cross section of ^{2}H with respect to ^{1}H. This will be reported in the second part of this review.

2 - Structural studies of PM by neutron diffraction and specific deuteration

2-1 : the arrangement of the transmembrane helices in BR

These studies were initiated some 20 years ago under the leadership of G. Zaccai, D. Engelman and J.-L. Popot (Engelman & Zaccai, 1980; Trewhella et al., 1983, 1986; Popot et al., 1986, 1989; Samatey et al., 1994). In all cases, the incorporation of deuterated amino-acids in BR was done biosynthetically, taking advantage of the fact that this Archae has a very simple metabolism and incorporates almost directly the amino-acids of the growth medium. Thus the labelling was directed by simply manipulating the nature and amounts of hydrogenated/deuterated amino-acids in the culture. Indeed, the absence of spillover of deuteraition to aminoacids in BR other than the selected ones in the growth medium was verified. Yet, the deuterated amino-acids are spread over all the helices of BR. making the analysis of the results difficult. This drawback has been circumvented in some experiments by a reconstitution of the 7-helical bundle from two chymotryptic fragments (fragment C-2, encompassing the first two putative transmembrane helices; fragment C-1, comprising the rest of BR, see Popot et al., 1989), each of such fragments arising from a different PM culture with selective deuteration on some (or all of) amino-acids. This led to an abundance of diffraction data, and cross-controls of interpretations.

One must emphasize the assumptions which are necessary for the analysis of the neutron diffraction patterns; and of the differences observed under different deuteration conditions :

i) electron diffraction is carried out on single PM patches, giving the diffraction pattern of a 2D crystal; in neutron diffraction experiments, obtention of a correct signal/noise ratio needs the use of a stack of many PM patches; these patches are indeed parallel to one another, but with a rotational disorder which leads to a diffraction pattern characteristic of a powder; this leads to overlapping peaks in the diffraction pattern, and one has to split them into corresponding contributions; this is done with the help of the corresponding separated spots in the diffraction pattern of single patches obtained from electron diffraction data; this is valid only because of the relatively great homogeneity of diffraction properties within each of the components of PM (protein on one side, lipids on the other)

ii) the phases of the different diffracted neutron waves are unknown, and they are approximated by those obtained from electron diffraction experiments;

iii) the analysis of the differences in diffraction data obtained from all-hydrogenated versus selectively deuterated samples can be carried out in two different ways

- calculation of the so-called difference-Fourier maps, but this is valid only if the amount of labelling is low enough (≈ 20%), and provided one can neglect the noise brought about by the fact that BR is not centrosymetric; this allows to directly visualize the location of the label
- use of the so-called model building, by calculation of the theoretical diffraction pattern of a model, and then selection by minimal mean square deviation with the measured map; this has to be used if the amount of labelling exceeds ≈ 20%; because the number of adjustable parameters is higher that the number of diffraction peaks, several models are most often left possible.

These approaches have led to the description of BR as an inside-out protein, with hydrophobic amino-acids facing the exterior of the molecule (in contact with the lipids) and hydrophilic amino-acids facing the interior of the protein (lining the proton channel). It has allowed to correlate the putative transmembrane helices (i.e. stretches in the sequence) to the electron microscopy density maps (i.e. spatial positions in the 3-D structure). It has allowed to define the orientation in space of these helices. All these results were fully confirmed by the high-resolution structure determined only very recently (Pebay-Peyroula et al., 1997).

These studies indeed need (and rely on) the knowledge of a structure of the system to start with, but can well operate with low resolution data (say ≈ 10 Å); this is because of the high contrast between ^1H and ^2H brough by selective deuteration. In the example of BR, the accuracy of helix rotational orientation determination was about 20°, leading to aminoacid positions defined with an accuracy of 1-2 Å. Yet, the exact positions of side chains remained beyond the possibilities of this approach. The potential application of structural studies by neutron diffraction and selective deuteration encompass any crystalline (2D or 3D) system known at low resolution.

2-2 the localisation of retinal in BR

Retinal, the natural chromophore of BR, is synthetized and incorporated in wild type BR during cell growth. Its localization, using deuterated retinal and neutron diffraction, is also a story beginning 20 years ago. In the first studies, the approach was either to remove retinal from BR (by bleaching in the presence of hydroxylamine, King et al., 1979), or to inhibit its synthesis (cultures in the presence of nicotine. Jubb et al., 1984), and then add extrinsic deuterated retinal. The preferred approach now is to use a retinal deficient mutant (retinal$^-$; Seiff et al., 1985; Heyn et al., 1988; Hauss et al., 1990). Using retinal synthetized and labelled on any part of its structure (polyene chain, Schiff base end, cyclohexene ring), localization of its different parts has been reported.

Because the amount of labelling brought by retinal is always low, the difference Fourier maps analysis has been used and controlled by model building. This allowed:

i) to localize the nitrogen of the Schiff base between helices 2 and 6, and the ring in the vicinity of helix 4 (Seiff et al., 1985; Heyn et al., 1988)

ii) to define the depth of the chromophore with respect to the membrane plane (cyclohexene ring at ≈ 10Å and Schiff base end at ≈ 17 Å from the surface), and the tilt of the molecule with respect to the membrane plane (≈ 40°) (Hauss et al., 1990)

iii) to describe the orientational change of retinal due to photon absorption (in the so-called dark and M states) (Hauss et al., 1994)

1-3 the localisation of glycolipids in PM

In the course of a study between two BR species (wild type and mutant D96N) by Weik et al. (1998a), differences of neutron scattering densities at the level of lipids were observed, which could correspond to 1 glycolipid replacing 1 phospholipid. The eventual importance and role of lipids in the structure and function of the PM had been also put forward previously (Glaeser et al., 1985; Grigorieff et al., 1995).

Several characteristics of lipids and glycolipids in PM prompted Weik et al. (1998b) to explore the localization of glycolipids by neutron diffraction with selective duteration of these glycolipids

i) the lipids in PM consist of 10% neutral lipids, 27% glycolipids (essentially a sulfated-triglycosylarchaeol « TGA-1 » with a polar head group consisting of glucose, mannose and galactose), and 63% phospholipids; outside the patches of PM, only traces of TGA-1 are present; this raised the question of the role of the glycolipid in BR trimeric regular array in PM, and therefore of the localization of TGA-1 with respect to BR.

ii) feeding *H. Salinarum* cultures with $^{2}H_{7}$-glucose labelled exclusively the head group sugar moieties of TGA-1, without any spillover to other lipids and to BR (Weik et al., 1998b).

iii) the lateral diffusion of lipids in PM was shown to be low enough to allow their localization by electron diffraction, and neutron diffraction should as well allow this localization. The nature of the head groups of lipids could not be determined by electron diffraction, because of orientational disorder; by specific deuterium labelling of the sugars in the headgroups, localization of glycolipids would be feasible

The diffraction patterns of natural PM and PM deuterated on glycolipids was then analyzed by difference Fourier and verified by model building (using the same approach as in § 2-1 for superposition splitting and phasing of diffracted waves). Because of the 3-fold rotational axis of symmetry in the BR trimer, each difference peak (related to one BR molecule) was present at three copies with symmetry relationship in each PM unit cell (containing a BR trimer). Two difference peaks appeared per BR: one in the space inside the trimer, and one located between the trimers near outward-looking helices G and A in the structure (Grigorieff et al., 1996; and see fig 4 in Weik et al., 1998b).

The amount of glycolipid corresponding to each difference peak was then evaluated taking into account the amount of deuteration per glycolipid (measured by mass spectroscopy to correspond to a mean of 9 deuterons per glycolipid), and the intensity of the difference spectrum scaled by the intensity of neutron diffraction by an helix for which the localisation and the amino-acid content is non-ambiguous (i.e. helix B, Grigorieff et al., 1996). It was then calculated that

- one glycolipid per BR was located next to the helices facing the interior of the trimer; therefore 3 glycolipids were sequestered inside the BR trimer, and no other lipid was present in this region
- one glycolipid per BR was located next to the helices facing the exterior of the trimer. Phospholipids are therefore only present between the BR trimers.

The localization of the glycolipid difference peaks was then compared to the localization (in projection on the plane of the membrane) of selected aminoacids in BR, taken from the structure of Grigorieff et al. (1986). Aromatic aminoacids, and especially Trp, were chosen for this comparison, as these are often located at the exoplasmic hydrophobic-hydrophilic interfaces and have been proposed for stacking interactions with sugar residues (Cowan, 1993). All the aromatic residues on the exoplasmic side of BR are located vertically no further than 5Å into the membrane from the edge of the transmembrane helices; W80 and Y64 point toward the glycolipid peak in the trimer interior, and W12 is over the glycolipid peak outside the trimer structure. This feature is therefore completely compatible with the existence of interactions between these aromatic side chains and the sugar moieties of the glycolipids in the exoplasmic leaflet, although this information is limited to the projections on the plane of the membrane, without information perpendicular to this plane.

It could then be suggested that such specific protein-glycolipid interactions participate in the BR trimer and lattice formations in PM. Such hypothesis deserves further investigations as for its generality. It is interesting to note features existing in the closely related protein in the same organism, Halorhodopsin (HR) :

- HR probably forms trimers in the membrane (as seen from Circular Dichroïsm spectra, see Hasselbacher et al., 1988) and indeed possesses a conserved W80 residue, just as that which in BR interacts with the glycolipid inside the trimer
- HR does not form a 2D array of trimers, and the residue corresponding to W12 in BR, suggested to participate in lattice formation, is always a serine in the different HR studied.

3 - Dynamical studies of BR by elastic incoherent neutron scattering and selective deuteration of BR.

In a coherent radiation scattering experiment (as above), the atomic distribution in a particle is measured from the angular distribution of scattered intensities, and the scattering pattern results from the interference between waves scattered coherently by the atoms at different positions. In an incoherent neutron scattering, the waves that interfere

are those scattered by a single nucleus occupying different positions as a function of time (Bée, 1988). For neutrons scattered without energy change (elastic scattering), the angular distribution of the intensity of scattered neutrons contains information on the amplitudes of the motions of atoms as they move during the characteristic time of the neutron experiment (typically nanoseconds for the experiments presented below). In practice, the atoms involved are essentially ^{1}H-atoms (see introduction), and the observed movements in the nanosecond time range correspond to the thermal fluctuations of the aminoacid side chains to which they are attached.

In an elastic incoherent neutron scattering experiment, the intensity of the elastically scattered neutrons is related to the scattering angle (2Θ) by an expression which allows to derive the mean square displacements $\langle u^2 \rangle$ of ^{1}H-atoms (Smith, 1991)

$$\ln I\ (Q, el) = A - (\langle u^2 \rangle Q^2) / 6$$

where I (Q, e) is the elastic incoherent scattering for the scattering vector Q ($Q = 4\pi \sin \Theta / \lambda$).

The first experiments on myoglobin by Doster et al. (1989) measured $\langle u^2 \rangle$ as a fonction of temperature, and pointed to the existence of two temperature ranges : i) at low temperatures (20-200 K approximately), $\langle u^2 \rangle$ varies linearly with temperature, reflecting the existence of harmonic vibrational movements in the protein; the slope of the $\langle u^2 \rangle(T)$ curve represents the inverse of the mean force constants in the molecule; ii) above 200K (the transition temperature), $\langle u^2 \rangle(T)$ deviates from the harmonic behaviour, and large amplitude movements take place. In BR, the existence of large amplitude non-harmonic movements has been shown to be related to the function of the protein as a proton pump : they appear only on hydrated samples and at temperatures above the transition temperature (260 K in this case). Yet, it must be emphasized that two instrumental parameters must be taken into account in the interpretation of the obtained results : the energy resolution and the Q-range of the spectrometer, which define respectively the time-window and the amplitude-window of the observed movements (Réat et al., 1997). It was demonstrated that, for BR movements analyzed in a low Q-range, two different transition temperatures exist, one at ca. 150K and the other at ca. 260K, whereas movements analyzed in a higher Q-range present only one transition temperature (at ca. 230-260K).

To focus on the motions of selected groups in BR, which may be involved more directly in the functioning of the protein, a selective ^{1}H-^{2}H labelling was used (Réat et al., 1998). The part of BR selected for study is located toward the extracellular (EC) half of the protein, and includes the retinal and its close environment. Advantage was taken of the fact that Met and Trp residues were mostly located in this EC half. A special PM sample (selectively hydrogenated PM, SH-PM) was then prepared by growing *H. Salinarum* in a deuterated medium consisting of a mixture of all-deuterated aminoacids supplemented by an excess of hydrogenated Met and Trp, and in the presence of hydrogenated retinal. As controls and comparison, all-deuterated and all-hydrogenated PM (D-PM and H-PM respectively) were prepared under the corresponding conditions of all-deuterated or all-hydrogenated growth medium. In SH-PM, although the ^{1}H-atoms represent only 6% of the total ^{1}H or ^{2}H, their incoherent signal contributes ca. 72% of the

total scattering of the membrane; of the remaining 28%, ca. 7% is from ^2H from lipids, and ca. 21% is from ^2H in the unlabelled part of BR; the $<u^2>$ obtained for this sample is then dominated by the amplitudes of motions of the labelled atoms in BR.

All the experiments were carried out on hydrated samples, and analyzed in a low Q-range (0.6-1.8 $Å^{-1}$). They display the following characteristics:

- PM presents a first dynamical transition at ca. 150K, and a second one at ca. 260K. This second dynamical transition, absent from experiments carried out on dry samples, is interpreted as being due to solvent effect (melting of hydration water).
- PM present exactly the same transition temperatures and the same amplitudes of $<u^2>$; this testifies that deuteration has not altered significantly the observed global movements of PM.
- SH-PM reveals three major differences with respect to H-PM or D-PM :

i) the first transition temperature is observed at ca. 200K, i.e. about 50K higher than for H-PM or D-PM.

ii) no clear transition temperature is observed at the melting of hydration water (260K); the amplitudes of movements increase much less above 260K than for H-PM or D-PM

iii) the amplitudes of movements at room temperature are consequently much less in SH-PM (ca. 1.2 $Å^2$) than in H-PM or D-PM (2.1 $Å^2$)

These results show that the labelled groups are more rigid than the rest of the molecule, and that they are shielded from hydration water and melting of it. This was temptatively correlated to a need of heterogeneity of functional movements in BR. The stereospecific initial photoisomerization of retinal from the all-trans to the 13-cis conformation must be selected by the retinal binding pocket and is best done in a rigid environment; in the same idea, the switch of acessibility of retinal from the extracellular space (EC) to the cytoplasmic one (CP) would also be best performed in a rigid environment. On the other hand, the accessibility switch of retinal is associated with substantial conformational changes in the CP half of the protein, and this would require that the protein possesses soft regions. One therefore is lead to describe BR as a soft body around a rigid anchor, perhaps provided by the retinal pocket and the EC half of BR.

One must stress that the neutron approach provides the most direct and possibly unique quantitative data to the lubricant movements in the pico-nanosecond time range underlining functional movements in the micro-millisecond time range. The present study proves the sensibility of the method toward local determinations of movements (only 6% of the overall H-atoms in PM were hydrogenated). Such data are needed to test models from molecular dynamics simulations, and to answer questions as : does and how specific dynamics have to compromise between the requirements of flexibility and those of function ? has specific dynamics adapted to different conditions of solvent environment, temperature or pressure ?

4 - References

Bée M. (1988). Quasi-elastic neutron scattering: principles and applications in solid state chemistry, biology and materials science. *(Adam Hilger, Bristol, U.K.).*

Cowan S.W. (993). Bacterial porins: lessons from three high-resolution structures. *Curr. Opin. Struct. Biol. 3, 501-507.*

Doster W., Cusack S. and Petry W. (1989). Dynamical transition of myoglobin revealed by inelastic neutron scattering. *Nature (London) 337, 754)756.*

Engelman D.M. and Zaccaï G. (1980). Bacteriorhodopsin is an inside-out protein. . *Proc. Natl. Acad. Sci. USA 77, 5894-5898.*

Ferrand M., Dianoux A.J., Petry W. and Zaccaï G. (1993). Thermal motions afunction of bacteriorhodopsin in purple membranes: effect of temperature and hydration studied by neutron scattering. *Proc. Natl. Acad. Sci. USA 90, 9668-9672.*

Glaeser R.M., Jubb J.S. and Henderson R. (1985) Structural comparison of native and deoxycholate-treated purple membrane. *Biophys. J. 48, 775-780.*

Grigorieff N., Beckmann E. and Zemlin F. (1995). Lipid location in deoxycholate-treated purple membrane at 2.6 Å. *J. Mol. Biol. 254, 404-415.*

Grigorieff N., Ceska T.A., Downing K.H., Baldwin J.M. and Henderson R. (1996). Electron-crystallographic refinement of the structure of bacteriorhodopsin. *J. Mol. Biol. 259, 393-421.*

Hasselbacher C.A., Spudich J.L. and Dewey T.G. (1988). Circular dichroïsm of halorhodopsin: comparison with bateriorhodopsin and sensory rhodopsin I. *Biochemistry 27, 2540-2546*

Hauss T., Büldt G., Heyn M.P. and Dencher N.A. (1994). Light-induced isomerization causes an increase in the chromophore tilt in the M intermediate of bacteriorhodopsin: a neutron diffraction study. *Proc. Natl. Acad. Sci. USA 91, 11854-11858.*

Hauss T., Grzesiek S., Otto H., Westerhausen J. and Heyn M.P. (1990). Transmembrane location of retinal in bacteriorhodopsin by neutron diffraction. *Biochemistry 29, 4904-4913.*

Henderson R. and Unwin P.N.T. (1975). Three-dimensional model of purple membrane obtained by electron microscopy. *Nature 257, 28-32.*

Heyn M.P., Westerhausen J., Wallat I. and Seiff F. (1988). High-sensitivity neutron diffraction of membranes : location of the Schiff base end of the chromophore of bacteriorhodopsin. *Proc. Natl. Acad. Sci. USA 85, 2146-2150.*

Jubb J.S., Worcester D.L., Crespi H.L. and Zaccaï G. (1984). Retinal location in purple membrane of *Halobacterium halobium* : a neutron diffraction study of membranes labelled *in vivo* with deuterated retinal. *The EMBO J. 3, 1455-1461.*

King G.I., Stoeckenius W., Crespi H.L. and Schoenborn B.P. (1979). The location of retinal in the purple membrane profile by neutron diffraction. *J. Mol. Biol. 130, 395-404..*

Pebay-Peyroula E., Rummel G., Rosenbusch J. and Landau E.M. (1997). X-ray structure of bacteriorhodopsin at 2.5 Å from microcrystals grown in lipidic cubic phases. *Science 277, 1676-1681.*

Popot J.L., Engelman, D.M., Gurel O. and Zaccaï G. (1989). Tertiary structure of bacteriorhodopsin; positions and orientations of helices A and B in the structural map determined by neutron diffraction. *J. Mol. Biol. 210, 829-847.*

Popot J.L., Trewhella J. and Engelman D.M. (1986). Reformation of crystalline purple membrane from purified bacteriorhodopsin fragments. *The EMBO J. 5, 3039 3044.*

Réat V., Patzelt H., Ferrand M., Pfister C., Oesterhelt D. and Zaccaï G. (1998). Dynamics of different functional parts of bacteriorhodopsin: H-^{2}H labelling and neutron scattering. *Proc. Natl. Acad. Sci. USA 95, 4070-4975.*

Réat V., Zaccaï G., Ferrand M. and Pfister C. (1997). Functional dynamics in purple membrane. In *Biological macromolecular dynamics,(Adenine, Guiderland, N.Y.)* pp. 117-122.

Samatey F.A., Zaccaï G., Engelman D.M., Etchebest C. and Popot J.L. (1994). Rotational orientation of transmembrane alpha-helices in bacteriorhodopsin; a neutron diffraction study. *J. Mol. Biol. 236, 1093-1104.*

Seiff, F., Wallat I., Ermann P. and Heyn M.P. (1985). A neutron diffraction study on the location of the polyene chain of retinal in bacteriorhodopsin. . *Proc. Natl. Acad. Sci. USA 82, 3227-3231.*

Smith J.C. (1991). Protein dynamics: comparison of simulation with inelastic neutron scattering experiments. *Q. Rev. Biophys. 24, 227-291.*

Trewhella J., Anderson S., Fox R. Gogol E., Khan S. and Engelman D.M. (1983). Assignement of segments of the bacteriorhodopsin sequence to positions in the structural map. *Biophys. J. 42, 233-241.*

Trewhella J., Popot J.L., Zaccaï G. and Engelman D.M. (1986). Localization of the two chymotryptic fragments in the structure of renatured bacteriorhodopsin by neutron diffraction. *The EMBO J. 5, 3045-3049.*

Weik M., Patzelt H., Zaccaï G. and Oesterhelt D. (1988b). Localization of glycolipids in membranes by in-vivo labelling and neutron diffraction. *Mol. Cell. 1, 411-419.*

Weik M., Zaccaï G., Dencher N.A., Oesterhelt D. and Hauss T. (1988a). Structure and hydration of the M-state of the bacteriorhodopsin mutant D96N studied by neutron diffraction. *J. Mol. Biol. 275, 625-634.*

PREPARATION, USES AND ABUSES OF PERDEUTERIATED PROTEINS

David Brockwell[1], Serena Cooper[2], Lu Yu[3], Debra Bloor[1], David Attwood[1], Simon J. Craskell[3], John R. Helliwell[2] and Jill Barber[1]

[1]*School of Pharmacy and Pharmaceutical Sciences*

and

[2]*Department of Chemistry,*

University of Manchester, Manchester, UK, M13 9PL

[3]*Michael Barber Centre for Mass Spectrometry,*

UMIST, PO Box 88, Manchester UK, M60 1QD

Many NMR and neutron scattering experiments involving perdeuteriated proteins have been carried out over the past several years. Most depend upon the assumption that perdeuteriation does not profoundly affect the physicochemical and biological properties of a protein. There are good reasons to believe this. Perdeuteriated ribosomes reconstituted with a single protiated protein are functional1. Perdeuteriated Staphylococcal nuclease has essentially the same structure as the protiated protein2. However, there are also good reasons to doubt that perdeuteriated proteins are always very similar to their protiated counterparts. A perdeuteriated protein has a molecular weight approximately 5% higher than that of the corresponding protiated protein. The short C-D bond also increases the density of the protein. Crespi and Katz showed that perdeuteriation decreases the thermal stability of phycocyanins3. In the present study we have set out to compare the properties of protiated and perdeuteriated elongation factor Tu (EFTu) and glutathione S-transferase.

A deuteriophilic E. coli strain, MRE600D was prepared by adaptation of E. coli MRE600 to M4-succinate / D2O medium followed by plating on agar based on the same medium. Single colonies were selected, grown up and subcultured in triplicate. The plate-growth-subculture cycle was repeated until reproducible growth rates, indicating genetic homogeneity, were obtained.

E. coli MRE600D was transformed (separately) with the plasmids pTrc99AtufA, which overproduces EFTu and pGEX-2T, which overproduces Schistosoma japonicum GST. Yields of EFTu obtained were 50-150 mgl-1 for protiated EFTu and 80-150 mgl-1 for the perdeuteriated factor. Yields of GST were relatively poor (up to 10 mgl-1) but similar for the protiated and perdeuteriated media.

Electrospray mass spectrometry was carried out on both the perdeuteriated and protiated EFTu following a long aqueous isolation procedure. The protiated protein was then incubated in D2O under mildly denaturing conditions and the perdeuteriated protein was incubated under the same conditions in H2O. Mass spectra allowed us to calculate that the perdeuteriated protein was 95% deuteriated on carbon and that 38 heteroatom-deuterons survived the isolation. The signal in the mass spectrum of the perdeuteriated protein is narrow (19 Da at half-height, the same value as for the protiated EFTu), indicating uniformity of deuteriation levels in the sample.

Trypsin-nicked EFTu (protiated and perdeuteriated) was crystallized. The 4 Å resolution data showed no significant differences between the two factors, and both these closely resembled the published structure of EFTu:GDP. Circular dichroism spectra were similar but not superimposable. Denaturation of the perdeuteriated and protiated factors was carried out at 55oC in D2O. The half-life of the perdeuteriated protein under these conditions was about half that of the protiated protein. Preliminary data indicate, however, that perdeuteriation confers stability to inactivation by chymotrypsin.

Electrospray mass spectrometry of perdeuteriated GST again showed that deuteriation at carbon was around 95%. Again the peak was narrow, indicating uniform deuteriation across the sample. This was in very stark contrast to the mass spectrum of a partially deuteriated sample prepared by growing the strain BL21pGEX-2T on Luria Bertini medium made up in D2O. The electrospray mass spectrum showed peaks corresponding to almost every mass value between 0% and 100% deuteriation.

Circular dichroism spectra of the protiated and perdeuteriated transferases were (again) similar but not superimposable. The KM for the model substrate, 1-chloro-2,4-dinitrobenzene was 0.95 + 0.06 mM for protiated GST and 1.10 + 0.11 mM for the perdeuterated protein, very similar, but not necessarily identical values.

Thermal denaturation was assessed by incubating protiated and perdeuteriated GST for 10 minutes at 10 different temperatures in the range 35 – 60 oC. The inactivation profiles followed the same general shape for the two proteins but the temperature at which half the enzyme activity was lost was 51.3 + 0.3oC for the protiated factor but 48.5 + 0.4oC for the perdeuteriated GST.

The degradation of protiated and perdeuteriated GST's by chymotrypsin was studied. GST (125 (l, 0.2 mgml-1) was treated with chymotrypsin (20 (l, 2 mgml-1) and the residual activity was measured at 9 intervals over 200 minutes. The half-life of the protiated GST was 50 minutes under these conditions, that of the perdeuteriated GST only 25 minutes.

These results indicate that perdeuteriated EFTu and GST both have some markedly different properties from the parent protiated proteins, but that these differences are found in the behaviour of the bulk solutions rather than of the individual molecules.

RP May, V Nowotny, P Nowotny, H Voss and KH Nierhaus, EMBO J., 1992, 11, 373.

TR Gamble, KR Clauser and AA Kossiakoff, Biophys. Chem. 1994, 53, 15.

A Hattori, HL Crespi and JJ Katz, Biochemistry, 1965, 4, 1213.

SJ Cooper, D Brockwell, J Rafferty, D Attwood, J Barber and JR Helliwell, J. Chem. Soc. Chem. Commun. 1998, 1063.

DYNAMICS AND TRANSMISSION OF CONFORMATIONAL PERTURBATION ON C-TERMINAL TRUNCATION OF STAPHYLOCOCCAL NUCLEASE

M. Kataoka[1], M. Ferrand[3], A.V. Goupil-Lamy[2], H. Kamikubo[1], J. Yunoki,[1] T. Oka[1] and J.C. Smith[2]

[1] Department of Earth and Space Science, Graduate School of Science, Osaka University, Toyonaka 560, Japan.

[2] SBPM, DBCM, C.E. Saclay, 91191 Gif-sur-Yvette Cedex, France.

[3] Institut Laue Langevin, B.P. 156X, 38042 Grenoble Cedex 9, France.

ABSTRACT

Truncation of the 13 C-terminal residues of Staphylococcal nuclease leads to disordering of the protein which nevertheless retains its capacity to function and recovers its native structure on inhibitor binding. To probe structural and dynamical changes on truncation, we combined neutron scattering techniques and molecular dynamics simulations. Both the experiments and simulations indicate that truncation leads to an increase in the amplitude of the local internal motions. The simulations also provide evidence for rapid denaturation of the protein on truncation and transmission of the perturbation to the active site, suggesting that the structures of the C-terminal residues and the active site are interdependent. The implications of the results for the relationship between flexibility and folding of the native protein are hereafter discussed.

INTRODUCTION

In recent attempts to understand protein folding pathways much attention has been focussed on protein in non-native conditions, in particular in compact states that retain a degree of secondary structure. A battery of experimental and theoretical techniques has been applied to characterise these states (1-3) which have provided much information on their structural properties. A comprehensive physical characterisation of these systems is likely to be necessary for an appreciation of their thermodynamic properties. This requires that the structural data be refined and complemented with information on the internal dynamics of the protein.

Very recently several nuclear magnetic resonance (NMR) relaxation experiments have been performed on partially-denaturated states of proteins (4-5). These experiments allow a limited amount of information to be obtained on the dynamics of individual labelled atoms on timescales shorter than the overall molecular tumbling relaxation time (typically a few nanoseconds), given an analytical model to interpret the relaxation data which involves order parameters and one or two characteristic dynamical time constants.

Inelastic and Quasielastic neutron scattering (INS & QENS) represent dynamical techniques complementary to NMR (6). In the experiments reported here the scattering from the sample is dominated by incoherent scattering from the hydrogen atoms, thus allowing the average dynamics of hydrogen atoms in the protein to be probed on the picosecond timescale and Angstrom length scale.

The physical characterisation of protein denaturation promises to furnish much useful information on folding and stability. The production of denatured protein involves the perturbation of either the environment of the protein (by varying, for example, the temperature or solvent composition), or the chemical structure of the protein itself, the latter approach allowing physiological external conditions to be retained. A particularly interesting example of denaturation on protein modification occurs on deletion of the 13 C-terminal residues of Staphylococcal Nuclease (Snase), a 149-residue protein with no disulfide bonds. Truncation of the C-terminus extremity leads to a state that is denatured but compact (7-9). Remarkably, the truncated protein conserves its enzymatic activity in the presence of salt and DNA (7). Moreover the addition of an inhibitor, deoxythynidine 3',5' biphosphate (pdTp), and Ca^{2+} to the truncated protein recovers a circular dichroism profile identical to the wild type and the radius of gyration reduces to 15.8±0.2Å, again close to the value for the native state (8). Therefore, the truncated protein retains its ability to fold.

The understanding of this reversible folding process on inhibitor binding will require a detailed characterisation of the physical properties of the truncated and native states. In particular, how the structural communication between the active site and the rest of the protein takes place. In that aim, we have investigated the dynamical properties of native and truncated Snase using quasielastic neutron scattering and molecular dynamics (MD) simulations. QENS, in which energy and momentum are exchanged between the neutrons and the sample, provides a direct information on the timescales and forms of equilibrium dynamics of atoms in proteins (6,10). MD is complementary to QENS in that motions of the similar time and length scales (ps-ns and Å) are sampled.

MATERIAL & METHODS

Sample preparation

Wild type (WT) and truncated (referred as to fragment, FR) Snase were expressed in *Escherichia Coli*, and purified with ion exchange chromatography (11-12). To maximize the signal from the proteins the experiments were performed in D_2O solution. The isolated proteins were dialysed against pure water and lyophilized. The lyophilized powder was dissolved in D_2O to exchange all labile protons, and then lyophilized. This procedure was repeated 3-4 times. The resulting powder was dissolved in D_2O and used as the specimen. The concentration of D_2O/protein solutions, measured spectrophotometrically, were almost similar: 82.0 mg/ml for WT and 78.8mg/ml for the FR.

Quasielastic neutron scattering

The neutron scattering experiments were performed on the IN5 time-of-flight spectrometer at the High-Flux Reactor at the Institut Laue Langevin. The incoming wavelength was 5.12Å, with an associated elastic energy resolution of about 100μeV (Full Width at Half Maximum). This means that motions on a timescale faster than ~50 ps could be detected. The instrumental set-up allowed spectra to be measured over the energy range 1eV to -1.2meV and the Q-range 0.3-2 $2Å^{-1}$. Spectra were collected at 300K for the two protein solutions and pure D_2O. Samples were contained in aluminium cells of 1.5mm thickness, leading to transmissions around 87-90%. The protein solutions were measured for 40 hours each and the solvent for 36 hours. The counting rate on each of the detectors were stable with time, indicating the absence of aggregation or precipitation during the experiment.

The raw data on the protein and solvent samples were corrected for detector efficiency with respect to a standard vanadium sample. The signal from the empty cell was subtracted taking into account sample geometry corrections for the attenuation of singly-scattered neutrons. The contribution of the solvent to the solution scattering was subtracted assuming that the scattering per mole of the solvent is identical in the pure solvent and in the protein solution and that the density of D_2O in the solution is 1.10567 g/cm^3. Corrected incoherent dynamic

structure factors, $S_{inc}(Q,\omega)$, were derived at 13 scattering angles for the native and truncated proteins, corresponding to a Q-resolution of about 0.2Å^{-1}.

Molecular dynamics simulation

In preliminary short MD simulations of the Snase systems it was found that truncation of the native protein led to significant denaturation on the 10^{-10}s timescale under physiological conditions (13). Simulations were performed on wild-type and truncated Snase molecules in explicit water at 300K using the CHARMM program (14), version 23. This version use the semi-empirical potential function with parameter set 22. The starting structures for both the simulations were derived from the 1.7Å X-ray analysis of native Snase (15, 1STN.PDB in Brookhaven Protein Data Bank. All protein atoms were included in the simulation. The proteins were immersed in boxes of water molecules containing counterions for electrical neutrality. The boxes were replicated with periodic boundary conditions. MD simulations were performed for 1.29ns on the truncated protein and 0.46ns on the native protein.

RESULTS

Quasielastic neutron scattering experiments

In a neutron incoherent-scattering experiment, the number of neutrons scattered into a solid angle $\delta\Omega$ with an energy bandwidth $\delta\omega$ at a given energy transfer $\hbar\omega$ and momentum transfer $\hbar\mathbf{Q}$ ($\mathbf{Q}=\mathbf{k}-\mathbf{k}_0$, where $\mathbf{k}_0$ and $\mathbf{k}$ are the incident and scattered wavevectors, respectively), is given by the differential scattering cross-section (6,10),

$$\frac{\partial^2_{inc}}{\partial\Omega.\partial\omega} = \frac{k}{k_0} S_{inc}(Q,\omega) \qquad [1]$$

$S_{inc}(Q,\omega)$, the incoherent dynamic structure factor can be expressed as the time Fourier transform of the intermediate scattering function, $I_{inc}(Q,t)$, a self-correlation function, defined in terms of Van Hove formalism (16) by

$$I_{inc}(Q,t) = \frac{1}{N}\sum_{l=1}^{N} b^2_{l,inc}\left\langle \exp\left\{-iQ.\hat{R}_l(0)\right\}\exp\left\{-iQ.\hat{R}_l(t)\right\}\right\rangle \qquad [2]$$

where $\hat{R}_l(0)$ and $\hat{R}_l(t)$ are the Heisenberg position operators of the "l" nucleus at time 0 and time t, each with an associated incoherent scattering length $b^2_{l,inc}$. The term in angle brackets is the self-correlation function averaged over a large number of molecules in equilibrium at temperature T. Incoherent neutron scattering considers only the individual contributions of each nucleus and can be interpreted to investigate individual atomic motions. It can be divided into three different scattering zones: elastic, quasieleastic, and inelastic. Incoherent inelastic neutron scattering accounts for nonzero energy transfer with vibrational modes in the molecule and is adapted to sample periodic motions on a timescale of 0.1-100ps. Incoherent quasielastic neutron scattering results from relaxational processes such as nonvibrational and diffusive motions, which are mainly stochastic, and, therefore, have a highest probability at zero energy transfer. Quasielastic scattering appears as a broadening of the elastic peak. Elastic scattering gives information on geometrical parameters of the motions involved. The presence of an elastic scattering component indicates that the dynamics is confined to a microscopic volume over the accessible timescale.

If we restrict the measurement of $S(Q,\omega)$ to the "elastic-quasielastic" domain, we can expressed $S(Q,\omega)$ as:

$$S_{inc}(Q,\omega) = A_0(Q)\delta(\omega) + S_{qe}(Q,\omega) \quad [3]$$

where $A_0(Q)$ is the elastic incoherent structure factor (EISF) and $S_{qe}(Q,\omega)$ is the quasielastic structure factor. The analytical forms of $A_0(Q)$ and $S_{qe}(Q,\omega)$ depend on the nature of the dynamics involved. However, as most of the dynamical diffusive processes are characterized by exponential relaxation decays, many simple dynamical models result in a Lorentzian form for $S_{qe}(Q,\omega)$. Consequently, the signal detected from the protein, can be decomposed as follows:

$$S_{inc}(Q,\omega) = A_0(Q)\delta(\omega)R(\omega) + [1 - A_0(Q)]L(Q,\omega) \otimes R(\omega) \quad [4]$$

in which $S_{inc}(Q,\omega)$ is expressed as the convolution product of the dynamic structure factor with $R(\omega)$, the instrumental resolution function. In the above expression, $L(Q,\omega)$ represents the lorentzian component. $R(\omega)$ was obtained by measuring the spectrum from a purely elastic incoherent scatterer (vanadium) and has an approximately triangular shape for IN5.

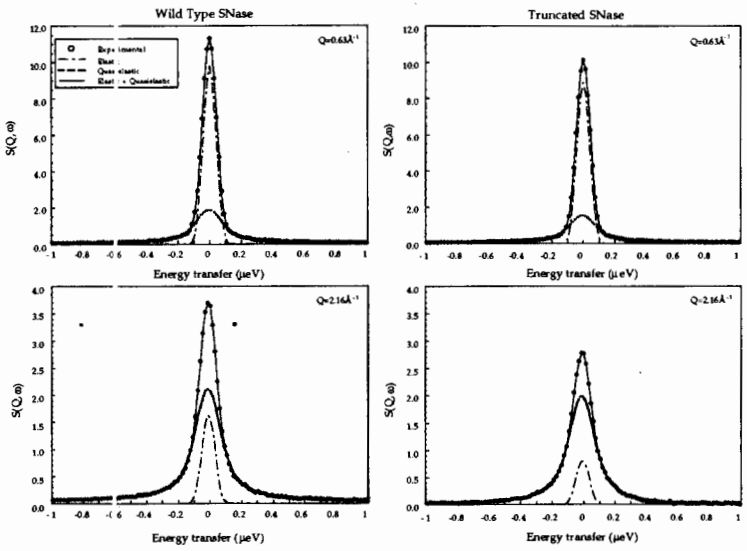

Figure 1. Dynamic structure factor with the results of fits of Eq. 4 to the data for native Snase (left) and truncated Snase (right). For both panels, top figure is the data at Q=0.63Å^{-1} and bottom at Q=2.16Å^{-1}. The open circles are the corrected experimental data and the solid lines are the results of the fits. The fits allow the scattering function to be decomposed into elastic (dot-dashed lines) and quasielastic (dashed lines) contributions.

In Fig. 1 are displayed $S(Q,\omega)$ for the native and truncated proteins at Q=0.63Å^{-1} and 2.16Å^{-1}. Low-Q and high-Q scattering give information on the long and short length scale dynamics, respectively. Whereas for the low-Q scattering profiles of the both proteins are similar, at high-Q the scattering from the fragment is less intense. Equation 4 was fitted

separately to all 13 scattering angles, with $A_0(Q)$ and the width of the Lorentzian as the variables. The results of the fits indicate that for both proteins the low-Q scattering is dominated by the elastic term (at Q=0.3Å-1, native and fragment scatter only elastically), whereas at high-Q the quasielastic scattering becomes more intense. The figures also show that in the truncated protein the quasielastic contribution is increased at high-Q relative to the elastic scattering when compared to the native Snase. The modification of the high-Q dynamic structure factor on truncation is consistent with an increase of the amplitude of the local motions of the denatured protein.

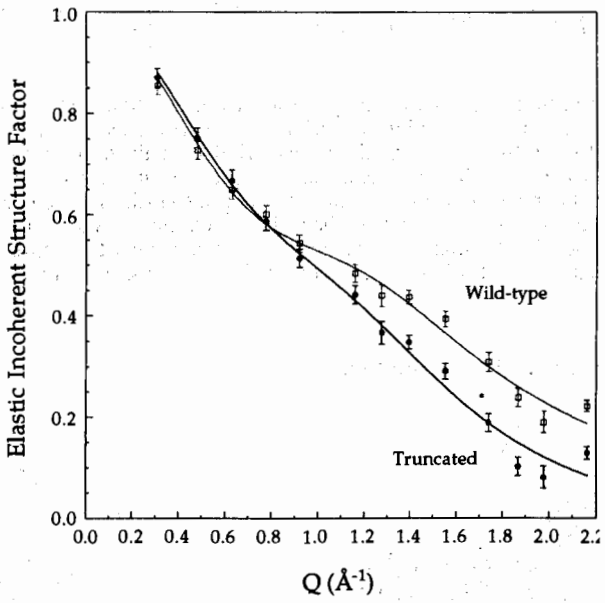

Figure 2. Apparent elastic incoherent structure factors for native (open square) and truncated Snase (filled circle). The experimental points were obtained from the ratio of the elastic to the (elastic+quasielastic) intensities as illustrated in Fig. 1, using the method described in reference [6]. The solid lines are results of fits of Eq. 6.

The difference in the scattering profiles leads to a difference in the EISF, which is determined by the geometry of the time-resolvable motions. In Fig.2 are presented $A_0(Q)$ for native and truncated Snase. In both protein states $A_0(Q)$ descends to a minimum at Q~2.0Å^{-1}. This is consistent with approximate diffusion-in-a-sphere behaviour with a sphere radius of about 1Å (17). However an additional feature can be observed at Q~1.5Å^{-1} in the native protein. This corresponds to a shoulder which has been evidenced in the EISF's of other proteins (18-19), and suggests the presence of a diffusive process over a longer length scale. Taking these considerations into account an approximate model of the dynamics was estimated by assuming that the position vector of each atom, $\hat{\boldsymbol{R}}(t)$, can be decomposed into three independent processes:

$$\hat{\boldsymbol{R}}(t) = \hat{\boldsymbol{R}}_{vib.}(t) + \hat{\boldsymbol{R}}_{sph.}(t) + \hat{\boldsymbol{R}}_{jump}(t) \qquad [5]$$

where $\hat{\boldsymbol{R}}_{vib.}(t)$ is a local Gaussian process, $\hat{\boldsymbol{R}}_{sph.}(t)$ is a uniform diffusion in a sphere of

where $\hat{R}_{vib.}(t)$ is a local Gaussian process, $\hat{R}_{sph.}(t)$ is a uniform diffusion in a sphere of radius R and $\hat{R}_{jump}(t)$ describe discrete jump motions between two sites separated by a distance d. The local Gaussian dynamics refers to dynamics that can be represented as $A_0(Q)=exp(-<u^2>Q^2/6)$, where $<u^2>$ is the mean-square displacement (20). A fraction $(1-p)$ of the protons is assumed to undergo the motion described by Eq.5, whereas the remaining p fraction undergoes only the Gaussian dynamics. The overall analytical EISF can be reduced to:

$$A_0(Q) = \left[p + \frac{1}{2}(1-p)\{1+j_0(Qd)\}\left\{\frac{3j_1(QR)}{QR}\right\}^2 \right] \exp\left\{-\frac{1}{6}\langle u^2\rangle Q^2\right\} \qquad [6]$$

where j_0 and j_1 are zeroth- and first-order spherical Bessel functions. The fit of Eq. 6 to the native protein is shown in Fig. 2 and the resulting parameters are $p=0.50$, $d=5.48$Å, $R=1.097$Å and $<u^2>^{1/2}=0.49$Å±0.02Å. The quasielastic line widths obtained correspond to relaxation times of ~20-40ps. $A_0(Q)$ for the native and truncated proteins are identical to within statistical error over the small Q-region (<1.0Å^{-1}). However there is a significant difference in the form of the atomic fluctuations for Q-values greater than ~1.3Å^{-1}. On Fig. 2 is also shown the result of a fit of the above model to the truncated protein EISF, in which only the Debye-Waller factor is varied ($<u^2>$). This gives a RMS displacement of 0.60±0.02Å, increase from 0.49Å±0.02Å in the native Snase.

Molecular Dynamics Simulations

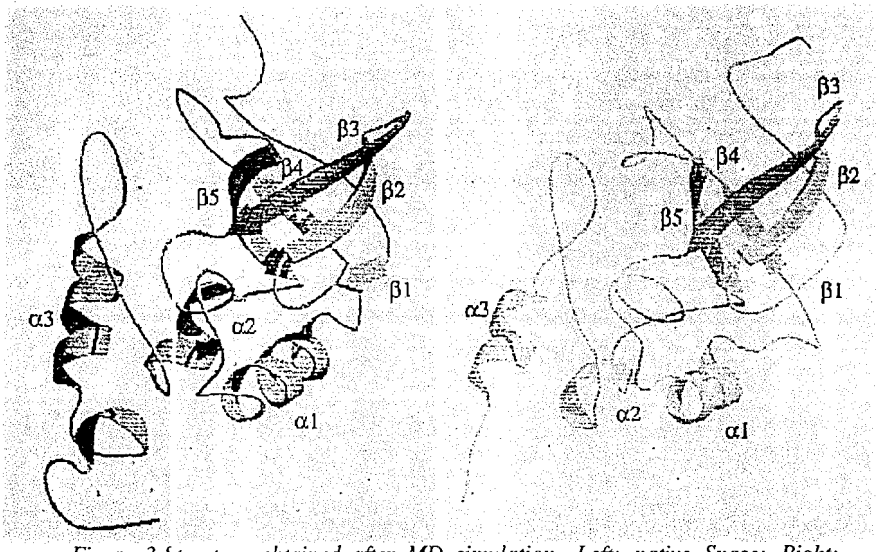

Figure 3: Structure obtained after MD simulation. Left: native Snase; Right: truncated Snase. Copied from reference [22].

Fig. 3 show the structure of native and truncated Snase at the end of each MD simulation. Whereas the native protein has retained its structure (RMS deviation from the energy-minimised crystal structure is 1.9Å over the last 100ps), the truncated protein has lost much of the structural features of the native state (RMSD~3.4Å). Helix α3 has moved away from the rest of the protein. The β barrel is still compact and stands β2 and β3 are particularly stable, in accord

with ^{1}H NMR experiments which demonstrated that a peptide with the sequence of the loop β2-β3 retains the native-like β-turn structure in solution (21). Interactions involving strands β1, β4 and β5 are less specific, leading to a structural relaxation of parts of their internal structure.

Inspection of the structure of the residues involved in binding of the inhibitor, pdTp, evidences for important structural modifications of the active site (22). While the X-ray structure is preserved in the simulation of the wild-type protein, that of the truncated protein is significantly modified. The residues inside the cavity undergo a significant surface-area decrease and form a nonnative hydrophobic cluster. Moreover fluctuations of strands β4 and β5 induce a drop of the loop β4-β5 onto the top part of the active site.

An interesting question is how the active-site collapse came about. In the native state there is a hydrophobic cluster involving residues L137, I139, W140 that are removed in the truncated protein and P42, A58, L105,V104, L108 and A109 that are not. Truncation of the protein largely perturbs the hydrophobic cluster. In addition the H-bond between G107 and I139, which is present in the X-ray structure and throughout the native protein MD simulation, is absent from the denatured protein due to the truncation. The removal of the hydrophobic cluster and of this crucial H-bond leads to displacement of helix α3 away from the rest of the protein and also destabilizes helix α2, which moves away from the β barrel and loses about half of its helical structure. The collapse of the active site is mainly a consequence of these two structural changes.

DISCUSSION

Neutron scattering applied here for the first time to study a partially-denatured protein, provides a particularly direct way of obtaining information about its internal dynamics. The results indicate that there is an increase in the amplitude of the ps-timescale average local fluctuations on truncation of the 13 C-terminal residues of Snase and this increase is quantified.

The simulation data indicate an increase of the solvent accessibility of the protein. This is accompanied by a change in the number of internal (protein-protein) hydrogen bonds, which remains stable at ~193 in the native protein simulation but decrease progressively to ~155 in the truncated protein MD.

The RMS fluctuations obtained from the experimental EISF is ~1.6Å for both the native and truncated proteins. This will contain contributions from both internal and external (rigid molecule) displacements. This value can be compared to those obtained from a calculation of the internal fluctuations of the native (1.0Å) and truncated (1.2Å) proteins along their simulated atomic trajectories. Although direct comparison of the nonequilibrium truncated protein simulation with the equilibrium neutron experiment should be made with caution, the MD values are consistent with experiment in the case that the whole-molecule diffusion contributes to the experimental system. The increase in the internal fluctuations of 0.2Å on truncation is of similar magnitude to that obtained from the experimental EISF.

The denaturation seen in the nonequilibrium MD simulation of the truncated protein is in agreement with a variety of experimental results. However, the simulation has probably not completely reached the experimental state. Among this phenomena that will not reach equilibrium on currently-accessible MD timescales is the cis-trans isomerization of the Pro peptide groups, which typically have isomerization rates of ~10^{-2}s^{-1}. The K116-P117 peptide group is mostly *cis* in the wild-type protein (23-24) but mostly *trans* in the high-temperature fully denatured form (25). This peptide group remains *cis* during both MD simulations. One possible consequence consists in the simulated radius of gyration, which evolves from 15.1Å at the beginning of the simulation to 15.8Å at the end, far away from the experimental value of 21.2±0.2Å (8). Manual isomerization of this *cis* bond at the end of the simulation of the truncated protein leads to a radius of gyration of 19.5Å and a pair distribution function, *p(R)*, in agreement with experiment (22).

The truncated protein retains its ability to bind the inhibitor pdTp and in doing so recovers the native structure (8). This suggests that the structures of the active site and of the truncation

region are interdependent. The present MD result is consistent with this assumption, showing denaturation of the inhibitor-binding pocket on truncation. This appears to be initiated by the structural changes involving the above-mentionned hydrophobic cluster and the G107-I139 hydrogen bond. If the simulation provides a realistic model of the truncated form, this finding suggests two possible models of the sequence of events leading from inhibitor binding to recovery of the native structure. One possibility is that the inhibitor binding induces a change in the active site structure that leads to refolding of the denatured parts. Alternatively, in the unliganded truncated state an equilibrium may exist between the native-like and collapsed active site proteins. The binding of the inhibitor would shift the equilibrium to the native-like structure. The latter model implies considerable flexibility of the unliganded truncated form, consistent with the present neutron scattering results.

How can the present results provide insight into the folding mechanism of the wild-type Snase? The rapid communication of structural change between the active site and the denatured α-helical regions of the protein, implies that the sequence of events leading from active site formation to helix structuring is probably highly cooperative and effectively barrierless.

REFERENCES

[1] M. Karplus & D. L. Weaver, *Protein Science* (1994), **3**, 650-668.
[2] A. F. Chaffotte, C. Cadieux, Y. Guillou & M. E. Goldberg, *Biochemistry* (1992), **31**, 4303-4308.
[3] K. A. Dill, S. Bromberg, K. Yue, K. M. Fiebig, D. P. Yee, P. D. Thomas & H. S. Chan, *Protein Science*(1995), **4**, 561-602.
[4] H. J. Dyson G. Merutka, J. P. Waltho, R. A. Lerner & P. E. Wright, *J. Mol. Biol.* (1992), **226**, 795-817.
[5] P. A. Jennings & P. E. Wright, *Science* (1993), **262**, 892-896.
[6] M. Bée, *Quasielastic Neutron Scattering*, Adam Hilger, Bristol (1988).
[7] D. Shortle & A. K. Meeker, *Biochemistry* (1989), **28**, 936-944.
[8] J. M. Flanagan, M. Kataoka, D. Shortle & D. M. Engelman, *Proc. Natl. Acad. Sci. USA* (1992), **89**, 748-752.
[9] J. M. Flanagan, M. Kataoka, T. Fujisawa & D. M. Engelman, *Biochemistry*, **32**, 10359-10370.
[10] J. C. Smith, *Quart. Rev. Biophys.* (1991), **243**, 227-291.
[11] D. Shortle, *J. Cell. Biochem.* (1986), **30**, 281-286.
[12] A. T. Alexandrescu, C. Abeygunawardana & D. Shortle, *Biochemistry* (1994), **33**, 1063-1072.
[13] A. Lamy & J. C. Smith, *J. Am. Chem. Soc.* (1996), **118**, 7326-7328.
[14] B. R. Brooks, R. E. Bruccoleri, B. D. Olafson, D. J. States, S. Swaminathan & M. Karplus, *J. Comput. Chem.* (1983), **4**, 187-217.
[15] T. R. Hynes & R. O. Fox, *Proteins: Struct. Funct. Genet.* (1991), **10**, 92-105.
[16] L. Van Hove, *Phys. Rev.* (1954), **95**, 249-262.
[17] F. Volino & A. J. Dianoux, *Mol. Phys.* (1980), **41**, 271-279.
[18] V. Receveur, P. Calmettes, J. C. Smith, M. Desmadril, G. Coddens & D. Durand, *Proteins: Struct. Funct. Genet.* (1997), **28**, 380-387.
[19] J. Fitter, R. E. Lechner, G. Büldt & N. A. Dencher, *Proc. Natl. Acad. Sci. USA* (1996), **93**, 7600-7605.
[20] S. Lovesey, *Theory of Neutron Scattering from Condensed Matter*, Oxford University Press, Oxford (1984).
[21] M. R. Ermacora, D. W. Ledman & R. O. Fox, *Nature Struct. Biol.* (1996), **3**, 59-66.
[22] A. Goupil-Lamy, *Ph. D. Thesis* (1997), Université Paris VI.
[23] P. J. Loll & E. E. Lattman, *Proteins: Struct. Funct. Genet.* (1989), **5**, 183-201.
[24] P. A. Evans, C. M. Dobson, R. A. Kreutz, G. Hatfull & R. O. Fox, *Nature* (1987), **329**, 266-268.
[25] D. P. Raleigh, P. A. Evans. M. Pitkeathly & C. M. Dobson, *J. Mol. Biol.* (1992), **228**, 338-342.

INFLUENCE OF ETHANOL ON THE MEMBRANE STRUCTURE: SANS STUDY

M.A. Kiselev [1], A.M. Kisselev[1], S. Borbely[2], P. Lesieur[3]

1) FLNP, JINR, Dubna, 141980 Moscow region, Russia
2) Research Institute for Solid State Physics, Budapest, Hungary
3) LURE, Bât. 209-D, Université Paris-Sud, F-91405 Orsay cedex, France

Abstract

The influence of ethanol on the structure of dipalmitoylphosphatidylcholine (DPPC) large unilamellar vesicles (LUVs) was studied by small-angle neutron scattering (SANS) in the gell phase ($L_{\beta'}$) and the liquid crystalline phase (L_{α}). In the region of the ethanol concentration (C_{et}) from 0 to 1.2 M at T=25°C the DPPC membrane exhibits $L_{\beta'}$ phase and demonstrates slight decrease of rate of 0.3 Å/M of the membrane thickness on increase of C_{et}. The abrupt decrease in the membrane thickness at C_{et} higher than 1.2 M corresponds to the formation of the interdigitated phase ($P_{\beta I}$). The $L_{\beta'}$ phase and $P_{\beta I}$ phase coexist at 1.2 M ≤ C_{et} ≤ 2.7 M. At C_{et} = 2.7 M the membrane thickness equal to 33.2±0.7 Å. Above the ethanol concentration of 2.7 M the interdegitated phase induces the intervesicle interaction and the appearance of multilamellar vesicles at C_{et} = 6.2 M. The interdigitation of hydrocarbon chains along with the intervesicle interaction is absent in the L_{α} phase.

Introduction

The studies of ethanol influence on the membrane structure have been performed by various techniques: densitometry and calorimetry[1,5], X-ray diffraction[2,5], fluorescence technique[3,4,6] and dynamic light scattering[5,6]. The information about ethanol influence on the repeat distance, membrane thickness, thickness of solvent in the intermembrane space and diffusion of ethanol through membrane has been obtained using the techniques described above. For these studies the dipalmitoylphosphatidylcholine (DPPC) and dimyristoilphosphatidylcholine (DMPC) membranes have been generally used. The conclusion about creation of ethanol-induced inderdigitated phase ($P_{\beta I}$) has been made[1,5,6]. The most interesting parameter of the phospholipid/ethanol/water system is the so-called critical ethanol concentration C_r - the mole ethanol concentration that corresponds to the fully inderdigitated phase in which the hydrocarbon chains are embedded into each other (this leads to a decrease of DPPC membrane thickness down to the value of about 30 Å). The C_r value is of importance because the ethanol-induced lipid interdigitation may play etiological role in the alcohol-related damage of the gastric mucosal barrier[6,7]. From the phase diagram based on the density meter measurements the C_r is equal to 0.93 M for T=25°C [1]. The X-ray diffraction data[5] gives us C_r=0.7 M for the gell phase of DPPC membrane. These results are in the contradiction with the investigations of the proton permeability of DPPC membranes in the presence of ethanol[6] which demonstrated the increase of proton permeability at ethanol concentration of 1.2 M.

Despite a variety of publications the direct measurements of the membrane thickness for phospholipid/ethanol/water system have not been performed yet. For example, in the studies of U. Vierl et al[5] the dynamical light scattering have been used and DPPC bilayer thickness has been calculated from the relative diameter of unilamellar vesicles as a function

of the bulk ethanol concentration. SANS, compared with this method, gives us an advantage to measure the membrane thickness of large unilamellar vesicles (LUVs) directly/8,9,10/.

The investigations of the ethanol influence on the membrane structure are of interest because of the necessity to understand the mechanism of alcohol penetration through the membrane, but nevertheless this is not the only reason for these studies. The first reason that there is the possibility to use the ethanol/water solvent as a probe for the study of membrane–membrane interactions due to the difference in electrical and hydration properties of the ethanol/water mixture and pure water. The second one is related to the chance for comparison of the influence of ethanol on the membrane structure with that of other solvents commonly used as cryoprotectors, in our case with that of dimethyl sulfoxide (DMSO)/11/. The characteristics of the phospholipid membrane phase transitions depend sufficiently on the concentration of the DMSO or the ethanol molecules in the solvent. This dependence was studied by SAXS, SANS, WAXS and calorimetry/5,11/. The ethanol influence the phase transitions of DPPC membrane, but in different way, compared with the DMSO. For example, the pre-transition temperature increases with an increase of DMSO concentration; in the case of ethanol the pre-transition temperature decreases with an increase of ethanol concentration.

In this work the influence of the ethanol on the DPPC membrane thickness of LUVs was studied in the range of the ethanol concentration from 0 to 6.2 M at temperatures of 25°C and 50°C. The results obtained were compared with that of SANS study of the DMSO influence on the properties of LUVs and membrane structure.

SANS experiment

The 2% (w/w) DPPC suspension in D_2O was extruded through 2000Å pores of Nucleopore filter by using the LiposoFast device (Avestine, Canada). The large unilamellar vesicles (LUVs) made of DPPC molecules were created by the extrusion in heavy water. The samples with 1% DPPC concentration and ethanol mole concentration $C_{et} = X$ were prepared by the mixing in the equal volumes of extruded 2% DPPC suspension in D_2O and D_2O/C_2D_5OD ethanol solvent with $C_{et} = 2X$.

SANS measurements were performed at the YuMO time-of-flight small-angle spectrometer (pulse neutron source IBR-2) in Frank Laboratory of Neutron Physics (FLNP) and at the small-angle spectrometer (steady state reactor source) in Budapest Institute of Solid State Physics (ISSP). The spectra from YuMO spectrometer in FLNP were normalized to the scattering cross-section of vanadium, the spectra from small-angle instrument in ISSP - to the scattering cross-section of H_2O. The results obtained at these two spectrometers are in good agreement.

For extended unilamellar structures (sheets or vesicles) with a surface area S and a thickness of the layer d_l (or radius of gyration R_t), much smaller than the radii of curvature of the surface (or the lateral dimensions of the layer), the approximation of scattering cross-section, valid for scattering vectors q in the domain $2\pi/\sqrt{S} < q < 1/R_t$, is given by equation:

$$\frac{d\sigma}{d\Omega} = \frac{2\pi S(\Delta\rho\, d_l)^2}{q^2} \exp\left[-q^2 R_t^2\right], \qquad (1)$$

where $\Delta\rho = \rho_m - \rho_s$, is so-called contrast - the difference in scattering density of the membrane and the solvent. For the heterogeneous membrane scattering density distribution $\rho_m(r) \neq$ const and the measured gyration radius R_t connects with the membrane thickness d_l by expression/8/:

$$R_t^2 = \frac{d_l^2}{12} - \frac{b_l}{b_s} \cdot R_{t0}^2. \qquad (2)$$

R_t is the gyration radius calculated with respect to the contrast $\Delta\rho$, R_{to} is the gyration radius calculated with respect to ρ_m. b_l is the neutron scattering amplitude of the DPPC molecule, b_s is the neutron scattering amplitude of the solvent molecules in the specific volume of one DPPC molecule V=1156 Å^3. For DPPC membranes $R_{to} \approx 0.3d_l$ and for heavy water $b_l/b_s = 0.037$. In this case the thickness of the DPPC membrane can be calculated by relation $d_l = R_t\sqrt{12}$ with the accuracy of 2%. The substitution of deuterated ethanol instead of D_2O does not make the conditions of the experiment worse: $b_{d_2O} = 7.41 \cdot 10^{-11}$ cm, $b_{EtOD} = 7.15 \cdot 10^{-11}$ cm, $b_l = 2.76 \cdot 10^{-12}$ cm.

The fitting of experimental spectra by the equation

$$\frac{d\sigma}{d\Omega} = \frac{d\sigma}{d\Omega}(0) \cdot q^a \exp\left[-q^2 \, b\right] , \qquad (3)$$

was used in order to determine a morphology of the particles. For LUVs or sheets $a = -2$. The deviation of a value from $a = -2$ gives us the information about the other morphology of the particles: for the rod-like micelles $a = -1$, for spherical or ellipsoidal micelles $a = 0$.

Results and Discussion

The values of the DPPC membrane thickness measured at T=25°C as a function of the ethanol concentration are presented for the cases of the deuterated ethanol (circles) and the protonated ethanol (squares) in Figure 1. The membrane thickness was calculated by relation $d_l = R_t\sqrt{12}$, the R_t value was determined from experimental SANS spectra by fitting with equation (1). The divergence of results with the deuterated and the protonated ethanol is negligible in the region of the ethanol concentration from 0 to 0.5 M. With further increment of the protonated ethanol concentration the approximation $d_l = R_t\sqrt{12}$ gives, according to equation (2), underestimated values of the membrane thickness, compared to that of the deuterated ethanol.

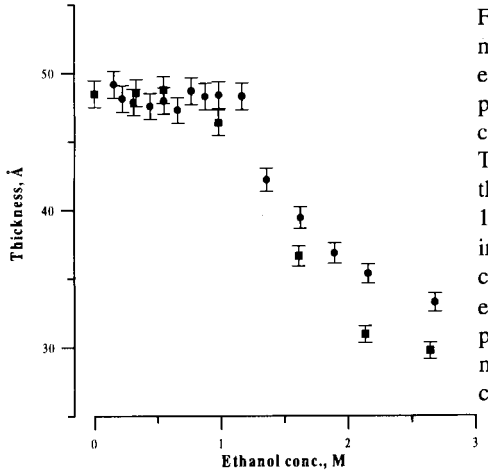

FIGURE 1. The dependence of the membrane thickness on the deuterated ethanol concentration (circles) and on the protonated ethanol concentration (squares), calculated from SANS spectra at T=25°C. The abrupt decrease of the DPPC membrane thickness at the ethanol concentration above 1.2 M corresponds to the formation of the interdigitated $P\beta I$ phase. At the ethanol concentration below 1.2 M the DPPC vesicle exhibits the $L\beta'$ phase. The usage of the protonated ethanol gives underestimated membrane thickness above the ethanol concentration of 0.5 M.

In the region of the ethanol concentration below 1.2 M the membrane thickness decreases slowly on increase of the ethanol concentration with the rate of 0.3 Å per mole of the ethanol concentration and DPPC membrane exhibits the $L_{\beta'}$ phase. The ethanol concentration of 1.2 M corresponds to the formation of the fully interdigitated phase. In the region of the ethanol concentration from 1.2 M to 2.7 M the interdigitated $P_{\beta I}$ phase coexists with the gel $L_{\beta'}$ phase. This results are in good agreement with that of the study of the proton permeability through the vesicle by fluorometry[6], which demonstrated the slow increase of the permeability in the region of the ethanol concentration from 0 to 1.2 M and sufficient monotonous increase of the proton permeability in the region of the ethanol concentration from 1.2 to 1.8 . In the case of the liquid L_{α} phase the absence of the abrupt increase in the proton permeability for $1.2\ M \le C_{et} \le 1.8\ M$ approves the direct connection of the proton permeability and the exhibition of the fully interdigitated phase by some part of the DPPC membrane.

The SANS curve deviates from the Guinier law for LUVs at the ethanol concentration above 2.7 M on further increase of it; from the equation (3) $a < -2$. The determination of the membrane thickness becomes impossible. Figure 2 presents the SANS spectra for LUVs with the deuterated ethanol mole concentrations of 0.0 and 3.2 and for multilamellar vesicles with $C_{et} = 6.2$ M at T=25°C.

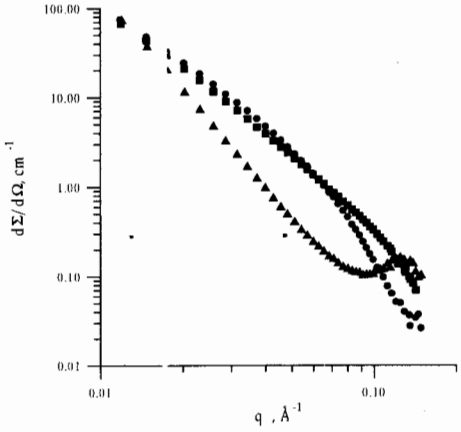

FIGURE 2. SANS curves for DPPC vesicles: in heavy water (circles) without ethanol, from equation (3) $a = -2.06 \pm 0.1$, the membrane thickness $d_l = 48.5$ Å; in D_2O/EtOD mixture with $C_{et} = 3.2$ M (squares), $a = -2.35 \pm 0.1$ and in D_2O/EtOD mixture with $C_{et} = 6.2$ M (triangles), $a = -3.69 \pm 0.02$. The diffraction peak at large value of q for the system with $C_{et} = 6.2$ M corresponds to the membrane repeat distance $d = 49.1 \pm 4$ Å.

The appearance of the diffraction peak for $C_{et} = 6.2$ M at $q = 0.128$ Å^{-1} is a result of the decrease in the repulsion between the unilamellar vesicles and the creation of the multilamellar vesicles. The membrane repeat distance $d = 49.1 \pm 4$ Å is obtained from the diffraction peak position. This value corresponds to the d value of the $P_{\beta I}$ phase measured by X-ray diffraction exactly[5]. Two possible explanations exist for the ethanol-induced intermembrane interaction and, as a result, for the LUVs aggregation in the $P_{\beta I}$ phase. The first explanation is based on the dehydration of membrane surface in the $P_{\beta I}$ phase, which results in the removal of the part of the membrane bound water. The second explanation is based on the energetic viewpoint: the membrane surface of the fully interdigitated vesicles is covered by both the polar headgroup and the nonpolar terminal methyl group. The nonpolar regions in the surface create Van der Waals contact points between vesicles that favors vesicle aggregation[6].

The second evidence of vesicles aggregation in $P_{\beta I}$ phase relates to the fact that on the increase of temperature up to 50°C only the L_α phase exists without any intervesicle interaction. It gives opportunity to measure the membrane thickness as a function of the ethanol concentration up to the concentration of 6.2 M. The results obtained are presented in Figure 3. The decrease of the membrane thickness in the L_α phase occurs as a result of the increase in the lateral membrane dimension. The surface area A of one DPPC molecule is equal to 62.9 Å^2 in the L_α phase for the case of the pure water solvent/11/. In order to make calculation we suppose that the volume occupied by one DPPC molecule is not changed under the alteration of the ethanol concentration, $V=A \cdot d_I=const$. Actually, due to the changes in the hydration of DPPC molecules V can not to remain constant as a function of the ethanol concentration, but this problem is still under discussion and other special investigations would be necessary in order to characterize the membrane hydration in the presence of the ethanol. At T=50°C the membrane thickness decreases from the constant value of 40.7 ± 0.2 Å in the region of the ethanol concentration from 0 to 1 M down to the value of 32.5 ± 0.7 Å at the ethanol concentration of 6.2 M. This decrease of the membrane thickness by the value of 8.2 ± 0.8 Å is a result of the increase in the value of A from 62.9 Å^2 to 78.8 Å^2.

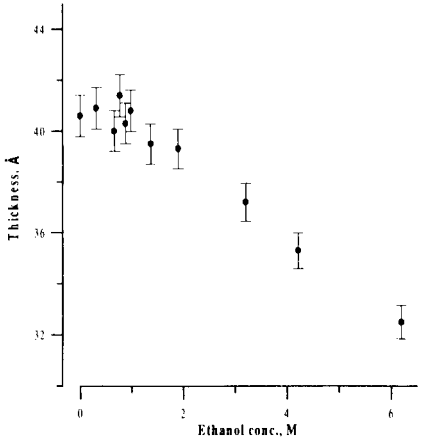

FIGURE 3. The dependence of DPPC membrane thickness on the ethanol concentration for LUVs at T=50°C. The membrane thickness has constant value of 40.7 ± 0.2 Å from 0 to 1 M ethanol concentration. With further increase of the ethanol concentration the membrane thickness decreases monotonously and has a minimum value of 32.5 ± 0.7 Å at the ethanol concentration of 6.2 M.

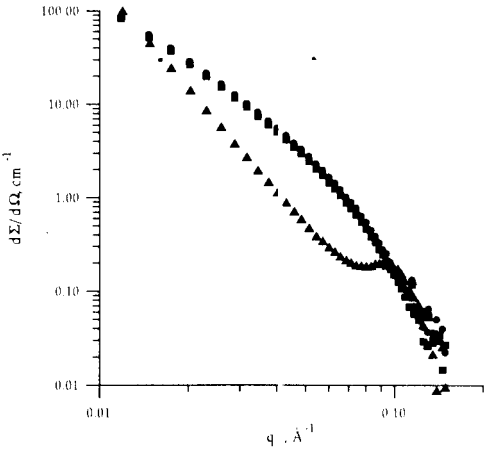

FIGURE 4. SANS curves for DPPC LUVs: in heavy water (circles) and DMSO/water mixture (square), the curves are practically the same and give the constant value of d_I=48.5±1 Å. The DMSO-induced dehydration has a maximum value at X_{DMSO}=0.02, which corresponds to a minimum value of the repeat distance d=58.1±0.8 Å/12/. At X_{DMSO}=0.2 (triangles) the SANS curve corresponds to the scattering from multilamellar vesicles with d=62.3 ± 5 Å.

The well-known cryoprotector dimethyl sulfoxide (DMSO) influences the DPPC membrane properties and structure sufficiently[12]. The presence of DMSO decreases the thickness of the intermembrane solvent, but the membrane thickness is not influenced by DMSO.

Figure 4 demonstrates the SANS spectra for LUVs in the presence of DMSO for DMSO mole fraction $X_{DMSO} = 0$, 0.1, 0.2 at T = 20°C. In the region of the DMSO mole fraction from 0 to 0.1 the structure of DPPC LUVs and the DPPC membrane thickness $d_l = 48.5$ Å are not influenced by DMSO. On further increase of the DMSO mole fraction the intervesicle interaction modifies the SANS spectra – the triangle curve at $X_{DMSO} = 0.2$. The position of the diffraction peak for $X_{DMSO} = 0.2$ corresponds to the repeat distance of 62.3 ± 5 Å, this value is sufficiently higher than the value of the DPPC membrane thickness $d = 58.1 \pm 0.8$ Å obtained from X-ray diffraction study of DPPC/DMSO/water system[12]. It was established by calorimetry, X-ray diffraction and SANS that DMSO induces the dehydration of the intermembrane space, but does not change the number of the water molecules connected with the membrane surface. DMSO does not penetrate in the region of the polar head groups. Ethanol penetrates in the region of polar head groups and consequently increases the membrane surface A per one DPPC molecule. The increase of A leads to the formation of the interdigitated phase from the gell phase of DPPC membrane. The SANS results demonstrate the creation of intervesicle interaction in both cases : the ethanol and the DMSO. It gives an additional reason for the explanation of the ethanol-induced intervesicle interaction and aggregation on the base of the ethanol-induced membrane dehydration.

Conclusions

The influence of the ethanol to the DPPC LUVs was studied at T=25°C and T=50°C. At T=25°C the region of the ethanol concentration from 0 to 1.2 M corresponds to the $L\beta'$ phase of the DPPC membrane. Above 1.2 M of ethanol the DPPC membrane consists of two phase mixture: the $L\beta'$ phase and the $P\beta I$. At the ethanol concentration of 2.7 M the increased amount of the vesicles in the fully interdigitated phase creates the measured membrane thickness of 33.2±0.7 Å. This value of the membrane thickness is close to the value for the pure fully interdigitated DPPC phase of 30 Å. Above the ethanol concentration of 2.7 M the main part of the vesicles exhibits the fully interdigitated phase, which leads to the formation of the intervesicle interaction and the vesicle aggregation. The multilamellar DPPC vesicles are created at the ethanol concentration of 6.2 Å as a result of the intermembrane interaction. From SANS results the critical ethanol concentration $C_r = 1.2$ M, at this concentration some fraction of the vesicles exhibits the fully inderdigitated phase, which leads to the abrupt decrease in the membrane thickness and liner increase of membrane permeability.

At T=50°C DPPC LUVs exhibit the L_α phase for the region of the ethanol concentration from 0 to 6.2 M. At the ethanol concentration from 0 to 1 M the membrane thickness is not influensed by the ethanol. Above the ethanol concentration of 1.0 M the surface area per one DPPC molecule increases linearly, which is in the agreement with $C_r = 1.2$ M obtained at T=25°C.

References

1. Kazio Ohki, Kazio Tamura and Ichiro Hatta. *Bioch. & Bioph. Acta*, 1028 (1990) 215-222.
2. Boris G. Tenchov, Haruhito Yao, and Ichiro Hatta. *Biophys. J.*, 59 (1989) 757-768.
3. Paulo F. F. Almeida, Winchil L.C. Vaz, T.E. Thompson. *Biochemistry,* 31 (1992) 6739-6747.

4. Chang-Hwei Chen and Stuart G. Engel. *Chem. & Phys. Lipids,* 52, (1990) 179-187.
5. Ulrich Vierl, Ludwig Lobbecke, Norbert Nagel, Gregor Cevc. *Biophys. J.,* 67 (1994) 1067-1079.
6. Junwen Zeng, Kirk E. Smith, Parkson Lee-Gau Chong. *Biophys. J.*, 65 (1993) 1404-1414.
7. J.M. Wilkers, H.J. Ballard, B.H. Hirst. *Gastroenterology,* 92 (1987) 1695.
8. V.I. Gordeliy, L.I. Golubchikova, A. Kuklin, A.G. Syrykh, A.Watts. *Prog. Coll. & Pol. Science,* 92 (1993) 252.
9. M. Dubnickova, M. Kiselev, S. Kutuzov, F. Devinsky, V. Gordeliy, P. Balgavy. *Gen. Physiol. Biophys,* 16 (1997) 175-188.
10. P. Balgavy, M. Dubnickova, D. Uhrikova, S. Yaradaikin, M. Kiselev, V. Gordeliy. *Acta Physica Slovaca,* submitted for publicatin, March 1998.
11. J.H. Nagle, R. Zhang, S. Tristram-Nagle, W. Sun, H. I. Petrache, R. M. Suter, *Biophys. J.,* 70 (1996) 1419-1431.
12. M.A. Kiselev, P. Lesieur, A.M. Kisselev, C. Grabiel-Madelmond, M. Ollivon. *Preprint JINR,* E14-98-91 (1998).

STRUCTURAL INVESTIGATIONS OF KIRROMYCIN BOUND TO BACTERIAL ELONGATION FACTOR TU BY NMR AND MOLECULAR DYNAMICS

David Brockwell, Debbie S. Marks, Deb Bloor and Jill Barber
School of Pharmacy and Pharmaceutical Sciences
University of Manchester, Oxford Road, Manchester, UK.

Bacterial elongation factor Tu (EFTu) has a molecular weight of 43kDa and is the most abundant protein in the *E. coli* cell. EFTu is involved in the chain elongation cycle of prokaryotic protein biosynthesis: when bound to GTP, EFTu is able to bind aminoacyl tRNA and catalyses its binding to the programmed ribosome. Upon cognate codon anti-codon interaction GTP hydrolysis occurs and EFTu.GDP leaves the ribosome. The action of EFTu is inhibited by the elfamycin antibiotic kirromycin (see Figure 1). EFTu.GTP is able to carry aminoacyl tRNA to the ribosome in the usual way, but after GTP hydrolysis, EFTu.GDP is unable to leave the ribosome. Consequently, resistance to kirromycin action is recessive.

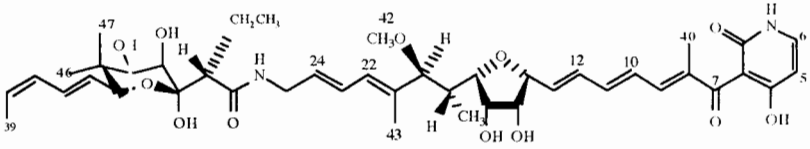

Figure 1. The structure of the antibiotic kirromycin

There is no crystal structure of kirromycin or its analogues and ROESY NMR spectra show no long range cross peaks and it may be assumed that the molecule is very flexible in solution. Several crystal structures for various forms of EFTu from *E. coli* and *Thermus* sp. have recently been published [2-6]. Whilst a quaternary complex of EFTu.GTP analogue.tRNA.kirromycin has been crystallised[7], no crystal structure is yet available.

Conventional ligand:protein 1D and 2D NMR experiments are not informative because of the large size of the protein and the tight binding of the kirromycin.EFTu.GDP complex (binding constant 1.3 x10^6M)[8]. These problems can be partially overcome by the use of highly deuteriated EFTu. Our laboratory has, in the past, developed a plasmid encoding EFTu under the influence of a strong chemical inducer (see Fig 2) and a 'wild-type' *E.coli* host has carefully been adapted to deuteriated d_4-sodium succinate medium. This clone expresses deuteriated protein to at least the same level as wild-type protein (100-150mg/L).

Initial 2D NOESY experiments using d_{11}-Tris as the buffer were disappointing with very few peaks being visible. This was attributed to aggregation of the protein leading to decreased T_2 relaxation times. Subsequent experiments were carried out in phosphate buffer and showed far superior signal to noise. However this spectrum was complicated by a second set of signals appearing at the chemical shift of free kirromycin. This was attributed to a transferred NOE effect of kirromycin binding weakly to a denatured form of the protein (the NOESY spectrum of free kirromycin was essentially blank). A transferred NOE effect can be observed for ligands which interact weakly with their protein targets and hence exchange rapidly between free and bound states. Cross relaxation between ligand protons in the bound state is transferred to the free state by chemical exchange. In a transferred NOE experiment, NOE information is transferred from the bound to free state so that the final NOESY spectrum exhibits the chemical shifts of the free drug but the NOEs due to bound state. In order to test whether this second set of signals was due to a denatured form of EFTu, a sample of deuteriated EFTu was allowed to denature at room temperature for 2 days. After the addition of a further 2 molar equivalents of kirromycin a TRNOESY spectrum was acquired. Many

crosspeaks were visible on this spectrum. As this TRNOESY spectrum was so successful it was decided to engineer an active species of EFTu which bound weakly to kirromycin. In order to estimate the bound conformation of kirromycin we therefore sought a weakly binding complex to obtain transferred NOESY (TRNOESY) spectra. (A375V)EFTu is a kirromycin resistant mutant protein which the literature indicated was suitable for such an experiment[8].

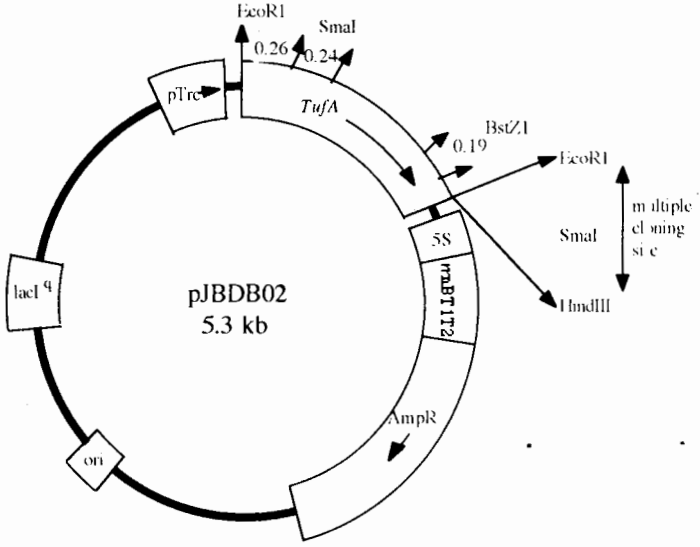

Figure 2. Plasmid map of pJBDB02

E. coli (A375V)EFTu $_A$ was obtained by recombinant DNA technology. The plasmid pTre99A*tuf*A (pJBDB02)[9] (see figure 2) was treated with the restriction endonuclease BstZ1 to excise the 189 base pair fragment from positions 961 to 1149 (corresponding to Gly-317 to Gly-379) giving plasmid pJBDB03. The 'missing' fragment bearing the required GCA to GTA point mutation at position 375 was generated using the polymerase chain reaction with the mutation contained within the rear primer. The fragment was blunt-end ligated into pUC18 Sma I/BAP vector using the SureClone Ligation kit (Pharmacia), sequenced, then excised and religated into pJBDB03 to give the required construct (pJBDB04). Expression of (A375V)EFTu$_A$ from *E. coli* MRE600pJBDB04 was assessed by growth of these cells to mid log phase on Luria-Bertani medium and induced with 1mM IPTG. The purity and molecular weight of the protein assessed by electrospray mass spectrometry (ESI-MS). The expression of (A375V)EFTu$_A$ was measured by the GDP exchange assay [10]. Expression of (A375V)EFTu$_A$ from *E. coli* MRE600pJBDB04 was 40mgL^{-1}. ESI-MS showed that after purification (A375V)EFTu$_A$ was essentially uncontaminated by wild type EFTu and had a molecular weight of 43229.7±1.4 Da.

A TRNOESY experiment was carried out in the following manner. Aliquots of a solution of (A375V)EFTu$_A$ (0.15mM) were added to a solution of kirromycin (1mM, 0.7ml sodium phosphate buffer) in 1/80th of an equivalent increments until an approximate doubling in linewidths were observed.

The resulting TRNOESY spectrum (mixing time 120ms) is shown in Figure 3. This spectrum was very similar to that obtained for inactive wild-type EFTu. Assignment of the ^{1}H resonances of kirromycin has previously been reported[11]. Many long-range cross peaks were seen in this spectrum showing that the drug had conformational rigidity in the bound state.The data were analysed providing a set of 10 nontrivial distance constraints that were not observed

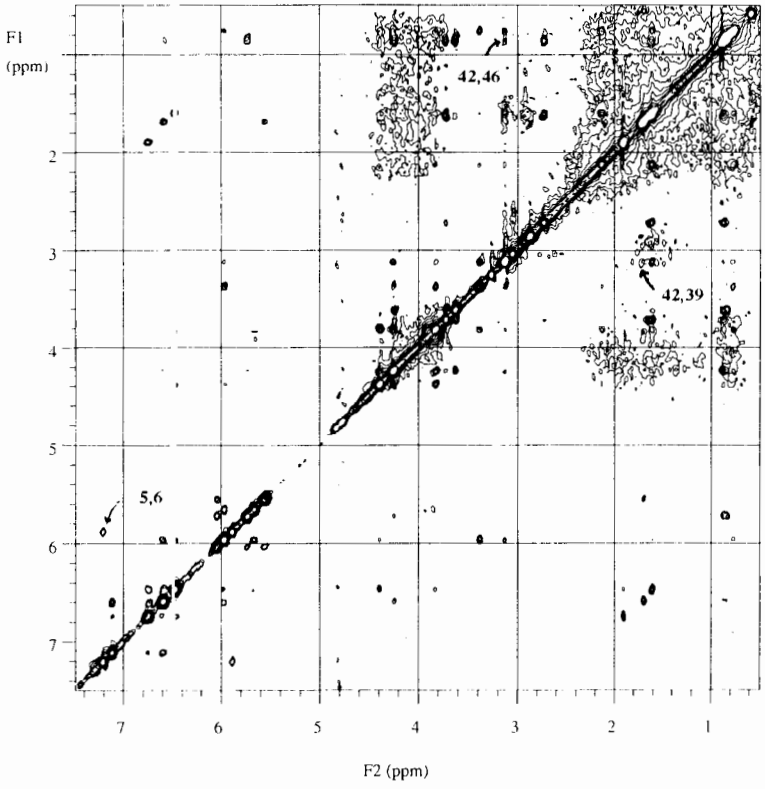

Figure 3. TRNOESY spectrum of 1mM kirromycin in phosphate NMR buffer with 1/40th molar equivalent (A375V)EFTu$_A$

in the ROESY spectrum of the free drug (see Table 1). Molecular modelling was now used to estimate the bound conformation(s). These distance constraints, together with torsional constraints on C7-C8-C9-C10-C11-C12-C13, C21-C22-C23-C24-C25 and C33-C35-C36-C37-C38 were used as a set of restraints in the molecular dynamics simulations and the systematic search. The molecule was built using SYBYL 6.3 on an INDY workstation and canonical MD was run for 2 nanoseconds at 600K step size 5 for each run. Partial atomic charges were calculated using the Gasteiger Marsili method[12] and energy function was calculated using the Tripos force field. The distance range restraints were used in the calculations as harmonic energy penalty functions using a force constant of 100 kcal/molÅ^2. 5 runs were carried out from different starting positions. The data were analysed using the molecular spreadsheet facility and the energy minimisations were carried out using the Simplex method initially for geometry optimisation followed by the Powell algorithm[13] until gradient convergence of 0.05. A systematic search was also carried out within SYBYL defining 7 bonds as rotatable with an angle increment of 20°.

Each run was examined and the resulting structures compared and energy minimised in the molecular spreadsheet facility. The 5 runs and systematic search produced

very similar ensembles of structures (200 structures per run) with no significant differences. Ten structures were chosen as representative of the varying conformations. The rmsd of the region from the pyridone to the furanic rings varied from 0.01 to 2.5 Å whereas the rest of the molecule overlaid with an rmsd varying from 0.01 to 0.2 Å.

The conformation of kirromycin in this complex may not be identical to that of the kirromycin.wild-type EFTu complex. However it is closely similar to of kirromycin bound to partially denatured EFTu suggesting that this is a favoured conformation.

Table 1. connectivities used as non-trivial distance constraints in molecular dynamics

First atom	Second atom
12	41
13	41
16	41
16	42
16	43
17	43
22	42
23	42
42	46
39	42

Further NOESY experiments on wild type deuteriated EFTu have proved to be disappointing with few peaks being visible above the background protein proton signals. Electrospray ionisation mass spectroscopy have shown that the protein used in this study was 95% deuteriated at non-exchangeable positions. It is hoped to improve upon this spectra in the future by utilising highly deuteriated d_4-sodium succinate as the carbon source and by the use of a larger sample volume by using a 8mm sample tube.

References:

1. Weijland, A, Hamark, R.H., Cool, P.H., Anborgh, P.H. and Parmeggiani, A. (1992) Mol. Microbiol. **6**, 683-688
2. Kjeldgaard, M. and Nyborg, J. (1992) *J. Mol. Biol.*, **223**, 721
3. Kjeldgaard, M., Nissen, P., Thirup,S. and Nyborg, J. (1993) *Structure*, **1**, 35
4. Berchtold, H., Reshetnikova, L., Reiser, C.O.A., Schirmer, N.K., Sprinzyl, M. and Hilgenfeld, R. (1993) *Nature*, **365**, 126
5. Nissen, P., Kjeldgaard, M., Thirup,S., Polekhina, G., Reshetnikova, L., Clark, B.F.C. and Nyborg, J. (1995) *Science*, **270**, 1464
6. Kawashima, T., Berthetcolominas, C., Wulff, M., Cusack, S. and Leberman, R. (1996) *Nature*, **379**, 511
7. Kristensen, O., Reshetnikova, L., Nissen, P., Siboska, G., Thirup, S. and Nyborg, J. (1996), *FEBS Lett.* , **399**, 59
8. Duisterwinkel, F.J., Kraal, B., de Graaf, J.M., Talens, A., Bosch, L., Swart, G., Parmeggiani, A., la Cour, T.F.M., Nyborg, J. and Clark, B.F.C. (1984) EMBO J. **3**, 113
9. Bloor D.J. (1992) PhD Thesis, University of Manchester
10. Arai, K-I, Kawakita, M. and Kaziro, Y. (1972) *J. Biol. Chem.*, **247**, 7029
11. Barber, J., Derome, A.E., Howard, T.D., Lian, L. and Tebb, G. (1989) *Magn. Reson. Chem.*, **27**, 748
12. Gasteiger J,Marsili M,(1980) Tetrahedron **36**,3219-3228
13. Powell M J D, (1977) Mathematical Programming, **12,** 241-254

STUDY OF EF-TU BY TRIPLE ISOTOPIC SUBSTITUTION

V.L. Aksenov[1], M.V. Avdeev[1], A.A. Timchenko[2], G. Zaccai[3] and I.N. Serdyuk[1,2]

[1]*Frank Laboratory of Neutron Physics, Joint Institute for Nuclear Research, 141980 Dubna, Moscow Region, Russia*

[2]*Institute of Protein Research, Russian Academy of Sciences 142292 Pushchino, Moscow region, Russia*

[3]*Institut de Biologie Structurale and University of Grenoble, 41 avenue des Martyrs, 38027 Grenoble Cedex 1, France.*

Introduction

Triple isotopic substitution (TIS) for studying the structure of biological objects in solutions was proposed by Pavlov and Serdyuk in 1987 [1]. Since that time thorough investigations of this method have been carried out and it has been applied mainly for the study of the polypeptide elongation factor Tu (EF-Tu) under different conditions.

In this review we summarize the experimental experience in this field and clarify the possibilities of TIS for different applications including the study of proteins in isolated state and within complexes, as well as the study of their surface and inner structure.

Theoretical background

The TIS method is based on the difference of small-angle scattering curves from two solutions (Fig.1). The first one contains the mixture of fully protonated and deuterated particles; the second one contains only partially deuterated particles. If the fraction of the deuterated particles in the first solution (δ) equals to the fraction of deuterium in the particles of the second solution

$$a_3(\mathbf{r}) = (1 - \delta)\, a_1(\mathbf{r}) + \delta\, a_2(\mathbf{r}) \qquad (1)$$

where $a_1(\mathbf{r})$ and $a_2(\mathbf{r})$ are the scattering densities of the unlabelled and deuterated particles, $a_3(\cdot)$ is the scattering density of intermediately deuterated particles in the second solution, then the difference of the intensities of two solutions ($I_{1,2}$) and (I_3) respectively will represent the vacuum scattering curve from the same particles but with different scattering density

$$I_{1,2}(q) - I_3(q) = N\, \delta\, (1 - \delta)\, I_F(q) \qquad (2)$$

where N is the number of particles in solution and I_F is the scattering intensity of a particle with the scattering density

$$a_F = a_1 - a_2 \qquad (3)$$

The TIS method leads to four main predictions [2]:

1) The contribution of interparticle interference and particle association to the difference scattering curve is eliminated.

2) The difference scattering curve is independent of the solvent isotopic content.

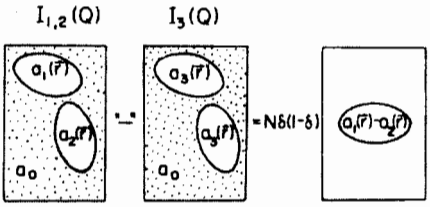

Fig.1. General scheme of the TIS method.

3) Any "small" or "large" molecules present in equal concentrations in solutions will be "invisible".

4) Any complex component of the constant scattering density of three types of particle will be "invisible" too.

In experiments one starts with the second solution. The partially deuterated particles are grown. Then the fraction of deuterium is determined from the match points of the protonated (γ_H), deuterated (γ_D) and partially deuterated (γ_{HD}) particles by the expression

$$(1 - \delta)\,\gamma_H + \delta\,\gamma_{HD} = \gamma_D \qquad (4)$$

which is obviously equivalent to (1). The found value of γ_D is used to prepare the first solution with the proper mixture of protonated/deuterated particles.

Tests of TIS with EF-Tu

The main predictions of the TIS method have been confirmed experimentally using EF-Tu from E.coli. The tests of predictions 2) and 3) were were carried out in Dubna in 1989 at the YuMO small-angle scattering setup of the IBR-2 pulsed reactor [3]. As an example we present a TIS scattering curve for EF-Tu plus glycerol in compare with the pure EF-Tu in Fig.2. One can see from these graphs that the difference scattering curves give the same parameters.

The influence of the interparticle interference to the TIS curve was studied by the D11 small-angle instrument at ILL in Grenoble, 1991 [4]. The TIS curves were the same for different concentrations. It should be pointed out that the interparticle interference is extracted without any model calculations in the TIS method.

The tests of the last prediction are presented below.

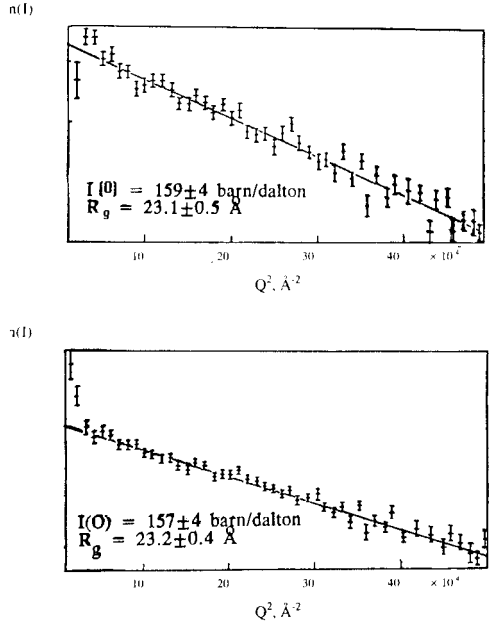

Fig.2. Guinier plot of the TIS difference scattering curve for EF-Tu (upper graph) and EF-Tu plus glycerol (lower graph). Parameters of the plots are the same for both graphs. Reproduced from [3]

Study of EF-Tu in ternary GTP*aminoacyl-tRNA complex

The scheme of TIS for the ternary complex is presented in Fig.3, b. The ternary complexes EF-Tu* GTP*aminoacyl-tRNA in H_2O were prepared by standard ways with the addition of aminoacyl-tRNA, pyruvate kinase, GTP, PEP and other molecules to both solutions in equal amounts [2]. Two kinds of aminoacyl-tRNA—leucyl-$tRNA^{leu}$ and phenilalanyl-$tRNA^{phe}$—were used. The experiments were performed on the D11 instrument in 1993. The results of this study are presented in Fig.4 and Table 1. They show clearly that for two different sets of experimental conditions there is no measurable difference between the radii of gyration of EF-Tu in a separate state and within two ternary complexes. This means that EF-Tu is a rather stable molecule during this part of the elongation cycle when it interacts with its legands.

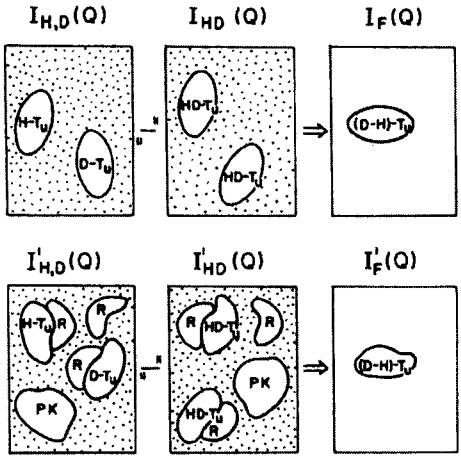

Fig.3. General scheme of the experiments. (a) TIS experiments with EF-Tu-GDP; (b) TIS experiments with the ternary complex EF-Tu•GDP•aminoacyl-tRNA. The difference in the shape of EF-Tu in (a) and (b) reflects possible conformational changes in EF-Tu upon complex formation.

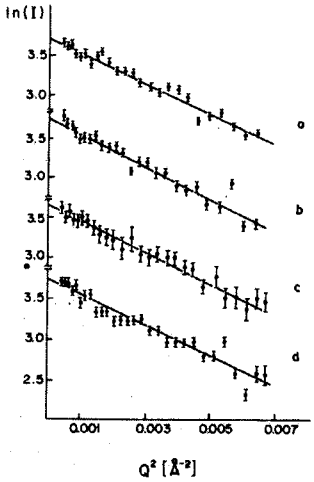

Fig.4. Guinier plot of the TIS difference scattering curve for (a) EF-Tu-GDP in H_2O in HMS buffer; (b) ternary complex EF-Tu•GTP•Leu-tRNA^{Leu} in the same buffer; (c) EF-Tu-GDP in H_2O in HLS buffer; (d) ternary complex EF-Tu•GTP•Phe-tRNA^{Phe} in the same buffer. Reproduced form [2].

Table 1. Parameters of the SANS curves—zero angle cross section $I_F(0)$ normalized by the concentration of EF-zTu and radius of gyration R_g— obtained for free EF-Tu-GDP and EF-Tu in ternary complexes

	$I_F(0)$, barn/g	R_g, Å
EF-Tu-GDP in H_2O in HMS buffer	167 ± 4	23.6 ± 0.4
EF-Tu•GTP•Leu-tRNA^{Leu} in H_2O in HMS buffer	170 ± 5	23.9 ± 0.7
EF-Tu-GDP in H_2O in HLS buffer	166 ± 3	23.6 ± 0.4
EF-Tu•GTP•Phe-tRNA^{Phe} in H_2O in HLS buffer	170 ± 5	23.4 ± 0.7

Study of the surface of EF-Tu

Here the results of the attempts to study the protein surface by TIS are presented. It was reported earlier (ex. [4]) that the surface of proteins has fractal properties. The fractal dimension [5] of the surface for different proteins was estimated using the atomic coordinates obtained by the X-ray crystallography. Another way to find the fractal dimension is small-angle scattering [6]. For large values of the modulus of the scattering vector (q) the scattering intensity (I(q)) of the fractal surface is connected with its dimension (D) by the following way [6]

$$I(q) \sim q^{-(6-D)}. \qquad (5)$$

For homogeneous particles the scattering curve coincides with the curve scattered by the surface [7], thus one needs to extract this intensity from the full intensity of the solution.

Assuming in the beginning that deuteration is rather homogeneous inside the particle we interpreted the TIS scattering curve of EF-Tu, which is a vacuum curve in reality, as the scattering curve of its shape. The experiments were carried out by the standard technique described above (Fig.3, a). The complex EF-Tu-GDP from E.coli with three levels of deuteration was isolated as in [2]. The measurements were performed on the YuMO and D11 small-angle scattering setups in the q-range 0.032 - 0.3 $Å^{-1}$. The difference scattering curve (Fig.5) in the interval of scattering vectors from 0.1 to 0.22$Å^{-1}$ gives a very good straight line with a slope which does not correspond to the Porod Law (q^{-4}). This slope corresponds to the surface fractal dimension 2.55 which is in reasonable agreement with theoretical calculations for globular proteins [7]. Unfortunately, the obtained interval of q is relatively narrow to attribute completely the observed slope to the roughness of the surface of this protein, and the observed slope in Fig.5 corresponds only to the beginning of the range where the fractal properties start to be significant.

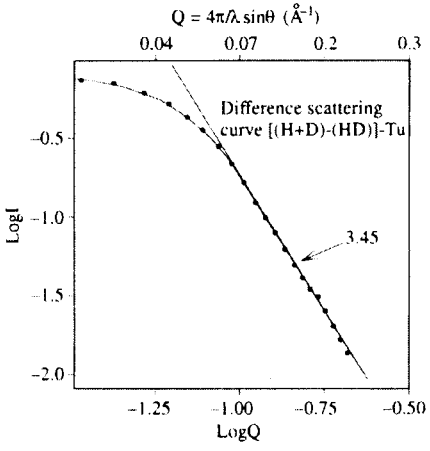

Fig.5. TIS curve for free EF-Tu. $\delta = 0.56$.

In principle, TIS allows us to increase the q-range of the scattering curve up to $0.8Å^{-1}$ as we can increase the concentration of EF-Tu in solution as much as we need without taking care for the aggregation. The restriction is the measuring capabilities of the SANS setups. To predict the behavior of the scattering curve at large q values, we calculated it using crystallographic X-ray data from the Protein Data Bank (PDB) [8]. We are forced to take the atomic coordinates of EF-Tu from Thermus Thermophilus as there are no data in PDB corresponding to the crystals of nonmodified EF-Tu from E.coli which was used in the experiments. We assume that the qualitative character of the scattering curves should be the same for this protein from both sources. The calculated TIS curve of EF-Tu is presented in Fig.6 together with the theoretical curve calculated by algorithm [9]. The slope of the latter for large q is 3.57 which differs a little from the previous value. It corresponds to the fractal dimension 2.63. From the former curve one can see that the deuteration is not a homogeneous process at the length less than 40Å as the correlation peak appears for large q, and vacuum curve of the nonpolar groups (CH, CH_2, CH_3, NH) where the replacement of hydrogen by deuterium takes place, does not differ much from the envelope curve. To understand whether it is possible to obtain the reliable information about the arrangement of these nonpolar groups inside the protein we compared the TIS curve with the scattering curve for these groups with unit scattering length for each group (in reality their scattering lengths are different). One can see that the difference between these curves is rather small (Fig.7). So using TIS for large q one can obtain the information on the correlation in the arrangement of the polar groups. Unfortunately, the signal corresponding to the surface is very small in this region.

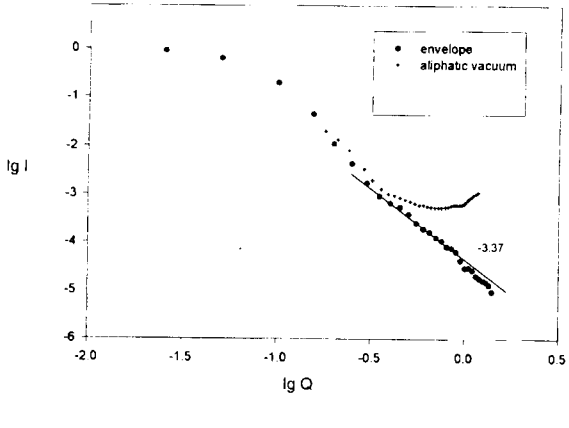

Fig.6. Envelope scattering curve (•) of EF-Tu from *Thermus Thermophilus* and the vacuum scattering curve of its nonpolar (aliphatic) groups. Intensity is normalyzed by zero angle cross section.

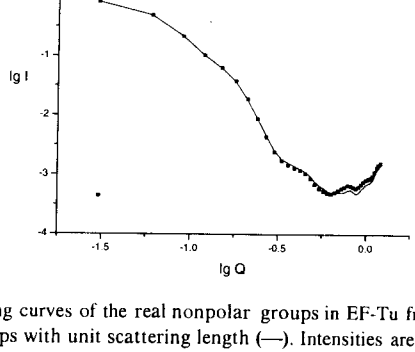

Fig.7. Vacuum scattering curves of the real nonpolar groups in EF-Tu from *Thermus Thermophilus* (■) and the same groups with unit scattering length (—). Intensities are normalyzed by zero angle cross section

Conclusions

Summarizing the experience in using the triple isotopic substitution technique we can make the following conclusions.

TIS is very useful for studies of biological complexes.

Using TIS one can study the modification of molecules during biological cycles.

Using TIS one can estimate the fractal dimension of the protein surface.

In the region of large scattering vectors TIS gives information on the arrangement of nonpolar atomic groups inside proteins.

References

1. M.Yu. Pavlov and I.N.Serdyuk, J. Appl. Cryst. (1987) 20, 105
2. I.N. Serdyuk, M.Yu. Pavlov, I.N.Rublevskaya, G.Zaccai, R.Leberman, Biophys. Chem. (1994) 53, 123-130
3. M.Yu. Pavlov, I.N.Rublevskaya, G.Zaccai, R.Leberman and Yu.M.Ostanevich, J. Appl. Cryst. (1991) 24, 243 - 254
4. Elber R., Fractal Analysis of Proteins. In "The fractal Approach to Heterogeneous Chemistry" Ed. by Avnir, D. 1989 John Wiley & Sons, Great Britain
5. Pfeifer, P., Obert, M. Fractals: Basic Concepts and Terminolgy, ibid.
6. Schmidt P.W., Use of scattering to determine the fractal dimension, ibid.
7. Fedorov B.A. & Schmidt P.U., Biofizika (1991) 36, 749 (in Russian)
8. Bernstein F.C., Koetzle T.F., Williams G.J.B., Meyer E.F.Jr. Brice M.D., Rodgers J.R., Kennard O., Shimanouchi T., Tasumi M. J. Mol. Biol. (1977) 112, 535
9. Pavlov, M.Yu., Fedorov, B.A. Biopolymers. (1983) 22, N6, 1507

International Workshop on Deuteration of Biological Molecules for Structural and Dynamic Studies. Applications to Neutron Scattering and NMR

Международное рабочее совещание «Дейтерирование биологических молекул для структурных и динамических исследований. Применение для нейтронного рассеяния и ЯМР»

E17,19-98-305

Ответственный за подготовку сборника к печати М.В.Авдеев

Макет Р.Д.Фоминой

Рукопись сборника поступила 26.10.98. Подписано в печать 5.11.98
Формат 60 × 90/16. Офсетная печать. Уч.-изд. листов 9,5
Тираж 120. Заказ 50989. Цена 12 р.

Издательский отдел Объединенного института ядерных исследований
Дубна Московской области